Contract Number: 622177

Deliverable D3.3

Long-term power supply sources for repository monitoring

Work Package 3, Task 3

Project Acronym	Modern2020
Project Title	Development and Demonstration of Monitoring Strategies and Technologies for Geological Disposal
Start date of project	01/06/2015
Duration	48 Months
Lead Beneficiary	AMBERG
Contributor(s)	*Esko Strömmer (ed., VTT), Héctor Luis Abós Gracia (ARQUIMEA), Francisco Alvarez (ARQUIMEA), Pierre Forbes (ORANO), Ecaterina Rosca-Bocancea (NRG) and Thomas Schröder (NRG)*
Contractual Delivery Date	31/08/2018
Actual Delivery Date	31/05/2019
Reporting period X:	3
Version	Final

Project co-funded by the European Commission under the Euratom Research and Training Programme on Nuclear Energy within the Horizon 2020 Framework Programme		
Dissemination Level		
PU	Public	X
PP	Restricted to other programme participants (including the Commission Services)	
RE	Restricted to a group specified by the partners of the Modern2020 project	
CO	Confidential, only for partners of the Modern2020 project and EC	

Modern2020 D3.3: Long-term power supply sources for repository monitoring
Dissemination level: PU
Date of issue of this report: 31/05/2019

Page 1
© Modern2020

History chart			
Type of revision	Document name	Partner	Date
Template, chapters 1-4 drafted.	Long-term power supply sources for repository monitoring v0	VTT	7.11.2017
Chapters 6.1, 6.2 and 6.4 drafted.	Long-term power supply sources for repository monitoring v0.1	VTT	17.1.2018
Chapter 5 added.	Long-term power supply sources for repository monitoring v0.2	NRG, VTT	25.4.2018
Chapters 6.4 and 6.5 added. Chapter 7 based on the text in the MS21 progress report added. Review of other chapters.	Long-term power supply sources for repository monitoring v0.3	NRG, VTT	21.5.2018
Chapters 5 and 6 edited. New text to Chapter 7 integrated and revised. Chapter 9 drafted.	Long-term power supply sources for repository monitoring v0.4	NRG, Orano, VTT	3.7.2018
Chapters 1-7 and 9 edited. New text to Chapter 8 integrated and revised, Abstract added.	Long-term power supply sources for repository monitoring v0.5	Arquimea, NRG, VTT	16.8.2018
Chapter 9 reviewed and revised. Chapter 8 reviewed. Small amendments in Abstract and Chapter 5 & 6.	Long-term power supply sources for repository monitoring v0.6	NRG, VTT	21.9.2018
Finalization of chapters 5 – 9.	Long-term power supply sources for repository monitoring, Final draft	Arquimea, NRG, Orano, VTT	23.1.2019

Reviewed by:

Johan BERTRAND (Andra).

Approved by:

This report has been approved by:

- José-luis Garcia-Sineriz, Work Package 3 Leader, *31/05/2019*
- Johan Bertrand, the Modern2020 Project Co-ordinator (on behalf of the Modern2020 Project Executive Board), *31/05/2019*

Modern2020 D3.3: Long-term power supply sources for repository monitoring
Dissemination level: PU
Date of issue of this report: 31/05/2019

Page 2
© Modern2020

Contents

Modern2020 D3.3: Long-term power supply sources for repository monitoring
Dissemination level: PU
Date of issue of this report: 31/05/2019

Page 3
© Modern2020

Modern2020 D3.3: Long-term power supply sources for repository monitoring
Dissemination level: PU
Date of issue of this report: 31/05/2019

Page 4
© Modern2020

Abstract

This document is the final technical report and summarizes the work performed in Task 3.3, *Alternative power supply sources*, of the EU H2020 project Modern2020. It integrates contributions by Andra, Arquimea, NRG, Orano, RWMC and VTT, and is prepared and compiled by VTT.

The objective of Task 3.3 has been to develop and demonstrate energy sourcing solutions for the wireless sensor instrumentation in nuclear repositories that are capable of extending the expected lifetime of the sensor instrumentation beyond that by chemical batteries, i.e. up to several decades. The energy sourcing solutions have also to eliminate the need for cables through the barriers, which would impair the safety function of these barriers.

Building on the results of the preceding project MoDeRn, Task 3.3 of project Modern2020 has been focused on relevant long-term power supply technologies for wireless repository monitoring sensors and involved the following subtasks:

- **Subtask 1**: Energy harvesting based on low thermal gradients (carried out by NRG)
- **Subtask 2**: Energy storage (carried out by Arquimea)
- **Subtask 3**: Wireless energy transmission (carried out by NRG and VTT)
- **Subtask 4**: Miniaturized nuclear generators (carried out by Andra, Orano and RWMC)

This report summarizes the work of all subtasks and partners contributing to Task 3.3 as follows:

- **Chapter 4**: Energy sourcing concepts of wireless sensor units for repository monitoring (related to all subtasks)
- **Chapter 5**: Energy harvesting on low thermal gradients (related to Subtask 1)
- **Chapter 6**: Wireless energy transfer (related to Subtask 3)
- **Chapter 7**: Miniature nuclear generators (related to Subtask 4)
- **Chapter 8**: Energy storage (related to Subtask 2)
- **Chapter 9**: Overall conclusions (related to all subtasks)

Referring to Table 9-1 (A rough comparison of the investigated energy sourcing options), the analyses and pilot systems in this report indicate that the proposed three power sourcing technologies (thermoelectric energy harvesting, wireless energy transfer, nuclear generators) are relevant and feasible for generating supply energy for repository monitoring wireless sensor units (WSUs). Nevertheless, they also have clear differences in their power output capability and way of application. In most cases, this in addition to the power sourcing requires an intermediate energy storage that accumulates the sourced energy for the further need of the sensor and communication payload. This also requires low duty cycle operation of the WSU, i.e. an operation scenario based on long (e.g. several hours or even several days) energy accumulation periods between short activity cycles for sensor measurements and wireless communication. In this operation scenario, the sensor and communication payloads are kept in an ultra-low power sleep mode or even totally unpowered, and activated periodically by an ultra-low power wake-up circuit. With this kind of WSU arrangement, which is also commonly applied to energy harvesting wireless devices in general, power sourcing levels even down to around 10 μW can be exploitable.

In addition to reporting some tangible pilot examples of the above mentioned power sourcing technologies and their verification results in the environment that partly represents the final repository environment, the report improves the understanding about the scaling of the capacity of the power sourcing by adjusting the design parameters. Moreover, the report improves the understanding of the effects of the repository environment on the behavior and performance of the power sourcing. Both of these will be of great importance in the follow-on actions towards complete wireless repository monitoring systems.

The report also improves the understanding for designing the intermediate energy storage subsystem that, depending on the power sourcing capacity, powering needs of the sensor and communication payload, required lifetime and environmental conditions, can be a critical part for the performance and the reliability of the entire repository monitoring WSU. This concerns especially the lifetime (aging) and

Modern2020 D3.3: Long-term power supply sources for repository monitoring
Dissemination level: PU
Date of issue of this report: 31/05/2019

Page 5
© Modern2020

the self-discharge of the energy storage components. Even though several energy storage technologies such as rechargeable batteries, electrostatic double-layer supercapacitors and newer type pseudocapacitors are commercially available, the design of an energy storage subsystem that can fulfil all requirements of typical repository monitoring WSUs can be a challenging task and may need iteration between the requirements and the design.

The work in Modern2020 Task 3.3 has mainly focused to the development and demonstration of the energy sourcing as a separate subsystem without other functionalities of the prospective complete WSUs such as sensor measurements and wireless communication. The achieved TRL levels are 3 – 5 depending on the investigated technology. The follow-on steps after project Modern2020 should be targeted to the further development, demonstration and verification of the energy sourcing parts as more complete building blocks. Beyond this, the follow-on steps should also be targeted to integration, demonstration and verification of more complete repository monitoring systems according to comprehensive repository monitoring strategies. In addition to the energy sourcing, these pilot systems should also involve the sensor and communication payload, encapsulation that can tolerate the target repository environment, and the system components behind the repository barriers. The verification of these comprehensive repository monitoring pilot systems should take place in a testing environment that emulates as much as possible the final repository environment. Since the repository environment does not enable repairing the devices after the installation, the future actions should also involve measures for improving the reliability such as redundancy, design by drift margins and component derating, and qualification and screening procedures.

Modern2020 D3.3: Long-term power supply sources for repository monitoring
Dissemination level: PU
Date of issue of this report: 31/05/2019

Page 6
© Modern2020

List of figures

Modern2020 D3.3: Long-term power supply sources for repository monitoring
Dissemination level: PU
Date of issue of this report: 31/05/2019

Page 7
© Modern2020

Modern2020 D3.3: Long-term power supply sources for repository monitoring
Dissemination level: PU
Date of issue of this report: 31/05/2019

Page 8
© Modern2020

List of Tables

Modern2020 D3.3: Long-term power supply sources for repository monitoring
Dissemination level: PU
Date of issue of this report: 31/05/2019

Page 9
© Modern2020

Glossary

AC:	Alternating Current
DC:	Direct Current
DoD:	Depth of Discharge
EBS:	Engineered Barrier System
EDLC:	Electrostatic Double-Layer Capacitor
EM:	Energy Management
EMD:	Energy Management Device
EMI:	Electromagnetic Interference
ESA:	European Space Agency
ESR:	Equivalent Series Resistance
HLW:	High-Level Waste
ICNIRP:	International Commission on Non-Ionizing Radiation Protection
ILLL:	Intermediate Level Long Lived
LF:	Low Frequency
LTRBM:	Long-term Rock Buffer Monitoring
OOK:	On/Off Keying
PCB:	Printed circuit board
RF:	Radio frequency
RPS:	Radio Isotopic Power System
RTD:	Resistance Temperature Detector
RTG:	Radioisotope Thermoelectric Generator
SAR:	Specific Absorption Rate
SoC:	State of Charge
TDM:	Time Division Multiplexing
TEG:	Thermoelectric Generator
TEH:	Thermoelectric Harvester
WDT:	Wireless Data Transfer
We, Wth:	Wattage unit of the electric and thermal power respectively
WSU	Wireless Sensor Unit

Modern2020 D3.3: Long-term power supply sources for repository monitoring
Dissemination level: PU
Date of issue of this report: 31/05/2019

Page 10
© Modern2020

1.   Introduction

The former MoDeRn Project has successfully developed and analyzed the capabilities of monitoring technologies for future nuclear disposal repository use in the fields of measurement techniques and probes, data transfer methods and energy supply. Among the main topics analyzed in the project MoDeRn was wireless technologies through the repository barriers for linking the sensor units in the inner repository to the outer environment without any physical paths such as electrical and optical cables that may entail risks of radionuclide transport out from the repository [1]. Among the prior technical issues that remained to be investigated in the follow-on projects were power supply sources that are capable of providing the necessary electric power for the operation of the wireless sensor units (WSUs) embedded in deep nuclear repositories. Supplying the power by chemical batteries is usually not a reasonable solution, since the chemical batteries feature relatively short lifetime due to their limited energy storage capacity and self-discharge, as well as materials not permitted inside some nuclear repositories.

Potential long-term power supply technologies for WSUs without chemical batteries, currently applied also in some commercial products, are energy harvesting, wireless power transfer and non-chemical batteries. In the energy harvesting, electric power is generated from inherent ambient energy such as light, thermal flows, mechanical vibration or electromagnetic radio frequencies. In the wireless energy transfer, most typically based on radio frequencies, the ambient energy for the sensor unit is generated or enhanced by a dedicated power transmitter. Non-chemical batteries can be based e.g. on a power converter generating electricity from the energy emitted by a radionuclide material.

Among the typical bottlenecks and risks of the existing alternative powering solutions in their application in deep nuclear disposal repository environments are their expected lifetime, wireless operation range and thermal constraints. Task 3.3 of the work package 3 in the project Modern2020 has focused on the adaptation of the relevant long-term power supply technologies for WSUs in future repository monitoring systems, and involved the following subtasks:

1. Energy harvesting based on low thermal gradients (carried out by NRG): This subtask has analyzed and developed methods for generating electrical power (energy harvesting) by thermoelectric generators (TEGs) that exploit heat produced by radioactive waste such as spent fuel or high-level waste (HLW) disposed in a geological disposal. Expected thermal gradients after long-term interim storage are small, therefore the focus of this subtask is to analyse the feasibility to harvest electrical power at temperature differences below 2 °C.

2. Energy storage (carried out by Arquimea): One of the outcomes of the project MoDeRn was that some kind of interim energy storage between the energy source and the sensor payload will be required due to the way in which the energy is used in radio-based repository sensor units. However, the energy storage technologies used in conventional wireless sensor applications are not suitable for long-term operation in repository environment. This subtask has investigated alternative energy storage technologies to obtain a suitable solution.

3. Wireless energy transmission (carried out by NRG and VTT): Based on the results of project MoDeRn on electromagnetic field propagation, inductive low-frequency radio based wireless energy transfer systems for powering repository monitoring sensors could be feasible. Two different medium range (up to 10 m or more) application scenarios of this have been investigated and demonstrated: wireless energy transfer through high electrical conductivity host rock and saturated components of the engineered barrier system (EBS), and a combined solution for wireless energy and data transfer through host rocks with low electrical conductivity (e.g. granite, rock salt).

4. Miniaturized nuclear generators (carried out by Andra, Orano and RWMC): This subtask has investigated the technical feasibility of a radioisotope thermoelectric generator (RTG) type power supply inside intermediate level long lived (ILLL) waste vaults. The operation of the RTG power supply is based on a combination of a radio isotopic heat source and a TEG. Thus, the physical operation principle is the same as in Subtask 1 but the technical implementation is much different.

The main part of the work in Task 3.3 has been devoted to analyze, develop and verify innovative power supply technologies for repository monitoring sensors to the proof-of-concept level. Potential power supply technologies have been verified by theoretical calculations, by simulations and by prototyping in

Modern2020 D3.3: Long-term power supply sources for repository monitoring
Dissemination level: PU
Date of issue of this report: 31/05/2019

Page 11
© Modern2020

a laboratory. Some verification activities have also been carried out by prototypes in field conditions that represent partly a real repository environment.

Modern2020 D3.3: Long-term power supply sources for repository monitoring
Dissemination level: PU
Date of issue of this report: 31/05/2019

Page 12
© Modern2020

2. Objectives of Task 3.3

The objective of Task 3.3 has been to develop and demonstrate energy sourcing solutions for the wireless sensor instrumentation in nuclear repositories that are capable of extending the expected lifetime of the sensor instrumentation beyond that by chemical batteries, i.e. up to several decades. The energy sourcing solutions have also to eliminate the need for cables through the barriers, which would impair the safety function of these barriers.

The work in Task 3.3 has been focused on three alternative power-sourcing technologies and on energy storage technologies for matching together the limited, sometimes also intermittent supply capability of the power sources, and the variable energy consumption of the sensor and communication payload. The results should support future implementation and integration of the powering parts into the repository monitoring sensors and entire monitoring systems, which among other things may include energy budged calculations of the repository monitoring sensors, and scaling the power and energy sourcing performance for the monitoring application needs by modifying the design parameters of the powering solution.

Modern2020 D3.3: Long-term power supply sources for repository monitoring
Dissemination level: PU
Date of issue of this report: 31/05/2019

Page 13
© Modern2020

3.   Scope of this report

This Modern2020 report, identified as D3.3, is the final technical report of the Task 3.3 of project Modern2020. Chapter 4 presents the alternative powering concepts from the monitoring system integration viewpoint. The outcome of all research subtasks focused to different technical building blocks is compiled hereafter in Chapters 5 - 8. Chapter 9 summarises general conclusions of all subtasks.

The aim of this report is to synthetize the progress achieved in the Task 3.3 by Andra, Arquimea, NRG, Orano, RWMC and VTT. Another aim is to support the evaluation of the readiness level of the investigated energy sourcing technologies. The report has been edited by VTT.

Modern2020 D3.3: Long-term power supply sources for repository monitoring
Dissemination level: PU
Date of issue of this report: 31/05/2019

Page 14
© Modern2020

4. Energy sourcing concepts of wireless sensor units for repository monitoring

The investigated alternative energy sourcing concepts for wireless repository monitoring sensors are depicted in Figure 4-1, Figure 4-2, Figure 4-3 and Figure 4-4. To illustrate the integration of the energy sourcing parts into entire monitoring systems, the other basic building blocks for measurement and communication are also included in the figures. The building blocks for sensor powering are indicated by red colour.
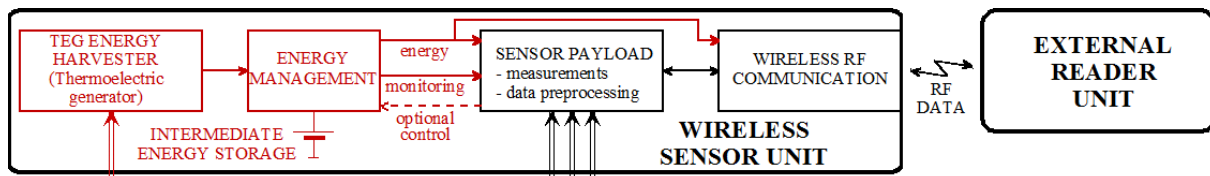
Figure 4-1. Conceptual illustration of a wireless repository-monitoring sensor powered by energy harvesting on thermal gradients.
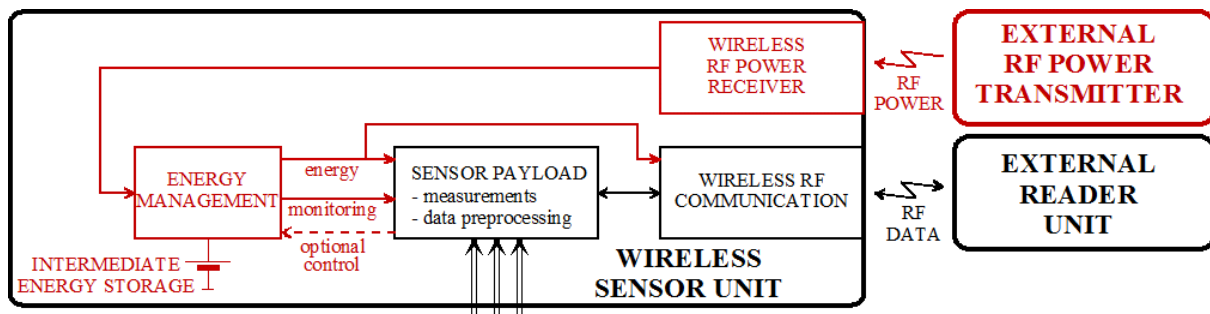
Figure 4-2. Conceptual illustration of a wireless repository-monitoring sensor powered by wireless energy transfer.
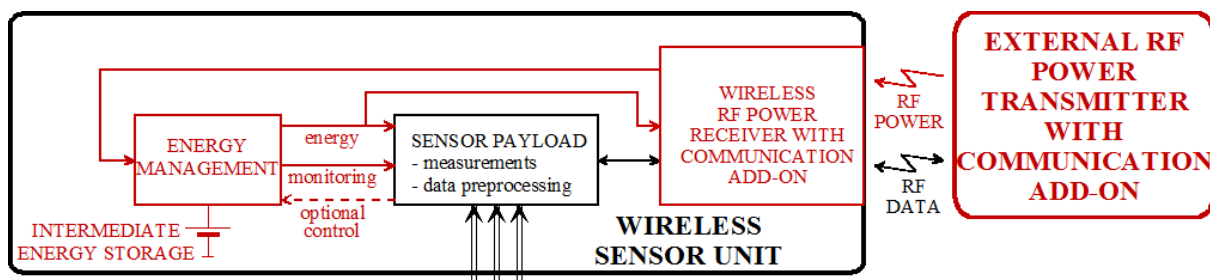
Figure 4-3. Conceptual illustration of a wireless repository-monitoring sensor powered by wireless energy transfer with wireless communication add-on.
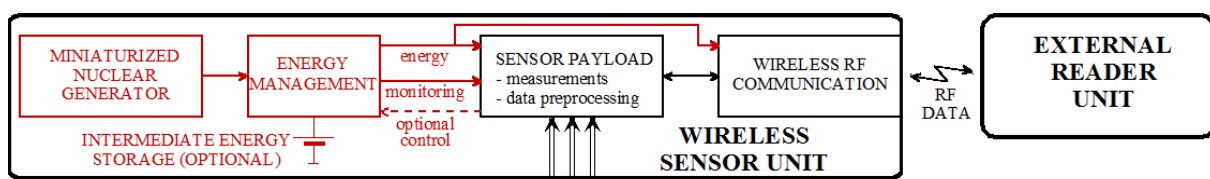
Figure 4-4. Conceptual illustration of a wireless repository-monitoring sensor powered by a miniaturized nuclear generator.

Modern2020 D3.3: Long-term power supply sources for repository monitoring
Dissemination level: PU
Date of issue of this report: 31/05/2019

Page 15
© Modern2020

The output power capability of the power sources in the previous figures is typically too limited for continuous powering of the wireless sensor unit with full activity. Thus, a typical operation scenario is to keep the power consuming parts, i.e. the sensor payload and the wireless RF communication, most of the time sleeping, which means that they are unpowered or in extremely low power consumption state. During the sleep mode, the wireless sensor unit will accumulate energy from the power source to the intermediate energy storage. After this energy accumulation period, the energy consuming parts will be waken up e.g. by an internal clock, by an energy storage monitoring circuit or by a signal sent by the reader unit, after which they carry out a short activity cycle involving measurements and communication that are powered mainly by the intermediate energy storage. At the end of this activity cycle, the power consuming parts will be switched back to the sleep mode, starting up the next energy accumulation period. The maximum rate of the sensor activity cycles depends on the output power from the power source and the energy consumed by the activity cycle. This is discussed more in the energy storage section of this report (Chapter 8).

A crucial part for the overall functionality of the system is energy management (EM) that connects the energy source, intermediate energy storage and the power consuming parts together. To avoid degrading the overall energy sourcing capability, the self-discharge of the intermediate energy storage and the self-power consumption of the EM have to be much lower than the mean output power capability of the power source. Among the tasks of the EM are:

- The EM optimizes energy acquisition from the power source by appropriate loading of it, such as the maximum power point tracking (MPPT).
- The EM controls charging and discharging of the intermediate energy storage.
- The EM makes necessary voltage conversions between the power source, the intermediate energy storage and the power consuming parts, and produces stable supply voltages to the power consuming parts.

Energy sourcing technologies are typically scalable to the powering needs of different sensor payloads. For this, following information about the sensor payload is typically needed:

- operation scenarios and their energy budged, e.g. energy consumed by each activity cycle of the sensor payload, what is the required rate of the activity cycles,
- supply voltages,
- peak current consumption of each supply voltage.

Modern2020 D3.3: Long-term power supply sources for repository monitoring
Dissemination level: PU
Date of issue of this report: 31/05/2019

Page 16
© Modern2020

5. Energy harvesting on low thermal gradients

5.1 Introduction

This chapter summarizes a feasibility study performed by NRG on the ability to use decay heat of High-Level Waste (HLW) containers to power wireless sensors units (WSUs) in a geological disposal facility. *Thermoelectric Generators* (TEGs) are widely applied to convert high temperature gradients into electric energy. However, the specific focus of this study are rather small temperature gradients as expected in a disposal situation. The focus of this research is therefore to understand the feasibility to harvest thermal energy from very small temperature gradients (<2°C), and to quantify the performance and efficiency of the different subcomponents of the energy harvesting system under disposal conditions.

5.2 Concept description

Due to the radioactive decay of the HLW, heat is produced in the waste containers. When the containers are disposed of in a geological disposal, the heat will diffuse through the engineered barrier system (EBS) into the host rock. Due to the heat input, temperatures will increase in the waste containers, the engineered barriers and the surrounding host rock, and a temperature gradient will settle throughout the system. The highest temperatures occur near the heat source, i.e. the waste canister, whereas temperatures drop further away from the source. As time progresses, the decay heat will decrease, and the temperatures as well as the temperature gradients will settle, finally to the ambient values before the disposal.

The heat flow can be converted into electrical power by the use of the so-called *Seebeck effect* that occurs in metals and semiconductors. The generated Seebeck voltage U_s can be calculated by the temperature difference ΔT between the hot and cold side:

$$U_S = \alpha \cdot \Delta T \tag{5-1}$$

with α the Seebeck coefficient in [V/°C]. To convert heat into electrical energy, a *Thermoelectric Generator* (TEG) is used. A TEG consists of one or several couples of n- and p-type semiconducting materials (Figure 5-1).
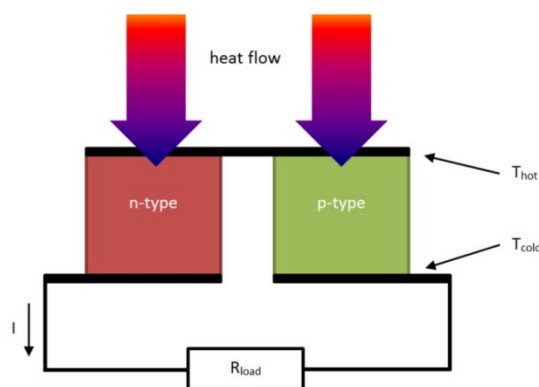
Figure 5-1. Basic principle of a TEG [2].

For the operating temperatures of interest, bismuth telluride is usually applied. Bi_2Te_3 has a Seebeck coefficient of about 220 µV/°C [3] and to provide high output voltages, often hundreds of couples are connected in series in a TEG module.

The induced voltage leads to a current I, dependent on the internal resistance R_{TEG} and the load resistance R_{load}, with the power output characterized by

$$P_{TEG,out} = I^2 R_{load}. \tag{5-2}$$

With N the number of $n+p$ legs, the current I generated by the TEGs can be estimated by

Modern2020 D3.3: Long-term power supply sources for repository monitoring
Dissemination level: PU
Date of issue of this report: 31/05/2019

Page 17
© Modern2020

$$I = \frac{N \cdot \alpha \cdot \Delta T}{R_{TEG} + R_{load}} .$$ (5-3)

At small temperature gradients, the little voltages generated by a TEG cannot be directly used to power WSUs: they have to be boosted up to higher voltage levels as required by sensor electronics (e.g. 2.2 - 5V). Furthermore, to provide sufficient energy to perform a measurement cycle, the small amounts of available power need to be accumulated and stored over longer periods. The electronic circuit that performs the voltage boosting, power conditioning and storage is shortly indicated as '*energy management device*' (EMD). The combination of a TEG-module and the EMD is indicated in this report as '*Thermoelectric harvester*' (TEH). The general set-up of a TEH is summarized in Figure 5-2 below:

- thermal energy is converted by a TEG module to electric energy with the efficiency η_{TEG}

- the electric energy is converted to a voltage of interest and stored by the EMD with efficiency η_{EMD}

- next to power losses during the electrical energy conversion, in the EMD also a (constant) self-power consumption can occur (P_{leak})
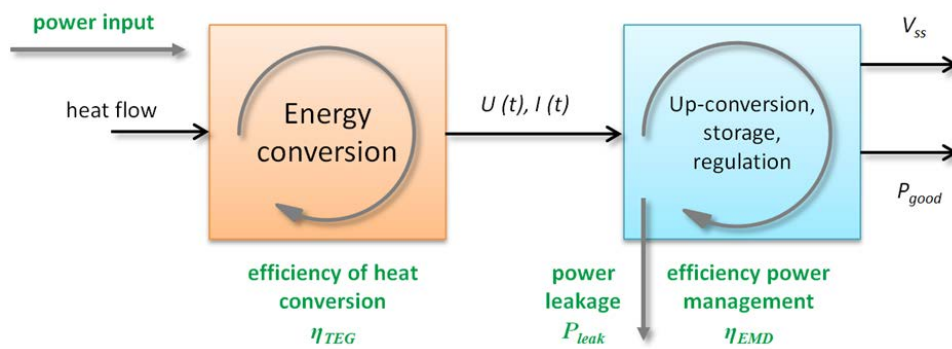
Figure 5-2. Principal set-up of a Thermoelectric Harvester (TEH).

The efficiency of the heat conversion η_{TEG} by the TEG module can be defined by

$$\eta_{TEG} = \frac{P_{TEG,out}}{q_{TEG}}$$ (5-4)

with q_{TEG} the heat flow through the TEG. The heat flow can be estimated by

$$q_{TEG} = N \cdot \alpha \cdot I \cdot T_{hot} + K \cdot \Delta T - \frac{I^2}{2} R_{TEG}$$ (5-5)

with K the thermal conductance of the TEG [3]. The efficiency of the up-conversion, storage, and regulation of the EMD η_{PM} is defined as

$$\eta_{EMD} = \frac{P_{EMD,out} - P_{leak}}{P_{EMD,in}}$$ (5-6)

Since the TEH operates under varying temperature gradients and load conditions, the overall efficiency cannot be expressed in a single number. Furthermore, the efficiency of the EMD and its self-power consumption depend on several factors as the input power and the load presented by the sensor electronics. From Figure 5-2 and Equation 5-6, it is evident that energy can only be collected as long as the input of power to the harvester is greater than the self-power consumption of the conversion unit. By collecting and storing energy over a longer period, even tiny energy amounts may accumulate until eventually, sufficient power is available to perform a measurement cycle of one or several sensors.

5.3 Feasibility analysis

5.3.1 Thermal analysis

This chapter shortly summarizes the thermal analyses performed by NRG. For a more detailed discussion of the analyses see Appendix 1.

The system of interest, for which the feasibility analyses are performed, is the generic Dutch OPERA disposal concept in Boom Clay [4]. In this concept, the heat producing HLW mainly consist of vitrified, reprocessed waste. The heat produced by this type of waste is due to the radioactive decay of the fission products contained in the glass. The main contributors to the heat output during the first hundreds of years are ^{90}Sr and ^{137}Cs. Figure 5-3 shows the evolution of heat production in a typical Cogema CSD-V container.
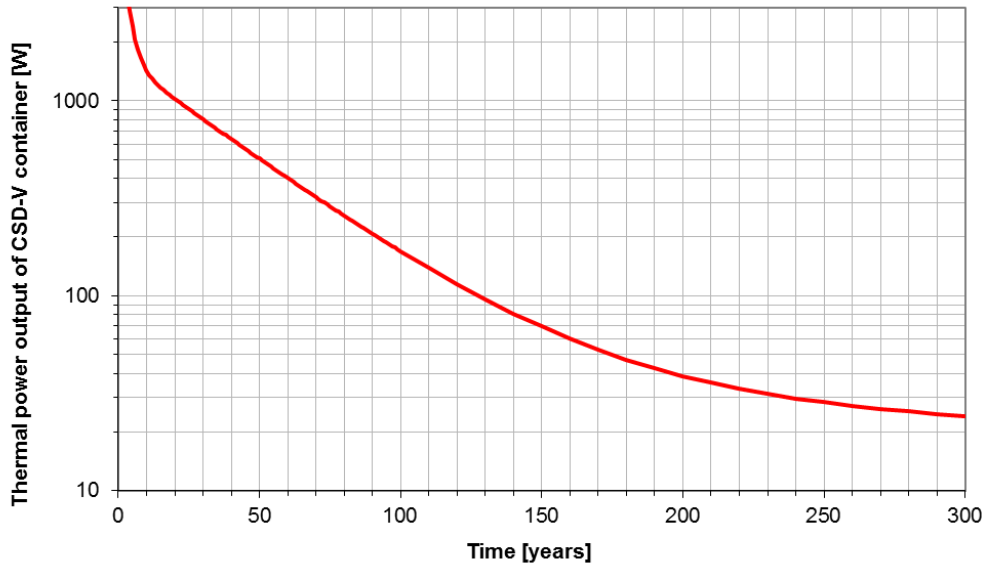
Figure 5-3. Heat production of a typical CSD-V container.

Directly after reprocessing, the thermal power output of the container is a few thousands watts. However, due to the long interim storage of at least 100 years in the Netherlands, at the moment of disposal, the power output will decrease to less than 200 W. After 200 years, i.e. 100 years of interim storage and 100 years of subsurface disposal, the thermal output is about 40 W per CSD-V canister.

The OPERA disposal concept makes use of a supercontainer (Figure 5-4) for vitrified waste that limits the radiation dose rate at the surface to less than 10 mSv/hr. The outer dimension of the supercontainer is 2.5 by 1.9 m (length by diameter), and the containers are stored horizontally in disposal galleries of about 45 m length (Figure 5-4).
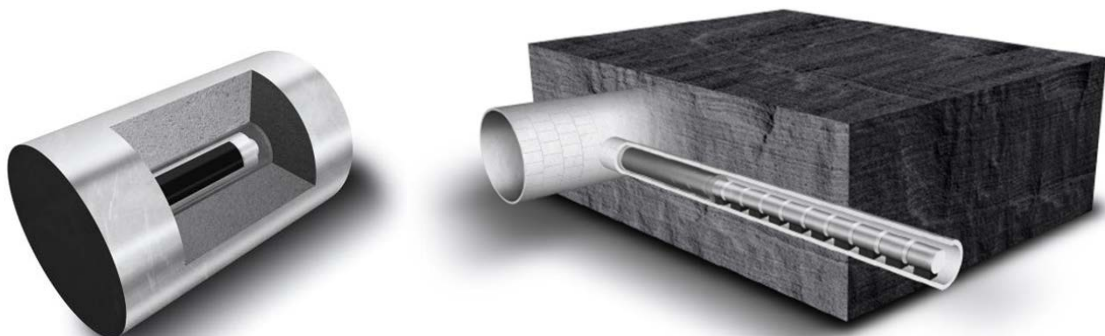
Figure 5-4. Artist impression of the OPERA Supercontainer and a HLW disposal gallery [4].

Figure 5-5 shows the evolution of the temperature gradients between different positions in a disposal gallery for vitrified waste: over the supercontainer buffer, over the backfill, over the gallery support, and in the first meter of Boom Clay. The gradients are calculated using a semi steady-state thermal model for a minimum surface interim storage period of 100 years. For longer interim storage periods, the gradients

Modern2020 D3.3: Long-term power supply sources for repository monitoring
Dissemination level: PU
Date of issue of this report: 31/05/2019

Page 19
© Modern2020

are even smaller (see Appendix 1). Hence, in order to provide energy over a relevant period of time, the TEH must be able to operate at temperature gradients of 2°C or less.
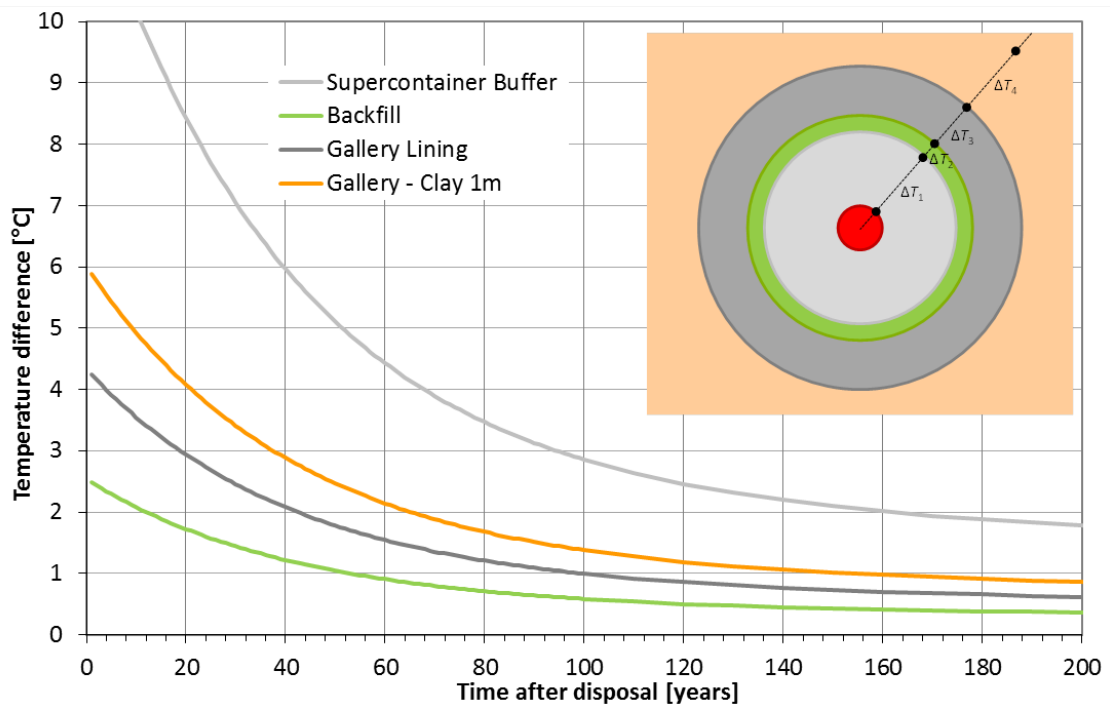
Figure 5-5. Estimated temperature gradient between several positions in the OPERA disposal concept for a Cogema CSD-V container after 100 years of interim storage.

5.3.2 TEH performance requirements

Many different types of TEGs are available on the market, the most are primarily used for cooling purposes, and their specifications are often limited to the relevant parameters for that particular purpose. Commercial EMDs require at least 20 mV to operate, leading to a preliminary requirement for the TEG to provide about 100 mV/°C in order to be able to harvest at low temperature gradients (<0.5°C).

For maximum output power and overall efficiency, the impedances of the TEG and the harvester, R_{TEG} and R_{load}, should be equal (Equations 5-2 and 5-3). However, a higher R_{load} might lower the minimum temperature gradient at which energy can be harvested. The load matching of TEG and EMD is not straightforward, because the oscillators used to convert the low voltages of the TEG show a complex, voltage dependent load resistance. To estimate and optimize the overall performance of the TEH solution, detailed measurements were necessary to quantify the TEG and its interaction with the EMD. These measurements are described in the next chapter.

5.4   Experimental set-up

A thermoelectric test bench was set-up to characterize the relevant performance parameters at very low temperature gradients (Figure 5-6). Resistance temperature detectors (RTDs) above and below the TEG allow quantifying the heat gradient over the TEG element. Two additional RTDs were installed to verify a homogeneous heat spreading over the TEG for the experimental conditions applied.

Modern2020 D3.3: Long-term power supply sources for repository monitoring
Dissemination level: PU
Date of issue of this report: 31/05/2019

Page 20
© Modern2020
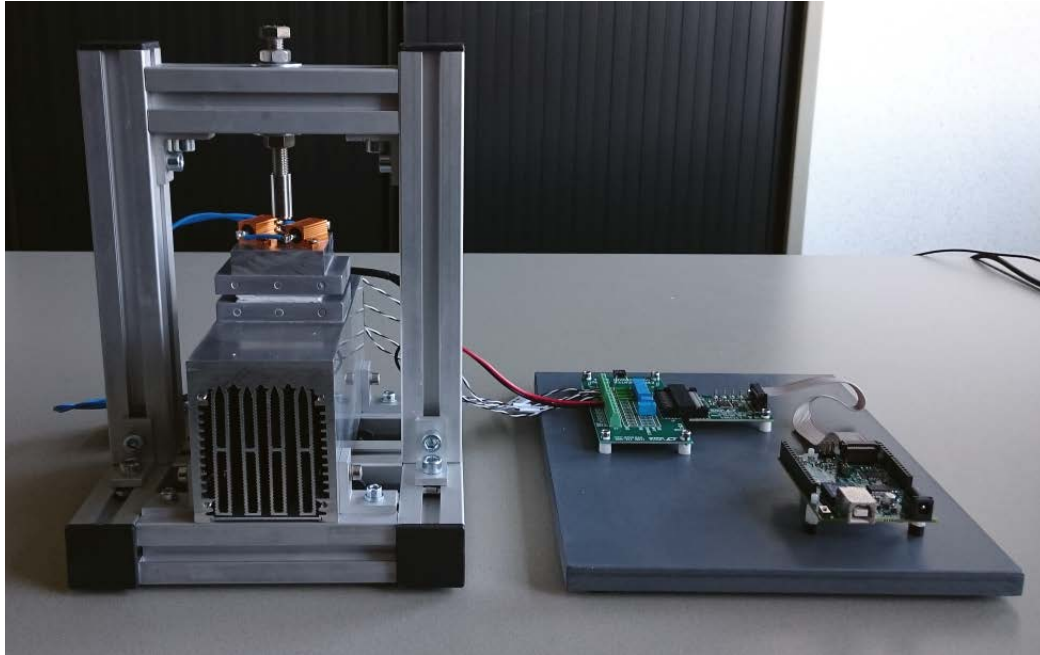
Figure 5-6. Thermoelectric test bench.

The small temperature gradients under consideration require careful calibration of all 4 RTDs: calibration measurements resulting in standard deviations typically below 0.0002˚C, and day-to-day differences in calibration values of less than 0.005 ˚C. Figure 5-7 shows the measured output voltage for two different types of 40 x 40 mm TEG's, TEG-1 (287 *p-n* legs) and TEG-2 (199 *p-n* legs). Measurements were performed without load and with a constant load of 3.3 Ω. For TEG-1 and TEG-2, an output voltage U_{TEG} of respectively 110 and 66 mV/˚C was found in the temperature gradient range of interest. With the load resistor, the output voltage drops to 28 and 43 mV/˚C, respectively.
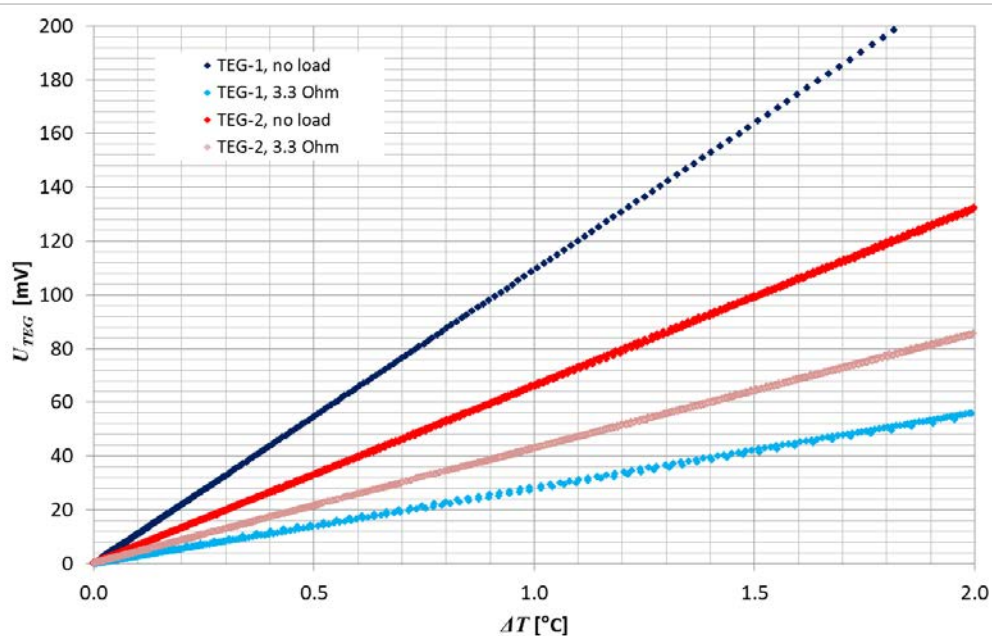
Figure 5-7. Measured output voltages U_{TEG} of TEG-1 and TEG-2.

Figure 5-8 shows the input resistance of the EMD as function of the input voltage, measured for two load resistances at the EMD's output.

Modern2020 D3.3: Long-term power supply sources for repository monitoring
Dissemination level: PU
Date of issue of this report: 31/05/2019

Page 21
© Modern2020
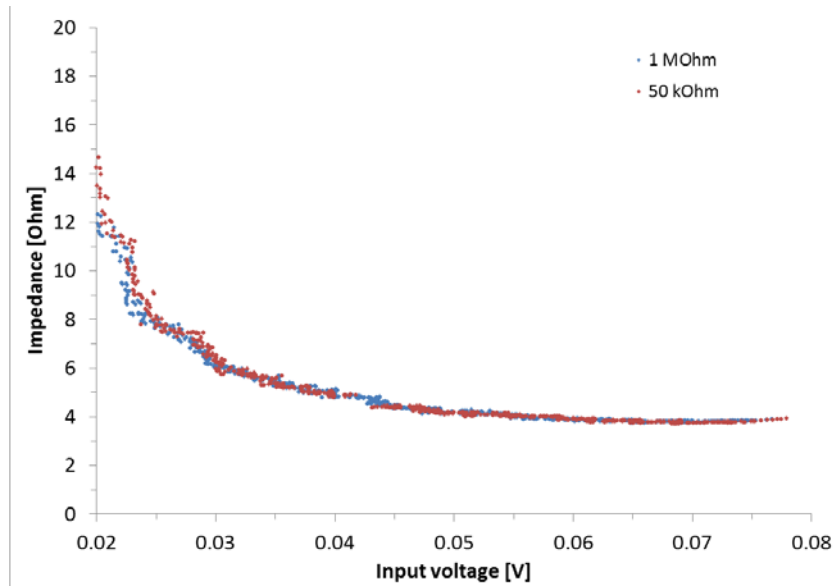
Figure 5-8. Input resistance of the energy management device.

By combining the measured voltage-temperature relation of the TEG (Figure 5-7) with the measured input resistance as depicted in Figure 5-8, for each TEG the voltage and power that is supplied to the EMD can be plotted as a function of the temperature difference (Figure 5-9). The figure shows that a temperature difference of about 0.5 °C results in a voltage U_{TEG} of about 27 mV, and about 50 to 100 μW is supplied to the EMD.
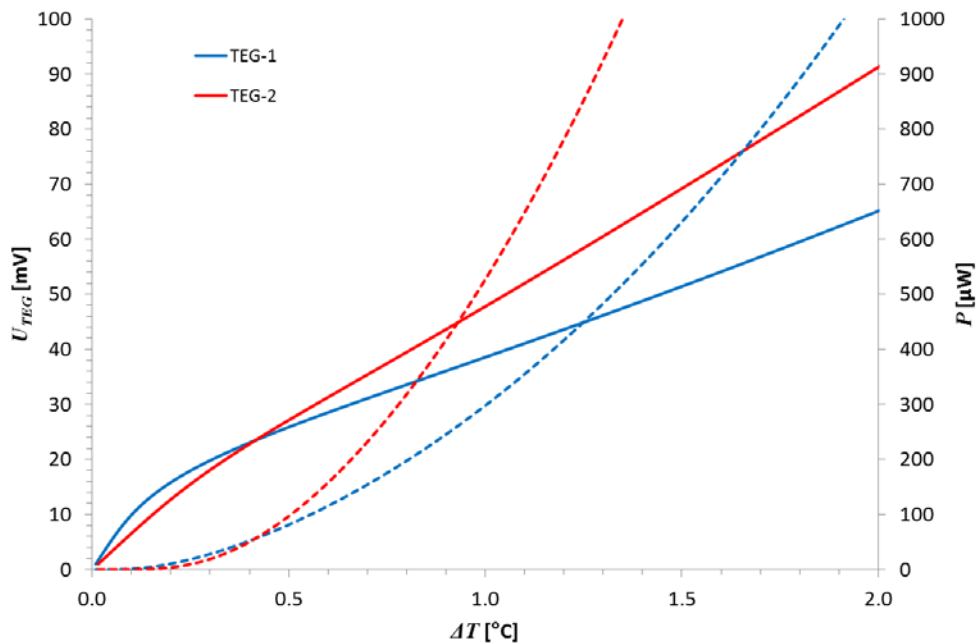
Figure 5-9. Estimated output voltage (solid line) and resulting power input (dashed line) of TEG-1 and TEG-2 into the energy management device.

Figure 5-10 shows the measured output voltage of the TEG, the power from the TEG into the EMD, and output power from the EMD, available for a WSU as a function of the temperature difference. Measurements were performed with six constant loads at the EMD's output, referring to output powers of 0, 1, 5, 10, 100 and 200 μW. A conversion efficiency η_{EMD} of the EMD of about 16 % was estimated, including an estimated power leaking P_{leak} of about 35 μW. The minimum temperature difference necessary for supplying any energy to the sensor was 0.50 °C and 0.44 °C for TEG-1 and TEG-2, respectively. The measured minimum input voltage U_{min} of the EMD is slightly above 20 mV.

Modern2020 D3.3: Long-term power supply sources for repository monitoring
Dissemination level: PU
Date of issue of this report: 31/05/2019

Page 22
© Modern2020
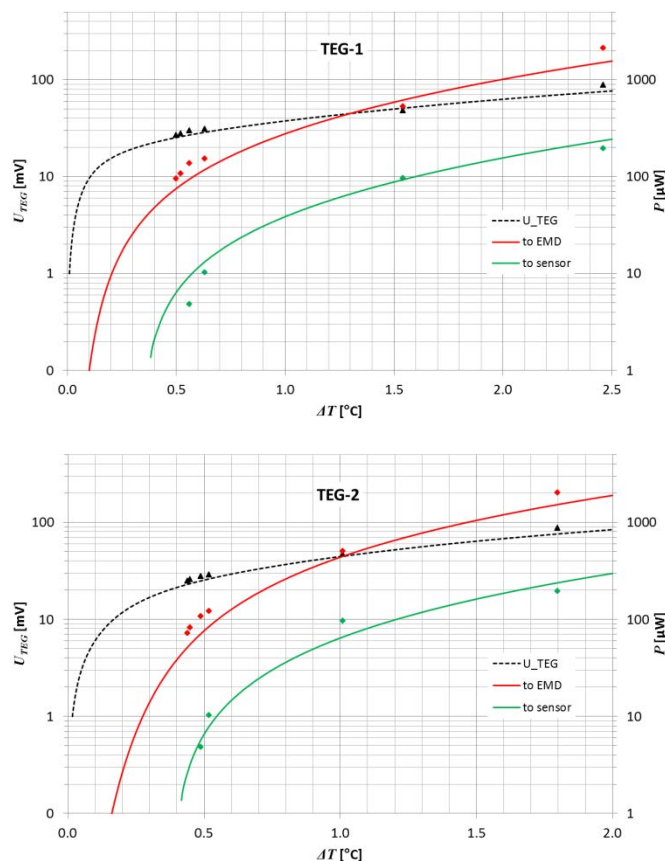
Figure 5-10. Calculated (lines) and measured (diamonds) TEG output voltage (black), power from the TEG to the EMD (red) and output power from the EMD (green).

On basis of the characterization of the TEGs and the EMD, a performance analysis for two application examples is performed in the next chapter.

5.5   Performance analysis of application cases

Based on the measurements and lessons learned in the previous chapter, in this chapter the results are translated to application cases. Six aspects need to be considered when setting-up a concept design and quantifying the overall performance of a thermoelectric harvester (see also Figure 5-2):

1.   the effective output voltage of the TEG U_s
2.   the minimum input voltage of the EMD U_{min}
3.   the self-power consumption of the EMD P_{leak}
4.   the conversion efficiency of the TEG η_{TEG}
5.   the conversion efficiency of the EMD η_{EM}
6.   the thermal losses due to heat conduction in the TEH (η_{cond})

The first three aspects mainly affect the minimum temperature difference at which the TEH can provide power, the latter three affect the efficiency of the TEH. All but the last parameter, η_{cond}, were measured or estimated in the previous chapter. The thermal losses due to heat conduction in the TEH are estimated by analysing the geometry and material properties of the TEH.

Several positions for the TEH are considered for the example case of the OPERA disposal concept, shortly introduced in Chapter 5.3. Conservatively[1], for the proposed design, two design requirements are applied:

---

[1] For a less conservative design concept see Chapter 7

Modern2020 D3.3: Long-term power supply sources for repository monitoring
Dissemination level: PU
Date of issue of this report: 31/05/2019

Page 23
© Modern2020

- the TEH should not alter the overall heat flow of the supercontainer & disposal cell, and
- the TEH should not bridge more than one EBS component.

For the first requirement, the overall thermal conductivity of the TEH should match with the thermal conductivity of the EBS component where the TEH has to be placed in (see Figure 5-5). With respect to the second requirement, two cases were analysed:

- a TEH inside the backfill, and
- a TEH inside the gallery lining.

Although a larger temperature gradient exists over the supercontainer buffer and the first meter of the Boom Clay (Figure 5-5), these cases are not considered, because both components have important safety functions. The TEH design to be placed inside the gallery lining has a length of 50 cm, the design for the backfill has a length of 15 cm. The temperature difference for the latter case is about 40% smaller than for the gallery lining (see Figure 5-5). For both designs, two TEH diameters are considered: 5 and 10 cm. All TEHs are based on TEG-2. Table 5-1 summarizes the four cases considered.

Table 5-1. TEH designs analysed for the OPERA disposal concept in Boom Clay.

Design	EBS position	Length	Diameter
TEH-1S	Gallery lining	50 cm	5 cm
TEH-1L	Gallery lining	50 cm	10 cm
TEH-2S	Backfill	15 cm	5 cm
TEH-2L	Backfill	15 cm	10 cm

From the geometry and material properties, the thermal losses inside the TEH are calculated: because a TEG is typically thinner than 4 mm, i.e. only a fraction of the overall TEH length, the resulting harvestable temperature difference over the TEG is lower than over the overall TEH. Besides, heat might flow alongside the TEG. These losses are expressed as *thermal design efficiency* η_{cond}, which defines the fraction of temperature difference over the TEH available for the TEG (Table 5-2). For each design, the thermal resistance R_{th} and an *equivalent area* can be calculated that represents the area of the backfill or gallery lining with a thermal resistance equivalent to the TEH. Furthermore, Table 5-2 depicts the minimum (external) temperature difference for which the TEH is expected to supply energy. For the temperature evolution as calculated for the case of the OPERA disposal concept (Figure 5-5), the TEH power output at different time steps can be estimated for all four TEH designs. Figure 5-11 shows the calculated power output as function of the time after disposal, and Table 5-2 gives an overview of the power output at 0, 50 and 100 years after disposal.

Table 5-2. Performance parameter of four TEH designs.

Design	η_{cond} [%]	R_{th} [K/W]	A_{eq} [m²]	T_{min} [°C]	P_{out} [µW] 0 yrs	50 yrs	100 yrs
TEH-1S	55	1.1	0.45	0.64	500	78	20
TEH-1L	78	0.8	0.64	0.46	1020	170	54
TEH-2S	80	0.8	0.66	0.46	370	52	8
TEH-2L	92	0.7	0.76	0.40	490	72	14

Figure 5-11 shows that harvesting of decay heat is potentially possible over periods of more than 100 years. The TEHs situated in the gallery lining harvest more power due to the large temperature difference. The TEHs with the larger diameter perform better than the smaller ones, due to lower losses during heat conduction. However, even the smallest TEH is able to provide power over a period of 100 years.
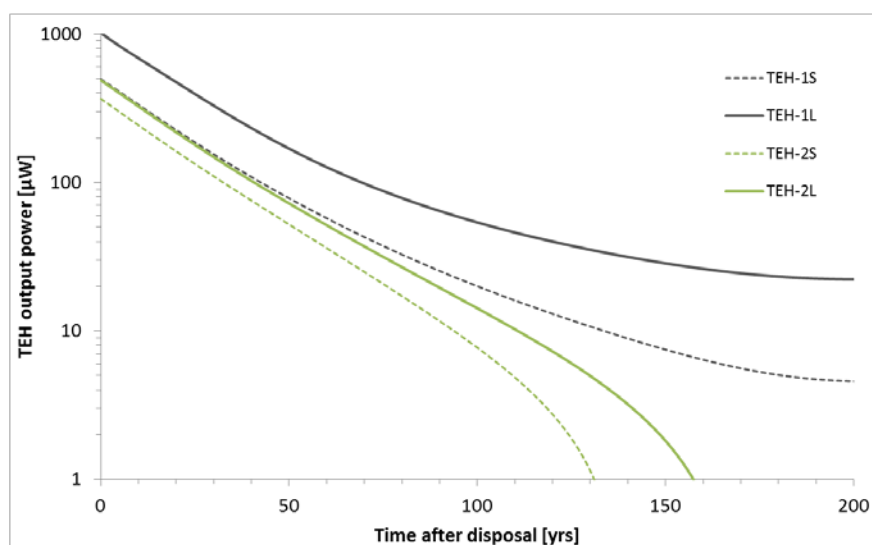
Figure 5-11. Calculated power output of four TEH concepts emplaced in the OPERA disposal concept for Boom Clay.

5.6 Conclusions

The results of this feasibility study show the principal potential to convert heat dissipated by HLW containers into electrical power. The performed measurements allow making a first estimate of the feasibility to harvest decay heat of HLW containers under very low temperature gradients as expected in a disposal situation after 100 years of interim storage. Conservative performance analyses were conducted under the assumptions that the TEH is situated in a single EBS component, and that the overall heat flow in the disposal cell is not altered. A better overall performance can be achieved when less restrictive design criteria are applied (compare with Chapter 7), or the TEH is placed in the supercontainer buffer or Boom Clay. Nevertheless, it could be shown that the considered TEH designs are able to provide power of a relevant period of time.

As part of the Carnot cycle, the efficiency of the TEG decreases linearly with the temperature gradient, and is generally low for the gradient range of interest (<2 ˚C). Together with the quadratic relation between power and temperature gradient, this results in a strong decrease of harvestable energy at low temperature gradients, independent of the technical implementation. Further losses take place due to the conversion losses in the TEH, the TEG, and the harvester electronics.

The quantitative outcomes showed that temperature gradient of less than 0.5 ˚C can be harvested, and converted to about 10 µW of electrical power. Limiting factors are the minimum input voltage of the harvester electronics, its efficiency and self-power consumption. Both might be improved in future, however, the strong decrease of the harvestable heat will be a limiting factor when it comes to gradients below 0.5 ˚C.

Efficient conversion and storage of energy harvested at low gradients (one to several hundred µW) can provide reasonable amounts of energy to WSUs with a low duty cycle in case these can be efficiently shut down, i.e. have very low quiescence currents when sleeping. The decrease in output power results in longer intervals between measurement cycles, but this might not be a problem for monitoring parameters that evolves only very slowly a few decades after disposal.

Further research is needed when it comes to qualifying the used materials and components with respect to long-term reliability and moderate radiation field as present in the considered disposal situation. Furthermore, since a combination of a TEG and EMD has been successfully assembled and tested in the test bench, and parameters affecting its efficiency have been determined, several options have been identified to improve the overall efficiency, e.g. the development of EMDs with lower power leaking and/or higher conversion efficiency. However, since improvement of one performance parameter is likely to result in a lower performance of others, the specific needs and requirements of a particular WSU need

Modern2020 D3.3: Long-term power supply sources for repository monitoring
Dissemination level: PU
Date of issue of this report: **31/05/2019**

Page 25
© Modern2020

to be known when designing a TEH for a disposal system as well as the thermal conditions at the location of interest.

In general, the results of this study show the principal feasibility to used decay heat of HLW containers to supply reasonable amounts of power to repository monitoring WSUs.

The novelty issue in project Modern2020 was applying TEHs close to HLW containers, exposed thus to relatively low temperature gradients. This powering concept was proven feasible by numerical modelling of the temperature gradients and testing integrated TEH prototypes in a laboratory test bench that emulated the estimated temperature gradients in the target operation environment. Thus, the TRL achieved in project Modern2020 is 4 - 5.

Modern2020 D3.3: Long-term power supply sources for repository monitoring
Dissemination level: PU
Date of issue of this report: 31/05/2019

Page 26
© Modern2020

6. Wireless energy transfer

6.1 Introduction

Chapter 6 of this report deals with the wireless energy transfer by inductive coupling between loop antennas. For this, two different pilot systems were constructed and evaluated:

- wireless energy transfer arrangement for powering of a repository monitoring sensor according to Figure 4-2 through high electrical conductivity host rock,

- wireless energy transfer arrangement with communication add-on for powering of, reading telemetry data from and sending telecommands to a repository monitoring sensor according to Figure 4-3 through host rocks with low electrical conductivity.

On the following pages, Chapter 6.2 summarises the methods and the results of a generic feasibility analysis and performance estimation of inductive energy transfer systems without medium interaction. The purpose of this inspection is to highlight principal features of the inductive energy transfer, to set a baseline to the target power transfer performance, and to improve the understanding of the relation between the performance and the design parameters. Chapter 6.3 presents the set-up description and the measurement results of a pilot system according to Figure 4-3 through host rocks with low electrical conductivity, and the comparison of the results with performance estimations without medium interaction. Chapter 6.4 presents principal considerations on the effect of the medium conductivity in inductive energy transfer systems, and the results of the field measurements above an electrical conductive subsurface. Finally, Chapter 6.5 presents the overall conclusions from the theoretical studies and both pilot systems.

Beyond the current state-of-the-art of the wireless energy transfer by inductive coupling, the report addresses following aspects:

- applying the existing theory to long wireless distances (10 m or more) with relatively low operation frequencies to enable the field propagation through repository barriers,
- experimental demonstrations of the previous,
- effects of conductive medium (repository barriers) to the behaviour and performance by theoretical analysis and experimental demonstrators,
- implementation of a bi-directional data transfer add-on without compromising the power transfer performance.

6.2 Feasibility analysis without medium interaction

6.2.1 System model

The feasibility analysis is based on a simplified system model in Figure 6-1 that presents a diagram of a typical inductive energy transfer system with operating range longer than the antenna dimensions (long-range inductive energy transfer system). The left side of the figure represents the RF power transmitter in parallel with (Figure 4-2) or in (Figure 4-3) the repository external reader unit. The right side of Figure 6-1 represents the wireless RF power receiver in the wireless sensor unit (WSU), located behind a geological or engineered barrier.

In the system model (Figure 6-1), the antennas are modelled by their lumped circuit parameters L_{TX} (power transmitter antenna inductance), L_{RX} (power receiver antenna inductance), R_{TX} (equivalent serial resistance modelling power loss in the transmitter antenna), R_{RX} (equivalent serial resistance modelling power loss in the receiver antenna), and M (mutual inductance between the antennas) for the characterization of the inductive coupling between the antennas. In the power transmitter, there are also an RF inverter producing RF power (P_{INV}) from the DC supply power (P_0) and a transmitter antenna tuning circuit. The power receiver on the right side of Figure 6-1 features a parallel tuning capacitor (C_2), an RF rectifier producing DC power (P_{L_DC}) from the received RF power (P_{L_AC}), and a DC load resistance that

Modern2020 D3.3: Long-term power supply sources for repository monitoring
Dissemination level: PU
Date of issue of this report: 31/05/2019

Page 27
© Modern2020

represents the electric load connected to the power receiver (the energy management and the power consuming blocks in Figure 4-2 and in Figure 4-3).
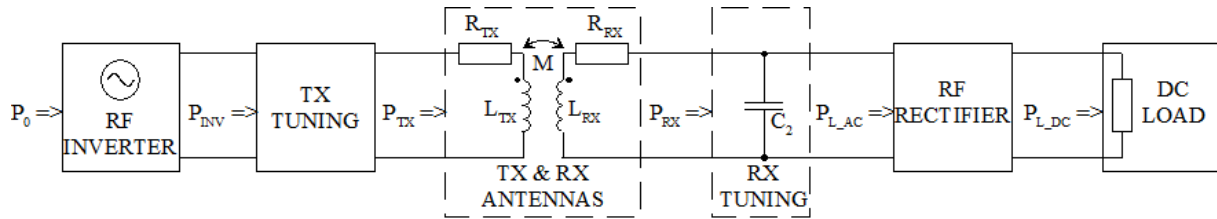
Figure 6-1. Block diagram of an inductive power transfer system with parallel tuned power receiver.

6.2.2 Power transfer efficiency

By assuming the tuning components lossless, the total power transfer efficiency for the given system is $\eta_{TOT} = \eta_{INV} \cdot \eta_{LINK} \cdot \eta_{REC}$, where $\eta_{INV} = P_{INV} / P_0$ is the RF inverter efficiency, $\eta_{LINK} = P_{RX} / P_{TX}$ is the link efficiency, and $\eta_{REC} = P_{L\_DC} / P_{L\_AC}$ is the RF rectifier efficiency. In a long-range inductive energy transfer systems the total DC-to-DC power transfer efficiency is dominated by the link efficiency η_{LINK}. For the theoretical estimation of the link efficiency, the antennas and their coupling can be characterized by the following parameters (f is the carrier frequency):

- coupling coefficient between the antennas: $k = \dfrac{M}{\sqrt{L_{TX}L_{RX}}}$,   (6-1)

- transmitter antenna Q-factor: $Q_{TX} = \dfrac{2\pi f L_{TX}}{R_{TX}}$,   (6-2)

- receiver antenna Q-factor: $Q_{RX} = \dfrac{2\pi f L_{RX}}{R_{RX}}$.   (6-3)

Maximising the theoretical link efficiency requires proper receiver antenna tuning and mutual matching of the load impedance and the receiver antenna inductance. In addition, the tuning and the impedance matching of the transmitter antenna is required for minimising the losses of the RF inverter and for adjusting the transmitted RF-power. By electrical network analysis, the following equation for the maximum theoretical link efficiency of long-range ($k^2Q_{TX}Q_{RX} \ll 1$) inductive energy transfer systems according to Figure 6-1 can be derived [5]:

- $\eta_{LINK\_MAX} = \dfrac{k^2 Q_{TX}Q_{RX}}{\left(1+\sqrt{k^2Q_{TX}Q_{RX}+1}\right)^2} \approx \dfrac{k^2 Q_{TX}Q_{RX}}{4}$.   (6-4)

The maximum link efficiency according to the previous equation with a specific receiver load requires tuning and matching of the receiver by applying the optimal values of L_{RX} and C_2 according to the following equations:

- $L_{RX\_OPT} = \dfrac{Q_{RX}\sqrt{k^2Q_{TX}Q_{RX}+1}}{2\pi f\left(k^2Q_{TX}Q_{RX}+Q_{RX}^2+1\right)}R_{L\_AC} \approx \dfrac{Q_{RX}}{2\pi f\left(Q_{RX}^2+1\right)}R_{L\_AC}$, and   (6-5)

- $C_{2\_OPT} = \dfrac{Q_{RX}^2}{(2\pi f)^2 L_{RX\_OPT}\left(k^2Q_{TX}Q_{RX}+Q_{RX}^2+1\right)} \approx \dfrac{Q_{RX}^2}{(2\pi f)^2 L_{RX\_OPT}\left(Q_{RX}^2+1\right)}$,   (6-6)

where f is the carrier frequency and R_{L_AC} is the equivalent AC load resistance comprised by the rectifier and the DC load in Figure 6-1.

In addition to charging the energy storage, the received DC power P_{L_DC} has to cover the self-discharge of the energy storage, the self-power consumption of the energy management and the sleep mode current of the sensor and communication payload that typically are totally a few microwatts or more. For this reason, 10 μW is considered as the minimum reasonable received DC power level.

Chapters 6.2.3 and 6.2.4 describe two different methods for defining the coupling coefficient k used for the estimation of the link efficiency by the previous equations. The first method is based on a rough approximation of the coupling coefficient from the antenna dimensions without applying the antenna

Modern2020 D3.3: Long-term power supply sources for repository monitoring
Dissemination level: PU
Date of issue of this report: 31/05/2019

Page 28
© Modern2020

self-inductances. The second method is based on the calculation of the coupling coefficient via the mutual inductance, requiring also the antenna self-inductances.

6.2.3 Maximum link efficiency by coupling coefficient approximation

In the case of two co-axial antennas with negligible effect of the intermediate and surrounding materials to the magnetic field, the coupling coefficient can be roughly estimated from the antenna diameters and the distance between the antennas as follows [6]:

$$- \quad k \approx \left(\frac{D_{TX} D_{RX}}{4x^2 + D_{TX}{}^2} \right)^{\frac{3}{2}}, \qquad\qquad (6\text{-}7)$$

where D_{TX} is the transmitter antenna diameter, D_{RX} (assumed to be smaller than D_{TX}) is the receiver antenna diameter, and x is the axial distance between the antennas.

After estimating the coupling coefficient by the previous equation, the maximum link efficiency can be estimated by applying Equation 6-4 with antenna Q-factors Q_{TX} and Q_{RX} that are measured from antenna prototypes in the final operation environment, estimated by simulations or pre-set as target values based on earlier experience of similar antennas.

6.2.4 Maximum link efficiency by mutual inductance calculation

In the case of two co-axial antennas without negligible effect of the intermediate and surrounding materials to the magnetic field and the power receiver antenna diameter remarkably smaller than the power transmitter antenna diameter (see also Figure 6-16), the mutual inductance can be estimated from the diameters of and the wireless distance between the antennas as follows [6]:

$$- \quad M = \frac{\mu_0 \pi N_{TX} N_{RX} D_{TX}{}^2 D_{RX}{}^2}{4\left(4x^2 + D_{TX}{}^2\right)^{3/2}}, \qquad\qquad (6\text{-}8)$$

where, in addition to the symbols in Chapter 6.2.3, μ_0 is the permeability constant, and N_{TX} and N_{RX} are the number of turns of the transmitter antenna and the receiver antenna, respectively. By applying Equation 6-1 with antenna self-inductances that are measured in the final operation environment, the coupling coefficient between the antennas can be calculated from the mutual inductance. The antenna self-inductances can also be estimated by simulations or by existing engineering formulas such as those in [7]. The theoretical link efficiency can again be calculated by applying Equation 6-4 as described in Chapter 6.2.3.

6.2.5 Results and discussion

Table 6-1 presents some sample calculation results of the DC-to-DC power transfer efficiency and the received DC power with optimal tuning and load matching of the receiver giving the maximum link efficiency. The coupling coefficient approximation method described in Chapter 6.2.3 is applied with three transmitter antenna diameters and three wireless distances.

Modern2020 D3.3: Long-term power supply sources for repository monitoring
Dissemination level: PU
Date of issue of this report: 31/05/2019

Page 29
© Modern2020

Table 6-1. Calculated power transfer performance with different power transmitter antenna diameters (D_{TX}) and axial distances between the antennas (x). The receiver antenna diameter (D_{RX}) is 150 mm and the transmitter DC supply power (P_0) 100 W. Other parameters are set as target values as follows: Q_{TX} = 50, Q_{RX} = 50, η_{INV} = 0.95, η_{REC} = 0.9.

Power transmitter antenna diameter	Axial distance between the antennas	Calculated coupling coefficient k [ppm]	Calculated max. DC-to-DC power transfer efficiency η_{TOT_MAX} [ppm]	Calculated max. received power $P_{L\_DC\_MAX}$ [µW]
1 m	5 m	57.2	1.75	175
1 m	10 m	7.2	0.028	2.8
1 m	20 m	0.9	0.0004	0.04
2 m	5 m	154.9	12.83	1283
2 m	10 m	20.2	0.22	22
2 m	20 m	2.6	0.0035	0.35
4 m	5 m	372.0	73.94	7394
4 m	10 m	54.8	1.60	160
4 m	20 m	7.2	0.027	2.7

The calculations in Table 6-1 were done for a coaxial alignment of the antennas and with assuming no attenuation by the intermediate materials such as rock or repository plug. Even though these may cause some signal attenuation, the calculation results in Table 6-1 indicate that transferring wirelessly a reasonable power level (10 µW or more as stated in Chapter 6.2.2) over 10 meters distance is possible. This requires e.g. a transmitter antenna diameter of 2 m or more, a receiver antenna diameter of 0.15 m or more, and a transmitter power level of 100 W or more. Increasing the received power via improved link efficiency is possible by raising these design parameters, especially the receiver antenna diameter. The received power can also be increased by raising the transmitter power level, but this is limited by the fact that the transmitter antenna dissipates a big majority of the RF power generated by the inverter (P_{INV}), which can cause overheating of the transmitter antenna.

Additional estimation results of the power transfer performance by the methods presented in Chapters 6.2.3 and 6.2.4 and their comparison to the measurement results by the pilot system are presented in Chapter 6.3.4 (Table 6-4). The potential influence of electric conducting media are discussed in Chapter 6.4.

6.3 Wireless energy transfer pilot with communication add-on through low electric conductivity host rock

6.3.1 Pilot system description

For the verification and performance evaluation of the wireless energy transfer through low electric conductivity host rock (bedrock), a pilot system according to Figure 6-2 was designed and prototyped by VTT Technical Research Centre of Finland Ltd. In addition to the wireless energy transfer, the system features wireless data uplink for reading telemetry data messages from the sensor and wireless data downlink for sending telecommand messages to the sensor ("all wireless in one"). The operation of the wireless interface between the reader and the sensor is based on inductive coupling between the antennas and 125 kHz carrier frequency. The data modulation method (both data uplink and downlink) is carrier on/off keying (OOK). TDM (time division multiplexing) scheme between the powering, data uplink and data downlink is applied, for which the sensor electronics involves an energy storage (e.g. a capacitor or a rechargeable battery) with associated control circuits (energy management) for accumulating energy during powering periods, during which the sensor and communication payload are held in the sleep mode.
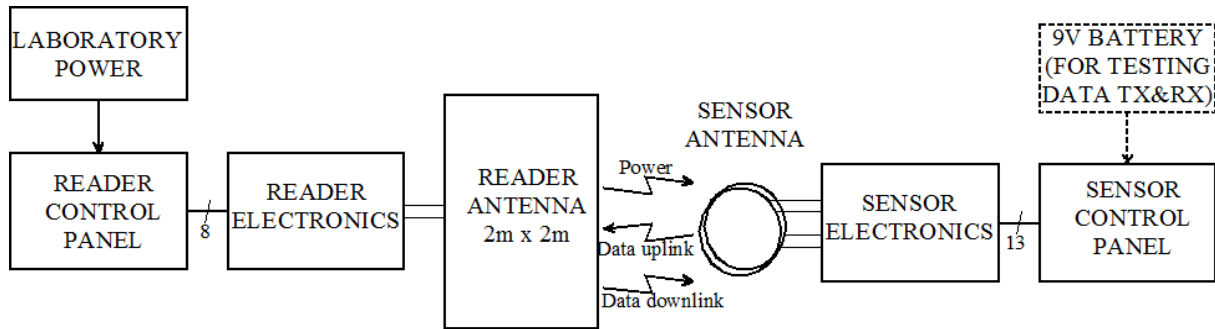
Figure 6-2. Modern2020 pilot system for evaluating wireless energy transfer through bedrock.

Figure 6-3 presents the internal structure of the reader electronics and the reader antenna (L_{TX}). The reader part features one shared antenna coil for power transmission, data uplink and data downlink. The reader electronics involves an RF inverter and reader antenna tuning capacitors (C_{1S} and optional C_{1P}). In addition, the reader electronics involves the circuits for uplink data demodulation and downlink data modulation.
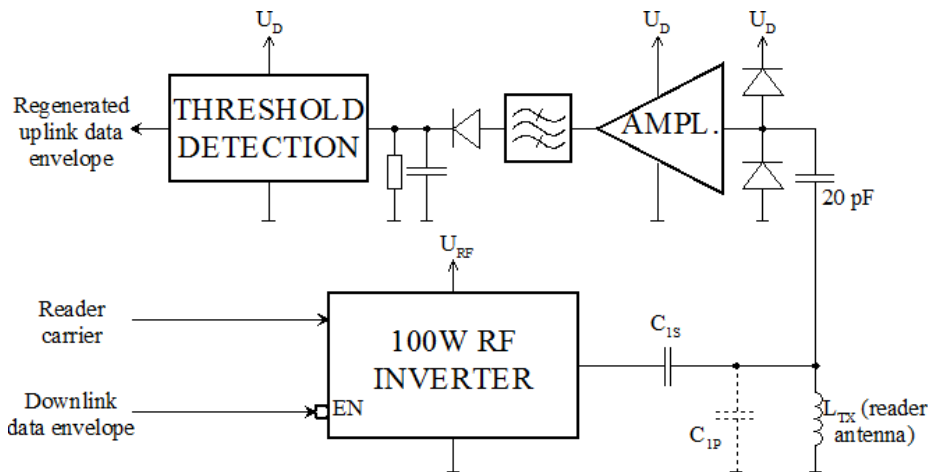
Figure 6-3. Block diagram of the reader electronics.

Figure 6-4 presents the sensor antenna coils and the internal structure of the sensor power reception path. The sensor part involves a shared antenna coil (L_{RX}) for the power reception and the data downlink and a separate antenna coil (L_{S_DU}) for data uplink. To improve the Q-factors of the antenna coils, both antenna coils are wound by Litz wire. With wireless distances substantially below 10 m, L_{S_DU} is not necessary, and the shared antenna coil L_{RX} can be applied to the data uplink, too. The power reception path involves embedded switches for controlling its operation states according to the table in Figure 6-4. The power reception path also involves tuning capacitors of the antenna coils (C_2, C_{2S_DU} and C_{2P_DU}), a rectifier, an energy storage capacitor (C_E), and interfaces to the data modulation and data demodulation circuits. In addition, the sensor electronics involves circuits for uplink data modulation and downlink data demodulation that are not included in Figure 6-4.

Modern2020 D3.3: Long-term power supply sources for repository monitoring
Dissemination level: PU
Date of issue of this report: 31/05/2019

Page 31
© Modern2020

Operation state	S1	S2	S3	S4	S5	S6
Sleep (EH)	C	C	C	O	O	O
Active	C	C	C	O	C	O
Uplink	O	O	O/C	O	C	C
Downlink	C	C	O	C	C	O
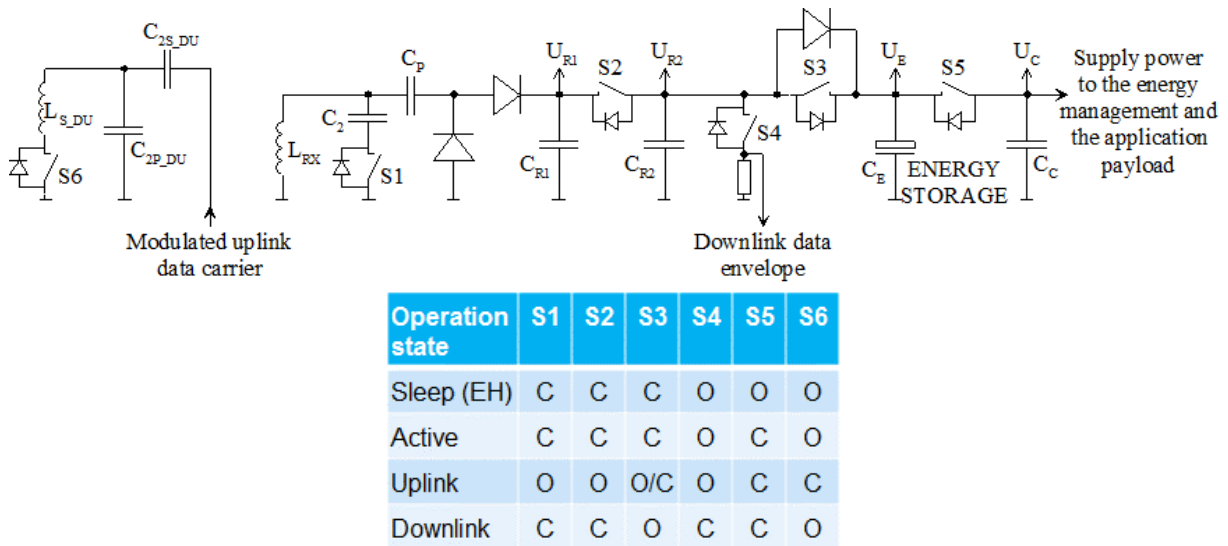
Figure 6-4. Block diagram and operation states of the power reception path in the sensor electronics (C = closed, O = open, EH = energy harvesting).

The pilot system also involves separate control panels for both the reader electronics and the sensor electronics for their manual control and monitoring. The control panels will later be replaced by microcontroller boards running the powering and communication protocol SW. The microcontroller board at the sensor end will also run the sensor payload driver SW or alternatively the driver SW for a separate sensor unit. The reader electronics and its control panel are powered by a laboratory power supply. The sensor electronics and its control panel can alternatively to the energy storage be powered by an external battery during testing the data uplink and data downlink.

Each of the four electronics units (reader electronics, sensor electronics and both control panels) are implemented by one separate customized PCB (printed circuit board) of the same size. Each PCB is encapsulated by a commercial off-the-shelf plastic box. Photos of the pilot system are in Figure 6-5 (the reader) and Figure 6-6 (the sensor).

Modern2020 D3.3: Long-term power supply sources for repository monitoring
Dissemination level: PU
Date of issue of this report: 31/05/2019

Page 32
© Modern2020
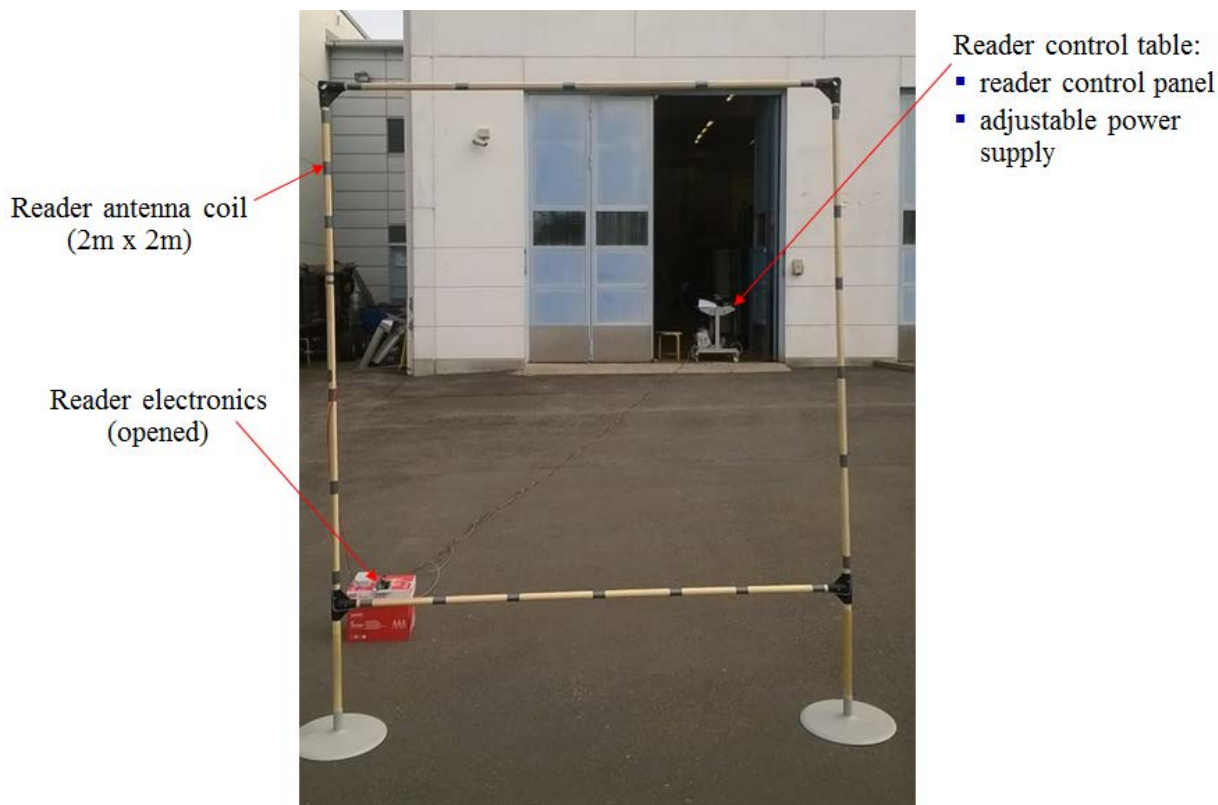
Figure 6-5. The reader part of the pilot system.

Figure 6-6. The sensor part of the pilot system.

Figure 6-7 presents the entire pilot system in two possible antenna configurations. The co-axial antenna configuration (left) can be applied e.g. for wireless interconnection through the repository plug or through the wall between the repository and an adjacent maintenance tunnel. The co-planar antenna configuration (right) provides shorter operation range but can be also applied e.g. around the repository plug if the plug contains metallic enforcements that prevents the operation through the plug.

Modern2020 D3.3: Long-term power supply sources for repository monitoring
Dissemination level: PU
Date of issue of this report: 31/05/2019

Page 33
© Modern2020

Figure 6-7. The pilot system in co-axial antenna configuration (left) and co-planar antenna configuration (right) through the air at VTT premises in Oulu, Finland.

6.3.2 Test set-up

The wireless energy and data transfer performance of the pilot system was first tested in co-axial antenna configuration (Figure 6-7 left) through the air at 10 m wireless distance. The tests were carried out outdoors at VTT premises in Oulu, Finland. The test results are presented in Chapter 6.3.3.

The wireless energy and data transfer performance of the pilot system was also tested in co-axial antenna configuration through the bedrock. The tests were carried out in the bedrock cave of the VTT Otaniemi premises in Espoo, Finland (Figure 6-8). The total distance between the antennas was about 8 m, 7 m of which was comprised of rock. There were some metallic structures close to the antennas such as the staircase close to the reader antenna and a big metallic box close to the sensor antenna. These are also visible in the photos of the reader antenna and the sensor in Figure 6-9. The test results are presented in Chapter 6.3.4.
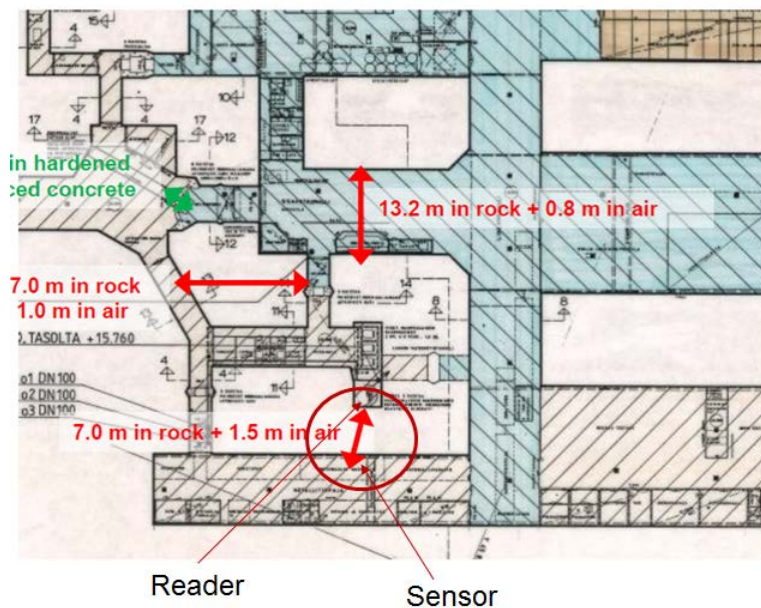
Figure 6-8. The bedrock cave in the Otaniemi premises of VTT (Kemistintie 3, Espoo, Finland).

Modern2020 D3.3: Long-term power supply sources for repository monitoring
Dissemination level: PU
Date of issue of this report: 31/05/2019

Page 34
© Modern2020

Figure 6-9. The pilot system in co-axial antenna configuration in the bedrock cave at VTT Otaniemi. The leftmost photo presents the reader antenna and the rightmost photo the sensor part.

6.3.3 Test results through the air

Table 6-2 presents the test results of the DC-to-DC wireless energy transfer with co-axial antenna configuration through the air (Figure 6-7 left) at 10 m wireless distance. The transmitted power level from the reader was adjusted via the inverter (RF) supply voltage and measured via its supply current. In this way, the DC supply power of the inverter was set to 100 W. The power was received to a DC load resistor (R_{L_DC}) connected to the RF rectifier output, the voltage over which was measured by a DC voltage meter. The test was repeated with a few DC load resistor values. The DC-to-DC power transfer efficiency was calculated from the measurement results.

Table 6-2. Wireless energy transfer measurement results through the air by the pilot system with co-axial antenna configuration and 10 m wireless distance.

Test settings		Measurement results		Calculated DC-to-DC efficiency		
Total DC load R_{L_DC} [MΩ]	RF supply voltage URFIN [V_{DC}]	RF supply current [A_{DC}]	DC load voltage U_{L_DC} [V_{DC}]	Transmitter RF supply power [W]	Receiver load power P_{L_DC} [µW]	DC/DC-efficiency [ppm]
10.00	29.4	3.41	16.14	100.3	26.0	0.260
5.00	29.4	3.41	14.62	100.3	42.7	0.426
3.33	29.4	3.41	12.75	100.3	48.8	0.487
2.50	29.4	3.41	11.24	100.3	50.5	0.504
2.00	29.4	3.41	9.98	100.3	49.8	0.497
1.67	29.4	3.41	8.93	100.3	47.8	0.476

Figure 6-10 and Figure 6-11 present measured signal graphs of the data downlink and the data uplink through the air with co-axial antenna configuration and 10 m wireless distance. In the data downlink, the unmodulated carrier power level was the same as in the energy transfer, corresponding 100 W inverter DC supply power. In the data uplink, the unmodulated carrier power level was about 100 mW. A 110 Hz square wave was used as a test modulation envelope in both data uplink and data downlink.

Modern2020 D3.3: Long-term power supply sources for repository monitoring
Dissemination level: PU
Date of issue of this report: 31/05/2019

Page 35
© Modern2020
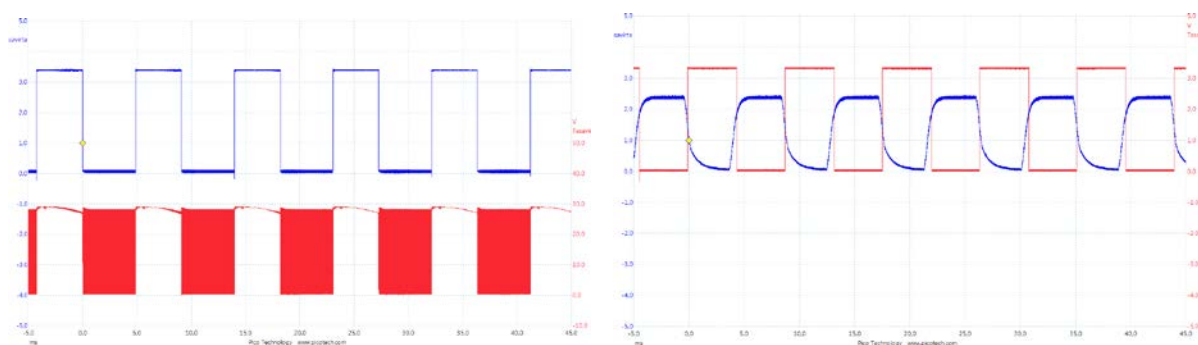
Figure 6-10. Oscilloscope graphs of the data downlink through the air by the pilot system with co-axial antenna configuration and 10 m wireless distance. The leftmost graph presents the transmitted downlink modulation envelope (blue) and the antenna signal (red) in the reader part. The rightmost graph presents the received rectified antenna signal (blue) and the regenerated downlink modulation envelope (red) in the sensor part.
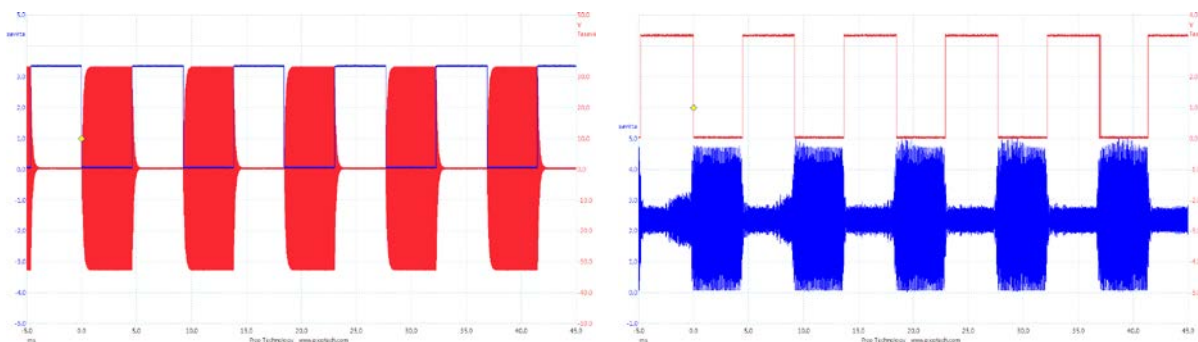
Figure 6-11. Oscilloscope graphs of the data uplink through the air by the pilot system with co-axial antenna configuration and 10 m wireless distance. The leftmost graph presents the transmitted uplink modulation envelope (blue) and the antenna signal (red) in the sensor part. The rightmost graph presents the received antenna signal (blue) and the regenerated uplink modulation envelope (red) in the reader part.

6.3.4 Measurement results through the rock

Table 6-3, Figure 6-12 and Figure 6-13 present the corresponding measurement results of the wireless energy transfer, data downlink and data uplink in the bedrock cave at VTT Otaniemi. The medium between the antennas was comprised of about 7 m thick rock and 1 m thick air. Because of the shorter distance between the antennas than in the tests through the air, the DC supply power of the inverter was decreased to 25 W. The nearby rock and metallic structures caused minor changes to the antenna self-parameters, which were compensated by re-tuning the antennas slightly. Otherwise, the test were made similarly to those reported in Chapter 6.3.3.

Modern2020 D3.3: Long-term power supply sources for repository monitoring
Dissemination level: PU
Date of issue of this report: 31/05/2019

Page 36
© Modern2020

Table 6-3. Wireless energy transfer measurement results through the rock (about 7 m rock plus 1 m air) by the pilot system with co-axial antenna configuration.

Test settings		Measurement results		Calculated DC-to-DC efficiency		
Total DC load R_{L_DC} [MΩ]	RF supply voltage URFIN [V_{DC}]	RF supply current [A_{DC}]	DC load voltage U_{L_DC} [V_{DC}]	Transmitter RF supply power [W]	Receiver DC power P_{L_DC} [μW]	DC/DC-efficiency [ppm]
10.00	15.7	1.59	26.07	25.0	68.0	2.723
5.00	15.7	1.59	19.92	25.0	79.4	3.179
3.33	15.7	1.59	16.23	25.0	79.0	3.166
2.50	15.7	1.59	13.70	25.0	75.1	3.007
2.00	15.7	1.59	11.86	25.0	70.3	2.817
1.67	15.7	1.59	10.44	25.0	65.4	2.620
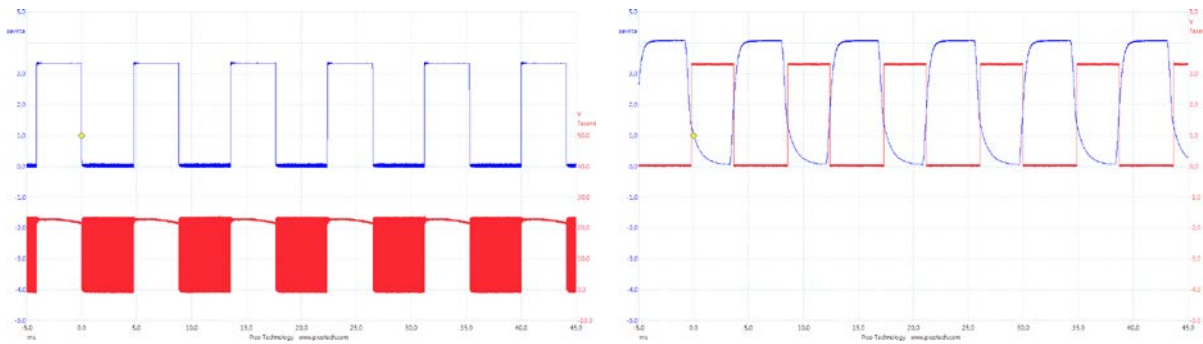
Figure 6-12. Oscilloscope graphs of the data downlink through the rock (about 7 m rock plus 1 m air) by the pilot system with co-axial antenna configuration. The leftmost graph presents the transmitted downlink modulation envelope (blue) and the antenna signal (red) in the reader part. The rightmost graph presents the received rectified antenna signal (blue) and the regenerated downlink modulation envelope (red) in the sensor part.
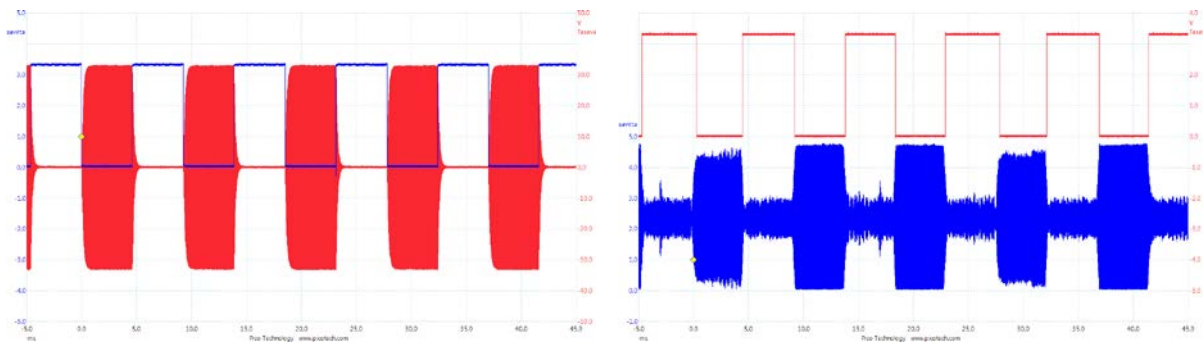
Figure 6-13. Oscilloscope graphs of the data uplink through the rock (about 7 m rock plus 1 m air) by the pilot system with co-axial antenna configuration. The leftmost graph presents the transmitted uplink modulation envelope (blue) and the antenna signal (red) in the sensor part. The rightmost graph presents the received antenna signal (blue) and the regenerated uplink modulation envelope (red) in the reader part. Some disturbances in the regenerated modulation envelope caused by nearby electric devices were occasionally observed.

Table 6-4 summarizes the energy transfer performance figures estimated by the methods in Chapters 6.2.3 and 6.2.4, and measured by the pilot system. The estimations were based on the antenna coil parameters measured from the prototypes in open space.

- power transmitter (reader) antenna: L_{TX} = 0.146 mH, Q_{TX} = 71.4, D_{TX} = 2.26 m, N_{TX} = 4,

Modern2020 D3.3: Long-term power supply sources for repository monitoring
Dissemination level: PU
Date of issue of this report: 31/05/2019

Page 37
© Modern2020

- power receiver (sensor) antenna: L_{RX} = 6.28 mH, Q_{RX} = 105, D_{RX} = 0.168 m, N_{RX} = 256.

Table 6-4. Measured vs. estimated power transfer performance.

Measured vs. estimated power transfer performance	Estimated by approximated coupling coefficient and measured antenna Q-factors		Estimated by calculated mutual inductance and measured antenna inductances and Q-factors		Measured with optimal load resistor at the receiver output	
Medium	10 m air	~7 m rock + ~1 m air	10 m air	~7 m rock + ~1 m air	10 m air	~7 m rock + ~1 m air
Transmitted DC power	100.3 W	25 W	100.3 W	25 W	100.3 W	25 W
Received DC power	132 µW	123 µW	56 µW	52 µW	50.5 µW	79.4 µW
DC-to-DC efficiency	1.32 ppm	4.93 ppm	0.56 ppm	2.08 ppm	0.504 ppm	3.18 ppm

6.3.5 Assessment of the human safety

Any RF device will expose nearby humans to RF radiation that can be harmful to the health. In the EU, the occupational RF exposures are regulated by the directive 2013/35/EU in which the exposure limits are derived from the ICNIRP (International Commission on Non-Ionizing Radiation Protection) Guidelines 1998.

The directive 2013/35/EU defines two procedures to show the compliance of an RF device with the exposure regulations. In the simplified procedure, the compliance is proven by the measurements, simulations or calculations of the electromagnetic field strength that has to be below the given action level (AL) value. The action level value for 125 kHz magnetic fields is 16 µT for thermal effects caused by the tissue heating through energy absorption from electromagnetic fields in the tissue, and 100 µT for non-thermal effects such as the stimulation of muscles, nerves or sensory organs. Another method is based on the exposure limit value (ELV) by SAR (specific absorption rate) analysis and requires more complicated assessment in practice. The AL value results in a conservative exposure assessment and automatic compliance with ELVs in all non-uniform exposure conditions.

Calculating the current in and the magnetic field around the transmitter antenna of the pilot system with 100 W transmitter power and comparing the field strength to the lower AL value above (16 µT) results to the fact that staying at least 2 m away from the transmitter antenna is safe. This is a rather conservative result. Closer distances are also possible but if they are necessary, closer analysis is required.

6.3.6 Conclusions

Wireless inductive energy transfer by using LF frequencies such as 125 kHz is a valid concept for powering repository-monitoring sensors through bedrock. The field attenuation caused by 7 m thick bedrock wall is minor and lower than the measurement accuracy of the pilot test set-up in general. Thus, the theoretical feasibility analysis methods for estimating the wireless energy transfer performance through the air in Chapters 6.2.3 and 6.2.4 are also valid for estimating the performance and its sensitivity to the design parameters such as the antenna dimensions and the distance between the antennas through the bedrock.

The reader part (power transmitter) of the pilot system with 100 W DC supply power was able to deliver slightly over 50 µW DC power to the sensor part (power receiver) at 10 m distance from the reader part. Higher power levels are also possible by the following design modifications:

- applying shorter wireless distance than 10 m,
- increasing the diameter of the sensor antenna (outer diameter 180 mm and mean diameter of the winding 168 mm in the tested set-up),
- increasing the size of the reader antenna (2 m x 2 m in the tested set-up),

Modern2020 D3.3: Long-term power supply sources for repository monitoring
Dissemination level: PU
Date of issue of this report: 31/05/2019

Page 38
© Modern2020

- increasing the antenna Q-factors (the reader antenna Q-factor 71.4 and the sensor antenna Q-factor 105 in the tested set-up), e.g. by using Litz wire also in the reader antenna, which however will make the antennas more prone to detuning,
- increasing the reader power level, which however is limited e.g. by the heating of the antenna coil.

More detailed energy transfer performance figures by the feasibility analysis and by the pilot system measurements are summarised in Table 6-4 above. The pilot system gave 50.5 μW received DC power by a 100 W power transmitter at 10 m distance through the air, and 79.4 μW by a 25 W power transmitter at about 8 m distance mainly through the bedrock. The former of the previous figures is rather close to the estimated received power level by the mutual inductance calculation method (56 μW). The latter of the previous figures is higher than the estimated received power level by the mutual inductance calculation method (52 μW). The most obvious explanation for this is that the total wireless distance in the pilot test set-up was slightly shorter than the assumed 8 m used in the feasibility analysis. In fact, half a meter shorter wireless distance than the assumed 8 m would explain the deviation. The coupling coefficient approximation method gave systematically more than twice as big performance figures as the mutual inductance calculation method. Thus, the coupling coefficient approximation method will give only rough estimations of the absolute performance but is anyway useful for estimating the sensitivity of the energy transfer performance to the antenna dimensions and the wireless distance roughly.

According to Equation 6-7, the coupling coefficient is proportional to the receiver antenna diameter to the power of 3/2. This will match together with Equations 6-8 and 6-1 if the receiver antenna inductance is directly proportional to the antenna diameter. According to the inductance calculation equation for multi-turn multilayer antennas given in [7], this is a fair approximation for antennas with remarkably longer diameter than the axial length. In the case of antennas with longer axial length than the diameter, the antenna inductance according to [7] is however proportional closer to the square of the antenna diameter, and thus, contrary to Equation 6-7, the coupling coefficient according to Equations 6-8 and 6-1 is directly proportional only to the antenna diameter without any power. Thus, the applicability of the Equation 6-7 to multi-turn antennas with relatively long axial length is poor.

Based on the feasibility analysis in general, the following relations concern the diameter of the antennas and the wireless operation performance:

- the received power level is inversely proportional almost to the sixth power of the wireless distance,
- doubling the diameter of both antennas will almost double the maximum wireless distance,
- doubling the diameter of the receiver antenna only will increase the received power by 6 - 9 dB.

A bi-directional communication add-on in an inductive energy transfer system ("all wireless in one") is feasible without compromising the energy transfer performance or the wireless distance. With such a low coupling coefficient between the antennas as applied in the pilot set-up, a separate antenna coil for data uplink is necessary at the sensor end. This is for keeping the RF voltage level of the sensor antenna reasonable with a reasonable power level of the data uplink. With higher coupling coefficients (e.g. shorter operation ranges), the power receiver antenna coil may be used for data uplink, too.

Among the future development needs of the pilot system towards the final use in the repository monitoring are the following:

- power budged calculations of the monitoring application,
- antenna customisation according to the required performance and available volume in the final application environment,
- selection of the energy storage fulfilling the requirements for its capacity, self-discharge and lifetime,
- improving the noise immunity of the data uplink,
- sensor encapsulation and protection against the harsh repository environment,

Modern2020 D3.3: Long-term power supply sources for repository monitoring
Dissemination level: PU
Date of issue of this report: 31/05/2019

Page 39
© Modern2020

- verification in the entire repository environment with ambient bentonite, moisture saturation, pressure etc.,
- replacing the control panels by microcontroller boards and development of the protocol SW and the sensor application,
- integration with the repository monitoring backend system.

6.4 Wireless energy transfer trough materials with high electric conductivity

This chapter summarizes a feasibility study performed by NRG on the ability to transfer energy wirelessly through the host rock or components of the engineered barrier system (EBS) into a disposal cell by magnetic induction techniques. Much research on wireless energy transfer over short distances has been performed in the last decade, and the main concepts developed there have been shortly summarized in Chapters 6.2 and 6.3. Some research is also performed on wireless energy transfer over longer distances (larger than the loop diameter), but this work is mostly limited to transfer through air, often using high frequencies in the MHz range. The focus of this contribution is to analyse the feasibility of wireless energy transfer by magnetic induction over larger distances through saturated media such as argillaceous host rocks or (partially) saturated EBS components that can be characterized as electrical 'good conductors', and to quantify the performance and efficiency of the different subcomponents as can be expected under disposal conditions.

6.4.1 General system analysis

In Chapter 6.3, evidence is given that the general approaches for energy transfer on shorter distances as can be found in the wider literature (see Chapter 6.2) can be successfully extrapolated up to distances of around 10 m (Table 6-4). However, some technical challenges may arise from the very low efficiencies with these distances that are in the ppm range (Table 6-1).

From Equations 6-4 and 6-7 and Table 6-1 it is evident that the antennas should be as large as possible, while the open space available to deploy an antenna in a geological waste disposal presents a limiting factor in many cases. Typical dimensions of deposition tunnels and the connecting access galleries (Figure 6-14) are summarized in Appendix 2, with maximum transmitter antenna diameters ranging between 4 and 7 m, and maximum receiver antenna diameters ranging between 0.7 and 4.8 m. When transferring energy through the deposition plug, the minimum wireless distance is defined by the plug length, ranging between 6.5 and 12 m.
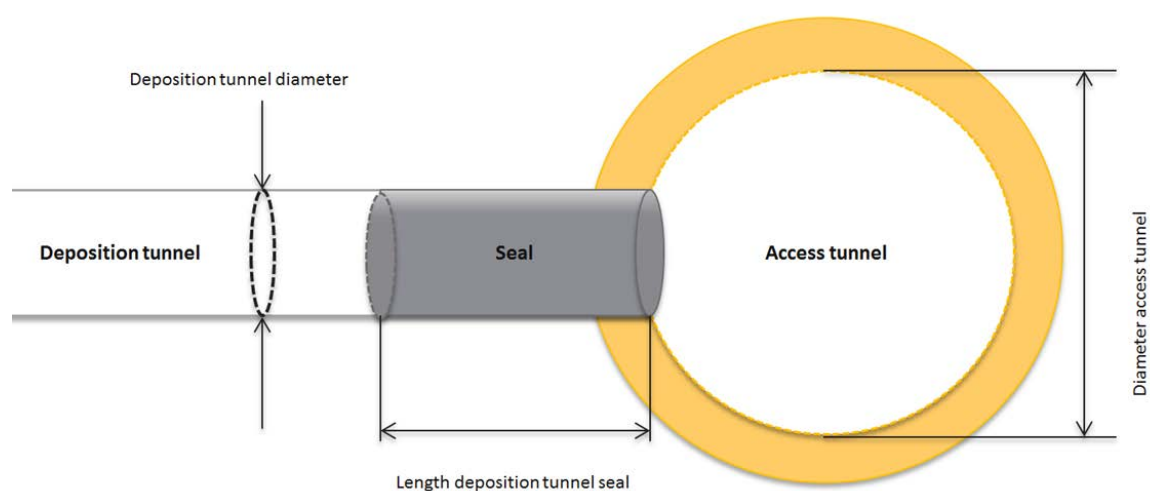
Figure 6-14. General outline of a deposition tunnel, separated by a seal from the access tunnel.

Modern2020 D3.3: Long-term power supply sources for repository monitoring
Dissemination level: PU
Date of issue of this report: 31/05/2019

Page 40
© Modern2020

The experiments summarized in the previous chapter were performed through electrical low conducting media (air and granite), which didn't show any significant effect to the magnetic field and the antenna parameters, while this chapter focus on the case of high conductive media, in which interactions cannot be neglected. To make a first judgement whether a certain pathway provides a 'high' or 'low' conductivity, the concept of *skin depth* [8], [9] can be used: the skin depths δ defines the distance at which a magnetic field is attenuated due to interactions with the medium by a factor of $1/e$, equivalent to -8.7 dB. In case of an electrical conductivity σ

$$\sigma \gg \omega \varepsilon_0 \varepsilon_r \tag{6-9}$$

with

ε_o permittivity constant ($8.9 \cdot 10^{-12}$ A$\cdot$s/V$\cdot$m)
ε_r relative permittivity [-],

the medium can be considered as a "good conductor", with the skin depth calculated by

$$\delta [m] = \sqrt{\frac{2}{\omega \mu_0 \mu_r \sigma}} \tag{6-10}$$

and

μ_o permeability constant ($1.257 \cdot 10\text{-}6$ V$\cdot$s/A$\cdot$m)
μ_r relative (magnetic) permeability [-]

In the absence of magnetic permeable materials - all analyses in this chapter are limited to that case - μ_r can be assumed to be equal to 1. Typical values for ε_r are around 3 - 40 for geological media [10], and are strongly dependent on the saturation [11]. The electrical conductivity σ of geological media can vary to a large extent, in the µS/m to mS/m range for crystalline rock, and mS/m to S/m range for argillaceous rock. The water-filled pore space of geological media or EBS components and the pore water composition can determine the overall conductivity significantly. The electric conductivity of fresh water is about 10^{-2} to 1 S/m, and the conductivity of saline water can be as high as 1 – 10 S/m. For the frequency and wireless distances of interest, argillaceous rocks with relevant water content are likely to behave as a "good conductor", while rock salt, granite or other crystalline rocks can be assumed to behave over a wide frequency range as a poor conductor. Unsaturated EBS components are expected to behave as poor conductor, while in a saturated state, the EBS may present a good conductor, dependent on the porosity and pore water composition. Table 6-5 gives an impression on the skin depth calculated for different conductivities of a medium. For wireless distances of 10 m and a conductivity of the wireless medium of 20 mS/m, as e.g. found in Boom Clay [12], interactions at 125 kHz are relevant.

Table 6-5. Skin depths as function of the electric conductivity of a medium at 125 kHz.

electric conductivity σ [S/m]	0.23	0.08	0.02	0.01
skin depth δ [m]	3	5	10	15

6.4.2   Magnetic field propagation

For a coaxial antenna configuration with a small receiver antenna, the field strength H over a distance d much smaller than the wavelength can be approximated by

$$H = \frac{IN}{2} \cdot \frac{r_{Tx}^2}{\sqrt{(r_{Tx}^2 + d^2)^3}} \tag{6-11}$$

with r_{Tx} the transmitter loop antenna's radius, I the current through the loop and N the number of turns of the antenna. In vacuum, the propagation velocity of an electro-magnetic wave is equal to the speed of light ($3 \cdot 10^8$ m/s). Under this condition, a 125 kHz-wave has a wavelength λ of 2.4 km. In water, the

propagation velocity in the near field is about nine times smaller, resulting in wavelengths of about 270 m. These wavelengths are beyond the wireless distance over which the energy transfer is anticipated (i.e. tens of meters). However, propagation of magnetic fields through electrical high conductive saturated clays, bentonites, and cementitious materials leads to secondary fields, and relevant smaller wave lengths apply. Under these conditions, strict near-field conditions do not apply.

In an infinite conducting medium, again assuming that the receiver loop diameter can be neglected, the magnetic field intensity vector $\bar{H}$ at a distance d to the antenna and at an angle θ relative to the antenna surface area can be calculated by (Eq. 84 and 85 in [13]):

$$\bar{H} = \frac{INA}{4\pi d^3} e^{-i\gamma} e^{-\gamma} \left[2 \cos \theta (1 + (1 + i)\gamma) \, \hat{d} + \sin \theta (1 + (1 + i)\gamma + 2i\gamma^2)\hat{\theta}\right] \qquad (6\text{-}12)$$

with $\gamma = d/\delta$, i the imaginary number and $\hat{d}$ and $\hat{\theta}$ the axial and radial unity vectors. For two coaxial loops ($\theta = 0$), Equation 6-12 can be simplified to the following scalar equation for the field intensity in the vertical direction:

$$H_{vertical} = \frac{INA}{2\pi d^3} e^{-i\gamma} e^{-\gamma} [1 + (1 + i)\gamma] \, . \qquad (6\text{-}13)$$

Finally, in a conducting half-space [14], magnetic field propagation can be estimated by

$$H_{radial} = \frac{INA}{2\pi d^3} T_{radial}; \quad H_{vertical} = \frac{INA}{2\pi d^3} T_{vertical} \qquad (6\text{-}14)$$

with

$$\left. \begin{matrix} T_{radial} \\ T_{vertical} \end{matrix} \right\} = \int_0^\infty \frac{x^3}{x + \sqrt{x^2 + iG^2}} \exp\left(-\sqrt{x^2 + iG^2}\right) \begin{Bmatrix} J_1(xD) \\ J_0(xD) \end{Bmatrix} dx \qquad (6\text{-}15)$$

In Equation 6-14 and Equation 6-15, J_0 and J_1 are Bessel functions of the first kind, d the axial and ρ the radial distance to the transmitter, $G = d \cdot (\sigma\mu\omega)^{1/2}$, and $D = \rho/d$. The validity of these equations is limited to the near-field, under the condition where both G and $G \cdot D \ll 1$. However, the wavelength λ may be of the same order of magnitude as the wireless distance or even smaller. Under these circumstances, near-field conditions are not valid anymore. Additional analyses are published that allow to analyse the case of a stratified medium (e.g., [14] [15]), but it should be clear that to address the geometrical complexity of a real disposal situation requires detailed numerical analyses. Nevertheless, comparing the different approximations for a simplified system representation allows to get a first insight whether signal attenuation might be a relevant factor or not, and can be helpful in establishing the target frequency range.

The equations above are valid for small receiver antenna size. For larger receiver antennas where the condition $r_{Rx}^2 \ll r_{Tx}^2 + d^2$ for the approximation in Equation 6-8 is not fulfilled, the mutual inductance of two coaxial loop antennas without interaction with the medium can be calculated by

$$M = \mu_o N_{Tx} N_{Rx} \sqrt{r_{Tx} r_{Rx}} \left[\left(\frac{2}{\vartheta} - \vartheta\right) K(\vartheta) - \frac{2}{\vartheta} E(\vartheta)\right] \qquad (6\text{-}16)$$

with

$$\vartheta = \sqrt{\frac{4 R_{Tx} R_{Rx}}{(R_{Tx} + R_{Rx})^2 + d^2}} \qquad (6\text{-}17)$$

and $K(\vartheta)$ and $E(\vartheta)$ the complete elliptical functions of the first and second order, respectively, and N_{Tx} and N_{Rx} the number of turns respectively of the transmitter and receiver coil [16]. Figure 6-15 shows an example of the strong decrease of the mutual inductances and coupling coefficients for smaller radii of the transmitter and receiver antenna coils, both normalized by the wireless distance d.

Modern2020 D3.3: Long-term power supply sources for repository monitoring
Dissemination level: PU
Date of issue of this report: 31/05/2019

Page 42
© Modern2020
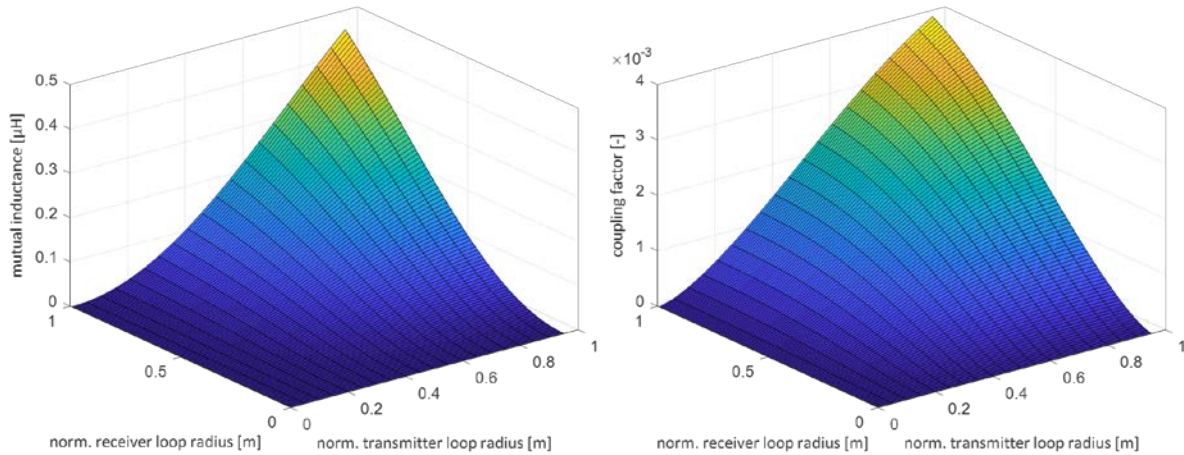
Figure 6-15. Mutual inductance (left) and coupling coefficient (right) of two coaxial, single turn coils as function of the normalized transmitter coil and receiver coil radius.

Figure 6-16 depicts a comparison of the mutual inductance calculated by Equation 6-16 or approximated by Equation 6-8. It shows that for antenna diameters smaller than the wireless distance, the approximation works well. It also shows that for wireless distances larger than the coil diameter, the mutual inductance and thus the link efficiency strongly decreases.
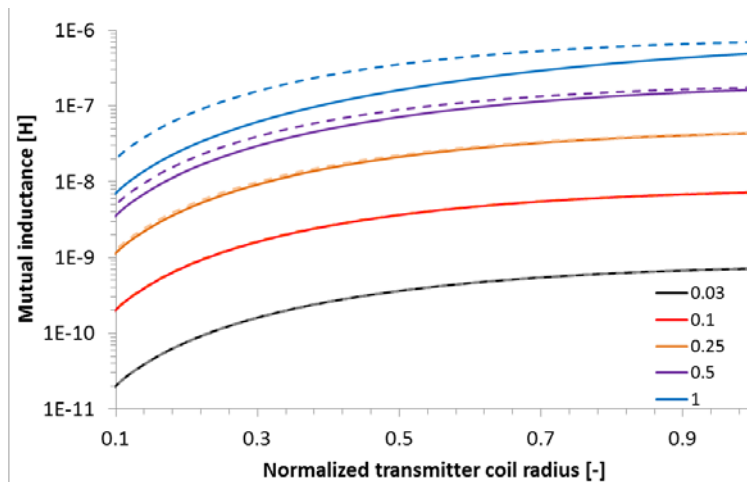
Figure 6-16. Calculated (solid line) and approximated (dashed line) mutual inductance of two coaxial, coils as function of the normalized transmitter coil radius for five normalized receiver coil radii.

6.4.3 Interactions of an antenna with its surroundings

At frequencies in the range of 125 kHz and free air conditions, the radiation resistance has little influence on the overall antenna resistance, and the antenna resistance is determined by losses due to the wire resistance. Under condition as present in many disposal situations, where EBS components as bentonite or cementitious materials get saturated, additional external losses may occur that might relevantly alter the overall antenna resistance. This eventually limits the maximum Q that can be achieved and may lead to degradation of the link efficiency η_{link}, compared to a "free air" situation as described in the previous chapter (Equation 6-4). In [17], the real part of the radiation resistance R_{rad} is estimated by

$$R_{rad} = \frac{N^2 \omega \mu}{4\pi} \iint \frac{e^{-\beta r_{12}}}{r_{12}} \sin(\beta r_{12}) cos\theta ds_1 ds_2 \qquad (6\text{-}18)$$

with

Modern2020 D3.3: Long-term power supply sources for repository monitoring
Dissemination level: PU
Date of issue of this report: **31/05/2019**

Page 43
© Modern2020

ds_1	differential element of length on the wire centre line
ds_2	differential element of length along inner surface of wire
r_{12}	distance between differential elements ds_1 and ds_2
β	$= (\omega\mu\sigma/2)^{1/2}$
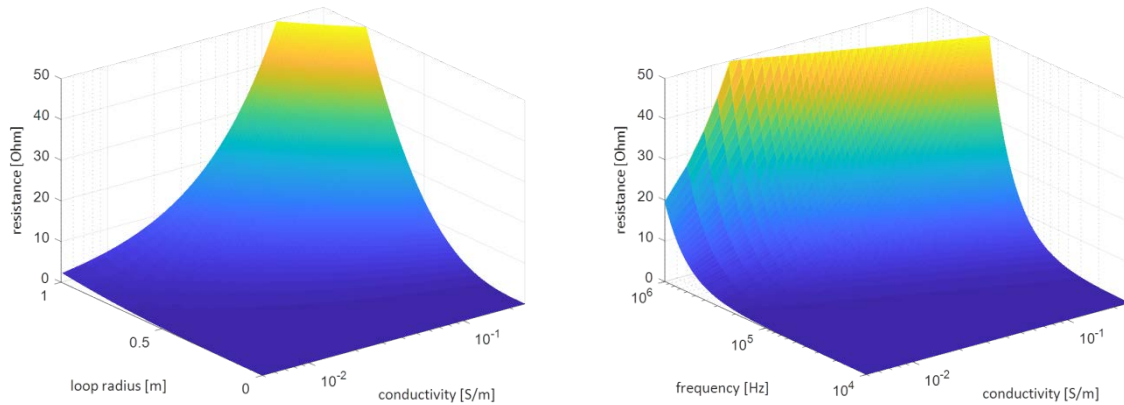
Figure 6-17. Calculated radiation resistance due to interactions with the medium of a 20-turn loop antenna as function of the electrical conductivity of the surrounding and the loop radius (left, f = 125 kHz) or the frequency (right, r_{loop} = 0.5 m).

Figure 6-17 shows that the radiation resistance is relevant in case of larger antenna diameter or higher conductivities. Comparable to the radiation resistance, the complex part of the radiation resistance, or reactance X_{rad} can be computed by

$$X_{rad} = \frac{N^2\omega\mu}{4\pi} \iint \frac{e^{-\beta r_{12}}}{r_{12}} \cos(\beta r_{12}) cos\theta ds_1 ds_2 \qquad (6\text{-}19)$$

Variations of the reactance during saturation might lead to a detuning of the antenna, consequently affecting the link efficiency. Dependent on the Q of the antenna, an adaption of the frequency or the antenna tuning might be necessary in order to avoid performance loss. However, Figure 6-18 shows a rather small effect of the conductivity for the analysed parameter ranges.
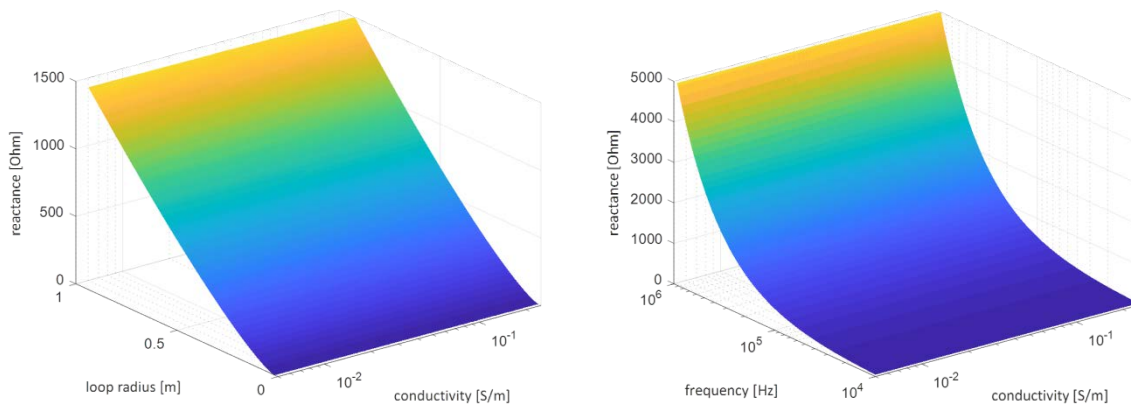
Figure 6-18. Calculated reactance due to interactions with the medium of a 20-turn loop antenna as function of the electrical conductivity of the surrounding and the loop radius (left, f = 125 kHz) or the frequency (right, r_{loop} = 0.5 m).

6.4.4 Experimental set-up

For the wireless energy transfer experiments, an experimental set-up was build, comparable to Figure 6-1, consisting of a programmable signal generator, a power inverter, a tuned transmitter antenna, a

Modern2020 D3.3: Long-term power supply sources for repository monitoring
Dissemination level: PU
Date of issue of this report: 31/05/2019

Page 44
© Modern2020

tuned receiver antenna and a load resistance (Figure 6-19). The mobile, battery powered inverter provides high currents to the inductive load of the transmitter antenna. As transmitter antenna, a 5-turn loop antenna with a radius of 2.25 m was used (L_{Tx} = 0.51 mH, R = 0.50 Ω). The receiving 20-turn loop antenna (Figure 6-21) had a radius of 0.5 m (L_{Rx} = 0.93 mH, R = 0.44 Ω). The receiver antenna was terminated by different load resistors in order to determine the optimum link efficiency.
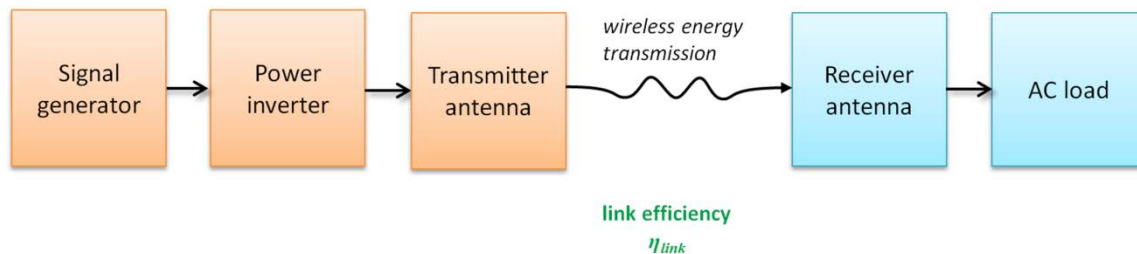
Figure 6-19. Set-up of the wireless energy transfer system.

To study the interactions with a conductive media, all wireless energy transfer experiments were performed in a coplanar configuration, with the antennas situated directly on the ground. The coplanar antenna configuration is a reasonable replacement of a coaxial configuration that allows a system evaluation of interaction with a conductive medium outside an URL facility, (see e.g. [12]). However, to compare the outcomes of a coplanar set-up with a coaxial configuration, corrections need to be made: for a small antenna, the field strength in a coplanar configuration is roughly half of the field strength of the (more favourable) coaxial configuration if the distances between the loop's centres are the same. This decreases the link efficiency of the coplanar configuration by a factor of four, i.e. a coplanar configuration with a centre-to-centre distance of 7.5 m has roughly the same link efficiency than a coaxial configuration at 10 m distance.

6.4.5 Field measurements

Several experiments were performed in order to substantiate the interactions of the antennas with the environment, as elaborated in the previous chapter. While large antennas are general favourable for high link efficiencies (see Eq. 16), it was argued in the previous chapter that a larger antenna might result in radiation resistances that limit the achievable Q-values and hence affect the overall performance. The principal effect of a conducting environment on the antenna parameter was demonstrated by measuring the receiver antenna's impedance in series with a capacitor of 1.68 nF at several heights above the surface, and directly on top of an unsaturated and an almost saturated grassland (Figure 6-20).

Figure 6-20. Field measurement of antenna impedance in a wet grassland in Ursem, NL.

Modern2020 D3.3: Long-term power supply sources for repository monitoring
Dissemination level: PU
Date of issue of this report: 31/05/2019

Page 45
© Modern2020

Figure 6-21 shows the effect of different heights and saturation degrees on the frequency dependent impedance of the loop antenna. Besides the wire resistance of 0.44 Ω, an additional resistance of 0.31 Ω was determined at the resonance frequency in the wet grassland. The effect of the conductive media is expected to be even larger when the antenna is covered on all sides.
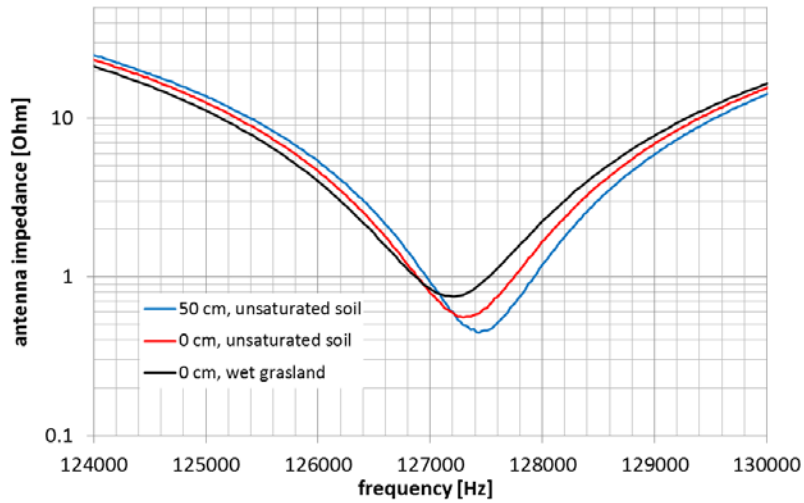
Figure 6-21. Field measurement of the receiver antenna's impedance with a 1.68 nF serial capacitor at two heights above an unsaturated soil and on top of wet grassland.

The reactance changed little, resulting in a small decrease of the antenna's resonance frequency from about 127.5 to 127.2 kHz, which is consistent with Equation 6-19 and Figure 6-18. Although the experiment did not allow to determine a precise value for the effective electrical conductivity of the antenna's surrounding, from Equation 6-19 a conductivity of about 0.02 S/m is estimated, assuming that effective conductivity seen by the antenna is half of this value.

Wireless energy transfer experiments were performed in Petten for a coplanar configuration with load resistances between 5 and 1000 kΩ. Figure 6-22 depicts the measured voltages (V_{pp}) for different load resistances and wireless distances of a receiver coil located on top of an unsaturated sandy soil. It shows that the voltage decreases with increasing the wireless distance and decreasing the load resistance.
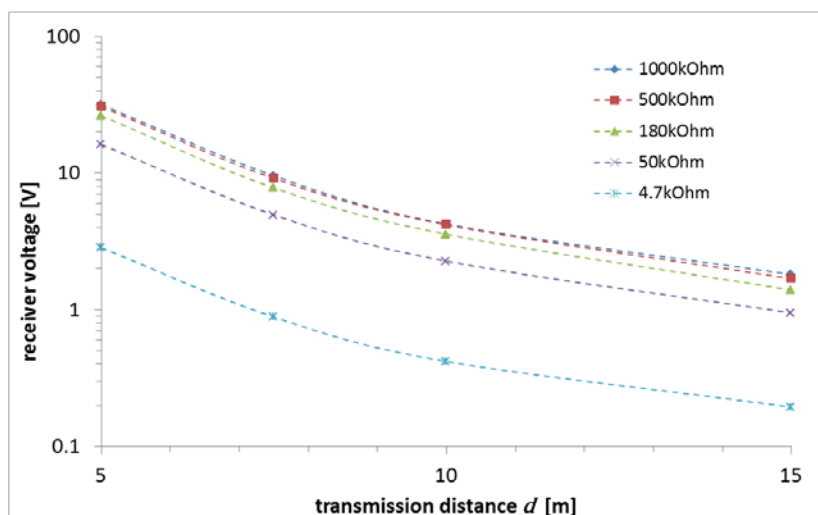
Figure 6-22. Measured voltages at different loads as function of the wireless distance between two coplanar antennas (Petten, unsaturated sandy soil).

Modern2020 D3.3: Long-term power supply sources for repository monitoring
Dissemination level: PU
Date of issue of this report: 31/05/2019

Page 46
© Modern2020

Figure 6-23 shows the power output determined by the measurements in Petten. The optimum load resistance is 50 kΩ, resulting in 2 - 700 µW of harvestable power over wireless distances from 5 - 15 m.
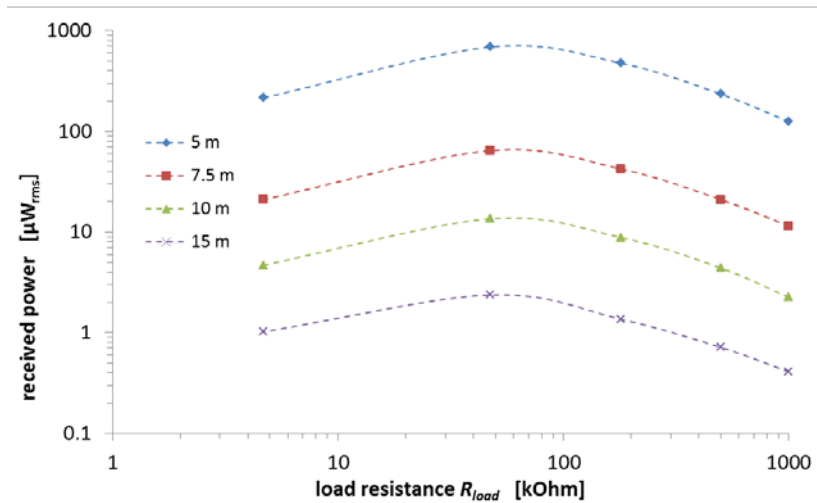
Figure 6-23. Load power for different wireless distances between two coplanar antennas as function of the load resistance (Petten, unsaturated sandy soil).

Figure 6-24 shows the power output by a measurement performed in the same manner, but now on a wet grassland in Ursem (NL). In both experiments, the same experimental set-up was used, including the antenna tuning. On the shortest wireless distance (5 m), the measured power is comparable to the unsaturated situation. However, with increasing wireless distance, increasing attenuation is observed in Ursem, compared to the unsaturated situation in Petten.
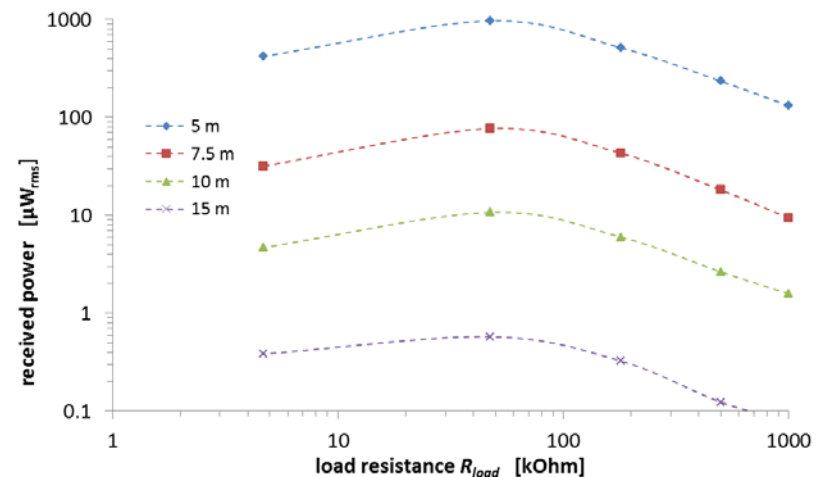
Figure 6-24. Load power for different wireless distances between two coplanar antennas as function of the load resistance (Ursem, wet grassland).

Table 6-6 compares the maximum power determined at a load of 50 kΩ in Petten and in Ursem. At 5 m wireless distance, in Ursem 40% more power is measured in the load than in Petten, despite the higher conductivity. This result is assumed to be related to experimental errors, e.g. variations of the inverter output power or slight detuning of the antennas.

Modern2020 D3.3: Long-term power supply sources for repository monitoring
Dissemination level: PU
Date of issue of this report: 31/05/2019

Page 47
© Modern2020

Table 6-6. Maximum load power measured in Petten (unsaturated sandy soil) and Ursem (wet grassland).

d	P_{load} [µW$_{rms}$]	
[m]	Petten	Ursem
5.0	690	970
7.5	64	77
10	14	11
15	2.4	0.6

Figure 6-25 shows the ratios of the load power of the wet vs. unsaturated situation. To compensate for the experimental errors noted above, the ratios are averaged for all loads larger than 4.7 kΩ, and are normalized by the average power measured on 5 m. For a wireless distance of 15 m, the higher conductivity in Ursem results in an additional attenuation of the power by a factor of 5, relative to the measurements performed in Petten.
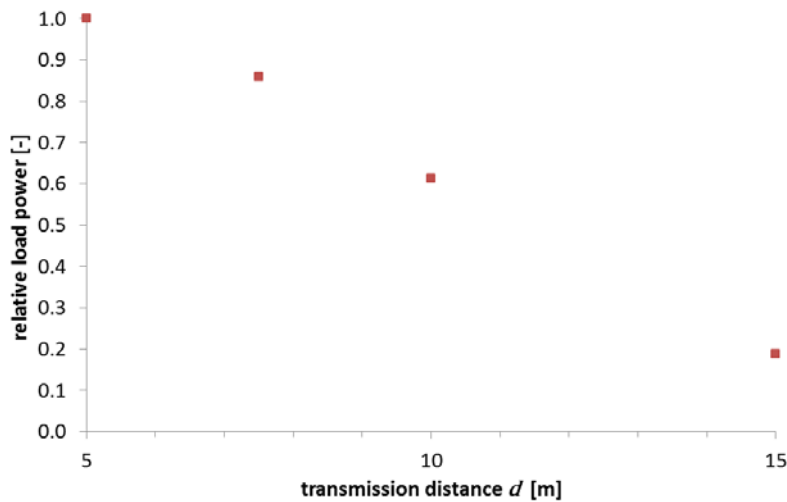
Figure 6-25. Ratio between the load power measured in Ursem (wet grassland) and in Petten (unsaturated sandy soil).

The measurement results allow some analysis of the link efficiency. In a first approach, the key parameters are calculated, assuming no interactions with the media. With Equation 6-16 and Equation 6-1, the mutual inductance and coupling coefficient for a coaxial case are computed for the wireless distances of interest. For a coplanar configuration, both values are assumed in a first approximation to be about half of a coaxial configuration [12]. A quality factor Q_{Tx} of 610 is estimated for the transmitter antenna by Equation 6-2, including 0.1 Ω additional resistance from the antenna connectors and connecting wires. For the receiver antenna, an effective Q-factor Q'_{Rx} of 66 is determined. The effective Q-factor Q'_{Rx} includes the influence of the load resistor R_{load} (50 kΩ) and is calculated by

$$Q'_{Rx} = \frac{R_{load}}{\omega L_{Rx}\left(\frac{R_{load}}{Q_{Rx}^2 \cdot R_{Rx}} + 1\right)} \tag{6-20}$$

([18]). With a tuning capacitor C_{Rx} in parallel with the receiver antenna, the link efficiency is estimated [19] by

$$\eta_{link} = \frac{k^2 Q_{Tx} Q_{Rx}^2}{(1 + \frac{Q_{Rx}}{\alpha} + k^2 Q_{Tx} Q_{Rx})(\alpha + Q_{Rx})} \tag{6-21}$$

with

Modern2020 D3.3: Long-term power supply sources for repository monitoring
Dissemination level: PU
Date of issue of this report: 31/05/2019

Page 48
© Modern2020

$$\alpha = \omega C_{Rx} R_{load} \tag{6-22}$$

The calculated values for the four wireless distances are summarized in Table 6-7.

Table 6-7. Calculated mutual inductance (Equation 6-16), coupling coefficient (Equation 6-1), and link efficiency (Equation 6-21) as function of the wireless distance, assuming no interactions.

wireless distance d [m]	mutual inductance M [H]	coupling coefficient k [-]	link efficiency η_{link} [ppm]
5.0	7.5E-07	1.2E-03	46495
7.5	2.6E-07	4.0E-04	5801
10	1.2E-07	1.8E-04	1163
15	3.6E-08	6.0E-05	111

The link input power [19] is calculated by

$$P_{link\ in} = I_{Tx}^2 \left(R_{Tx} + R_{eq} \right) \tag{6-23}$$

with

$$R_{eq} = k^2 L_{Tx} \omega \frac{\alpha \cdot Q_{Rx}}{\alpha + Q_{Rx}} \tag{6-24}$$

A current I_{Tx} of 0.5 A was measured in the transmitter antenna. The measured link efficiency $\eta_{link,meas}$ is the ratio between the input power $P_{link\ in}$ and the maximum load power P_{load} measured at the receiver antenna (Table 6-6). Table 6-8 summarizes the measured link efficiencies $\eta_{link,meas}$ as determined in Petten and Ursem, and the percentage of the $\eta_{link,meas}$ relative to the calculated link efficiency η_{link} in Table 6-7.

Table 6-8. R_{eq}, input power, link efficiency measured in Petten and Ursem, and fraction of the measured link efficiency compared to the calculated link efficiency (η_{link}) in Table 6-7.

wireless distance d [m]	R_{eq} [Ω]	$P_{link\ in}$ [W]	measured link efficiency $\eta_{link,\ meas}$ [ppm]		fraction of the calculated link efficiency η_{link} [%]	
			Petten	Ursem	Petten	Ursem
5.0	0.12	0.18	3835	5386	8.2	11.6
7.5	0.01	0.15	423	503	7.3	8.7
10	<0.01	0.15	90	72	7.8	6.2
15	<0.01	0.15	16	4	14.3	3.5

In general, the measured efficiencies are about one order of magnitude below the calculated efficiencies. Part of the lower efficiency can be attributed to experimental aspects, e.g. slight detuning of the antennas from the optimum resonance frequency or measurement errors. Part of if, in particular for the smaller wireless distances, is related to the estimation of the mutual inductance: the applied approximation from [12] is valid for small antennas only.

However, part of the effect might be attributed to interactions with the medium, as discussed in Chapters 6.4.2 and 6.4.3. Table 6-9 summarizes the link efficiencies calculated for several conductivities and wireless distances, accounting for a) the additional antenna resistance (Equation 6-18) that affects the Q (Equations 6-2 and 6-3) and hence the link efficiency, and b) the signal attenuation according to [12], Eq. 3 & 4. Because the antenna are positioned in a conducting half-space, for the calculation of the resistance, an effective conductivity equal to 50% of the value given in Table 6-9 is used.

Modern2020 D3.3: Long-term power supply sources for repository monitoring
Dissemination level: PU
Date of issue of this report: 31/05/2019

Page 49
© Modern2020

Table 6-9. Calculated link efficiencies for two coplanar loops, including interactions with the electric conductivity of the medium.

distance d [m]	link efficiency η_{link} [ppm]				
	electric conductivity σ [S/m]				
	0.01	0.02	0.05	0.1	0.2
5.0	14189	8405	3755	1972	916
7.5	1814	1131	543	277	106
10	394	257	122	55	15
15	45	30	11	3	0.4

The calculated link efficiencies in Table 6-9 show a strong decrease for higher conductivity values and larger wireless distances, and compared with the values calculated without interactions (Table 6-7), these values are closer to what is measured in Petten and Ursem. Looking to the largest wireless distances, where the effect of the conductivity is the strongest, and the relative contribution of the experimental error the smallest, electrical conductivities of about 0.02 S/m and 0.05 S/m could be reasoned for the Petten and Ursem situation, respectively. However, although both experimental and calculated values are linked with uncertainties, the results give some evidence that the considerations presented in Chapters 6.4.2 and 6.4.3 can be useful when designing a wireless energy transfer system in a disposal situation, where the skin depth is in the order of magnitude of the wireless distance.

6.4.6 Discussion and conclusions

In Chapter 6.4, the potential interactions of a wireless energy transfer system with electric high conductive media were studied. The concept of skin depth allows a first estimation whether interactions are relevant for a given wireless distance and conductivity of the medium (Table 6-5). Several approaches for a closer analysis of a disposal situation were summarized, addressing the signal attenuation by the medium. Additionally, effects of conductive media on the antenna properties were discussed. It was shown that for the frequency range considered, the interactions of the antenna with the media need to be considered in the system design. Unlike for energy transfer through air or low conducting media as granite, the optimum antenna size for a high conductive media might be smaller than the available open space in a disposal facility. The conductivity of the media affects the antenna's reactance, and thus the resonance frequency. However, the effect is relatively small, and for many disposal conditions, with a proper design no frequency adaptation during the monitoring period is necessary to compensate for the effect of the variable saturation level of EBS components on the resonance frequency.

Wireless energy transfer through conductive media was demonstrated in a coplanar configuration with a set-up optimized for link efficiency. Power levels between 10 µW and 1 mW have been demonstrated over wireless distances between 5 and 10 m, with a link input power of 0.2 W. At the chosen input power level, load voltages are more than 2V at 10 m wireless distance, allowing AC-DC conversion with rectifiers. However, higher voltages at the receiver antenna are beneficial for the AC-DC conversion efficiency and can be realized e.g. by an increase of the input power. For a wet grassland, a decrease of the link efficiency by a factor of five at the largest wireless distance was measured, demonstrating a relevant impact of the electrical conductivity of the medium. The measured link efficiencies were only about 10 % of the calculated values without accounting for interactions with the media. However, correction for the interactions provided a better match.

In conclusion, wireless energy transfer is also feasible through highly conductive media, but needs some additional considerations to allow optimum transfer efficiencies.

Modern2020 D3.3: Long-term power supply sources for repository monitoring
Dissemination level: PU
Date of issue of this report: 31/05/2019

Page 50
© Modern2020

6.5   Overall conclusions about the wireless energy transfer

Based on the system analyses, feasibility studies and experiments in Chapter 6, wireless inductive energy transfer by using LF frequencies such as 125 kHz can be envisaged as a promising concept for powering repository monitoring sensors in general. However, reasonable power levels by inductive energy transfer require remarkably higher coupling between the antennas than usually required for proper signal-to-noise ratio for wireless inductive data transfer. In practice, this means shorter operation range and/or a need to apply bigger antenna diameters compared to data transfer systems.

The feasibility analyses in Chapter 6.2 estimated roughly that reasonable received power levels (over 10 μW) for long-term accumulation of the energy from a wireless power transmitter at 10 m distance are possible. This can be achieved with reasonable size of the antennas (transmitter and receiver antenna diameters such as 2 m and 0.15 m respectively), reasonable Q-factor of the antennas (e.g 50), and reasonable RF power level to the transmitter antenna (e.g. 100 W). These analyses are valid if the performance degradation due to the medium interaction can be kept moderate (less than 50%). Wireless distances longer than 10 m and power levels higher than 10 μW are also possible e.g. by increasing the antenna diameters, in which the following rules of thumb are valid:

- the received power level is inversely proportional almost to the sixth power of the wireless distance if the distance is much larger than the antenna diameters,

- doubling the diameter of both antennas will almost double the attainable wireless distance,

- doubling the diameter of the receiver antenna only will increase the received power by a factor of 4 - 8.

However, in highly conductive media, additional, non-linear factors might play a role: here, the skin depth δ can serve as a first estimator if the above rules of thumbs are applicable.

Higher power levels or longer wireless distances are also possible by higher antenna Q-factors by increasing the wire diameter, which however demands more accurate tuning of the system, eventually require a system design with possible autotuning arrangements. However, the ability to increase the Q-factor and size of the antenna is limited by the increasing radiation resistance, certainly in case of an electrically good conducting media.

The experiments in Chapter 6.3 demonstrated that the bedrock with low electrical conductivity didn't show any remarkable degradation of the energy transfer performance due to 125 kHz magnetic field attenuation. Thus, the performance estimation methods for the operation ranges and power levels without medium interaction in Chapter 6.2 are valid for power transfer through repository barriers comprised of low-conductivity host rock. Some degradation of the performance can be attributed to a slightly antenna detuning that however can be compensated by adjusting the antenna tuning for the final operation environment. The experiments showed also that a bi-directional communication add-on in an inductive energy transfer system ("all wireless in one") is feasible without compromising the energy transfer performance.

The experiments in Chapter 6.4 demonstrated that energy transfer through an electric conductive media is feasible as well. With an optimized antenna design, link efficiencies of several hundred ppm over a wireless distance of 7.5 m were achieved with co-planar antennas, despite of interactions with the conducting medium. The antenna coupling with this co-planar configuration is roughly equivalent to a wireless distance of 10 m with a coaxial configuration.

For the wireless distance of interest (10 m), interactions with the medium need to be considered in the case of argillaceous host rocks, (saturated) bentonite or cementitious materials. These interactions strongly depend on the pore water composition. In case of higher conductivities (> 50 mS/m), lower frequencies than 125 kHz should be preferred in order to avoid large performance losses.

In conclusion, the contributions in Chapter 6 demonstrate the general feasibility to transmit energy wirelessly over distances typical for sealing constructions as projected in typical disposal facility designs for radioactive waste (about 5 - 15 m, Appendix 2). It was shown that the general concepts used for wireless energy transfer over short distances (smaller than the antenna radius) can be applied on longer distances reasonably well. Additional effort has been done to address the specific technical challenges

Modern2020 D3.3: Long-term power supply sources for repository monitoring
Dissemination level: PU
Date of issue of this report: 31/05/2019

Page 51
© Modern2020

that go along with the comparable small link efficiencies that can be achieved on these distances, and to address interactions with conductive media such as large metallic objects and saturated bentonite as present in many disposal concepts.

One aspect not addressed in the current research are interactions with magnetic permeable materials, applied in the EBS (e.g. steel reinforcement), present in monitoring components (e.g. extensometers), or the disposed waste canisters. Smaller magnetic permeable components might have a limited effect on field propagation, or could probably even be beneficial for the field propagation. Magnetic permeable materials as part of the EBS can potentially be avoided by transferring energy not over the shortest pathway - directly through the plug - but alongside of the plug. However, for future work it will be important to understand the interactions with the rather large, highly conductive waste containers.

The novelty issues in project Modern2020 were applying 125 kHz inductive wireless energy transfer:

- at relatively long distances,

- through natural or engineered repository barriers, in which the electrical conductivity can cause damping of the magnetic field, and

- with a bi-directional communication add-on without significant degradation of the energy transfer performance.

This powering concept was proven feasible by numerical modelling and by integrating the basic technical components together for experiments in laboratory environment and through repository barriers in environment that partly represents the target operation environment. Thus, the TRL achieved in project Modern2020 is 4 - 5.

Modern2020 D3.3: Long-term power supply sources for repository monitoring
Dissemination level: PU
Date of issue of this report: 31/05/2019

Page 52
© Modern2020

7. Miniature nuclear generators

7.1 Introduction

In this chapter, ORANO (previously AREVA) studies nuclear batteries, also called Radio Isotopic Power Systems (RPS), as a power sourcing alternative for wireless repository monitoring sensors. Nuclear batteries are currently used e.g. in long-range space missions as far as they are known to operate for very long lifetime. So far, the question arises whether RPS technology could be adapted for monitoring use within geological disposals.

For the past decades, the dominant RPS technology has been the radioisotope thermoelectric generator (RTG), which converts the decay heat of the radioisotopes into electricity through the Seebeck effect. RTG devices have been successfully employed on a number of space missions but not only. Ground applications have encompassed energy supply for remote lighthouses, coastal beacons and weather stations. In the early 90's, safety concerns led to remove some of those. New applications are under analysis as the use cases for autonomous underwater vehicles (AUV) as well as underwater stations [20], [21]. Today, RTG devices have a safer design, but their use is still limited mainly to space and nuclear environments.

RTG could also be a solution to provide autonomous power supply within a geological deep disposal of nuclear waste for monitoring and data transmission (including wireless) over a long period of time as considered in the framework of Modern2020. The constraints at a final radioactive waste disposal are indeed relatively similar to the one encountered in spacecrafts. In particular, RTG could be an option for areas of the repository where neither energy harvesting nor wireless energy transfer are possible.

Within the frame of project Modern2020, the main part of the work has been an exhaustive state of the art study on the possibilities offered by nuclear batteries and possible technical limitations of such a technology due to the physical conditions related to geological disposal. In addition, the work has involved a demonstration of the possibilities and technical limitations of an RTG type power supply inside intermediate level long lived (ILLL) waste vaults. This work is based on a preliminary design and thermal modelling of the RTG.

The aim of the state-of-art study was to perform an overview of miniaturized nuclear generator technologies in order to find the most suitable of them to develop an electrical power generator taking into account the constraints of geological lifetime disposal. The analysis is driven by the specifications (limit in vault concrete temperature, geometrical constraints) and environmental conditions provided by Andra [22].

The demonstration work focuses on a specific radioisotope that can be used to supply energy within RTG. So far, the isotopes most commonly used for space applications have been Plutonium (^{238}Pu), Americium (^{241}Am), and Polonium (^{210}Po). Due to the scarcity of ^{238}Pu and to radiotoxicity and high volatility of ^{210}Po, the focus has been on the feasibility for using ^{241}Am.

This work has been reported closer in a separate report related to Modern2020 milestone MS11 [23].

7.2 State-of-the-art

The main objective of the state-of-the-art survey was to evaluate the technological feasibility of nuclear batteries in general and especially RTGs for the use in a nuclear waste disposal monitoring application. The report [23] provides an overview of the current state-of-the-art of nuclear batteries in general and especially that of the RTG's. A preliminary review of the current available and/or emerging electrical power sourcing technologies allowed comparison between those based on radioisotopes (such as RTG's) and chemical batteries. The different battery technologies have been positioned against one another by using their specific energy and density. The review of chemical batteries involved primary, rechargeable and advanced (Li-x) batteries, which are found not to comply with the specifications for geological deep disposal. This is due to their short lifetime. In addition, no liquid is allowed within the cavities for safety reasons, which eliminates liquid cells.

Modern2020 D3.3: Long-term power supply sources for repository monitoring
Dissemination level: PU
Date of issue of this report: 31/05/2019

Page 53
© Modern2020

Betavoltaic systems, also known as betavoltaic cells, have been challenged, too. Currently they find applications in micro-electromechanical and electronic devices, implantable biomedical prosthetic devices, and in the military intelligence applications. They can potentially replace conventional chemical batteries in many ultra-low power applications, including those in extreme environmental conditions. However, they cannot be seen as a real alternative for the use in geological disposal repositories because of their ultra-low energy capacity that typically is in the class of a microwatt.

Radioisotope Thermoelectric Generators (RTG's) use a thermoelectric generator (TEG) to convert the heat released by the decay of radioactive material into electricity. The physical operation principle is the same as in the energy harvesting from thermal gradients (Chapter 5), but instead of exploiting the heat generated by the HLW, RTG's exploit the heat released by the decay of a specific piece on nuclear material in the immediate vicinity of the TEG. RTG's are presented to have demonstrated their success whenever simplicity and long lifetime are required. This has been proven since the beginning of the space programs. The power generation by radioactive decay is a mature technology for space missions. For example, the smaller Multi-Mission RTG, MMRTG, used on the Mars Science Lab Curiosity, has a mass of 44 kg and generates 125 W.

Among the technologies for converting the nuclear radiation energy to electricity (Figure 7-1), the thermoelectric conversion appears to be the most mature at the moment.
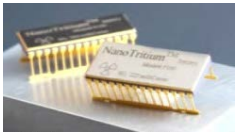
Conversion Technology	Description	TRL	Figures
Thermoelectric power conversion	Thermal energy from a radioisotope is converted via a TEG to produce a voltage difference	6 Larger satellites & Mars rovers	
Betavoltaic power conversion	Beta particles emitted from a radioisotope are absorbed by a p/n junction diode to produce electron-hole pairs	**5**	
Alphavoltaic power conversion	Alpha particles emitted from a radioisotope are absorbed by a p/n junction diode to produce electron hole pairs	2 Analysis-testing at NASA	
Thermophotovoltaic power conversion	Infrared radiation emitted from a hot radioisotope is absorbed with an infrared photovoltaic cell	2 Analysis-testing at Toronto University	
Piezoelectric power conversion	A miniature cantilever beam is bombarded with radiation from radioisotope source, and the vibrational energy is converted via piezoelectricity	2 Analysis-testing at Toronto University	
Small radioisotope power system	Stirling thermodynamic cycle power conversion from a radioisotope	2 Analysis-testing at NASA Glenn	

Figure 7-1. Future conversion technologies [24], [25], [26], [27].

Modern2020 D3.3: Long-term power supply sources for repository monitoring
Dissemination level: PU
Date of issue of this report: 31/05/2019

Page 54
© Modern2020

7.3   RTG design for geological disposal

Overall RPS performance is usually assessed from conversion system efficiency and specific power values. Conversion system efficiency is quite low, a few per cent, except for advanced generators such as Stirling generators which are not adapted to deep disposal applications because of the presence of gas and mobile mechanical parts.

Therefore, for the geological disposal application, one has to cope with a conversion efficiency of only a few %. Consequently, in an RTG type RPS, a sufficient amount of heat production will be necessary, while it could be limited when copping specifications related to geological disposal. As far as specific power value (after conversion) varies within 4 to 6 We/kg (electric wattage by kg of material used for heat production), one have to consider using kg or several hundred grams when designing RTG for geological disposal applications with electric power levels of several watts.

In general, the selection of isotope material for heat production in a nuclear battery is complex. It should consider the type of radiation, the half-life of the isotope, the decay energy of the radiation, the cost of the isotope or the possible other radiation forms emitted by the isotope (e.g., gamma rays) influencing shielding designs for nuclear safety purpose. A good summary of the selection criteria was already identified in [28]. In practice, these criteria limit appropriate materials to radionuclides with half-lives from 15 to 100 years that decay by alpha-particle emission over 99% of the time, of which only five exist.

Considering application to geological disposal monitoring, the equipment has also to be robust, economically acceptable and consistent with regulations. While ^{238}Pu is a much better power source, it is very difficult to obtain and can concur to nuclear proliferation [29]. An alternative to ^{238}Pu should be preferentially considered among the following [30]:

1. ^{209}Po (102 yr; 0.4855 W/g; bombardment of bismuth with protons in accelerator),
2. ^{249}Cf (351 yr; 0.1407 W/g; β-decay of berkelium-249 – made by intense neutron irradiation of plutonium),
3. ^{241}Am (433 yr; 0.1100 W/g; present in commercial spent fuel rods and "old" plutonium – from β-decay of ^{241}Pu),
4. ^{251}Cf (900 yr; 0.0545 W/g; multiple intense neutron irradiations of plutonium).

Among the material listed above, ^{241}Am is the preferred selection. It has a specific thermal power that is approximately one fifth of ^{238}Pu and a half-life that is approximately five times greater than that of ^{238}Pu. Photons can easily be shielded. In addition to this, ^{241}Am is also easily extracted from stockpiles of transuranic waste, the bi-product of nuclear fission reactors. ^{241}Am is actually a weaker power source, however its greater half-life ensures a long term energy production as required for monitoring geological disposals.

The order of magnitude to feed an RTG of 5We and following the assumptions of a 5 % conversion system efficiency, a radioisotope source of at least 100 Wth (thermal wattage) is required. This corresponds to about 100 cm³ or about 1 kg of Am_2O_3.

The conversion efficiency of a TEG is extremely sensitive to temperature difference and to thermoelectric materials itself. For disposal application, because of a lower difference in temperature between cold and hot sides, lower efficiency could be a disadvantage.

AREVA has studied and proven the concept of using Mg_2Si-HMS (Higher Manganese Silicide) type TEG in order to improve the efficiency of the system. The conclusion of this study told that the thermoelectric performance of the material is confirmed by thermal model and the correlated experiment. One obstacle to using this material into the RTG for deep disposal will be its availability and the difficulty of its production process.

Another possibility could be to investigate new materials. Among the potential thermoelectric materials are the following [31]:

- Silicon Germanium (SiGe): efficiency 6 - 7 %,
- Lead Telluride (PbTe) -TAGS: efficiency 5 – 7 %,

Modern2020 D3.3: Long-term power supply sources for repository monitoring
Dissemination level: PU
Date of issue of this report: **31/05/2019**

Page 55
© Modern2020

- Bismuth Telluride (BiTe): efficiency 2.5 - 4.5 %,

- Segmented PbTe-TAGS/BiTe: efficiency about 9 %,

- Skutterudites: efficiency > 9 %.

Bismuth Telluride (BiTe) is commonly applied in terrestrial commercial applications. Bi_2Te_3 is available in a variety of commercial standard units and operates most efficiently with a cold-side temperature of around 320 K. Combined with the availability of standard commercial modules and relatively low cost, this makes Bi_2Te_3 a suitable selection. For alternative new materials, additional investigations remain to be done. An option worth of consideration in the future would be a higher total thermal power by increasing the quantity of Am_2O_3 encapsulated radioisotope, allowing an Am_2O_3-based RTG to reach the same performance as a standard PuO_2-based RTG. Another option to improve the performance is a greater number of thermoelectric couples in the TEG.

In conclusion and regarding the RTG design for a geological disposal facility, the recommendation could be to use Bi_2Te_3 even if the maximum temperature is limited to 250 °C, because it is a well-known material with a mature and cost-effective production process.

7.4 Modelling

In order to check compliance with specifications regarding geological disposal monitoring ([22]), thermal modelling analysis has been performed for an RTG as designed in Chapter 7.3, i.e. [241]Am radiation source, 5 We electrical power and placed inside ILLL (Intermediate Level Long Lived) waste vaults of a geological disposal facility, Cigeo-project, France. The main objective was to verify the feasibility of the RTG inside a vault while respecting a thermal criterion on the concrete inside the vault for different simplified designs of the RTG. The RTG has been considered to be placed inside a vault as presented in Figure 7-2.
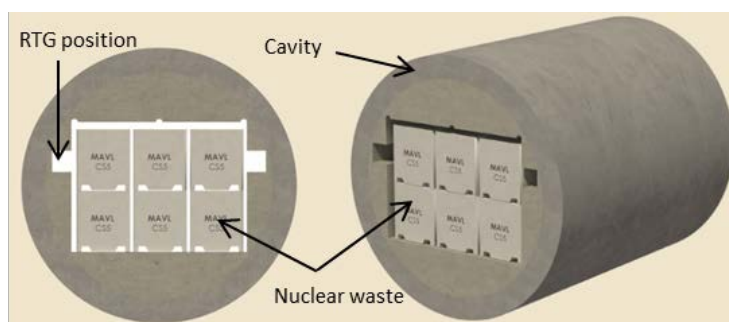
Figure 7-2. Underground geological nuclear waste disposal vault with RTG location.

The heat source ([241]Am) is surrounded by some insulation material and a few cooling plates with the role of generating a thermal gradient between the hot side (heat source of the RTG) and the cold side (concrete or geological material) as shown in Figure 7-3.
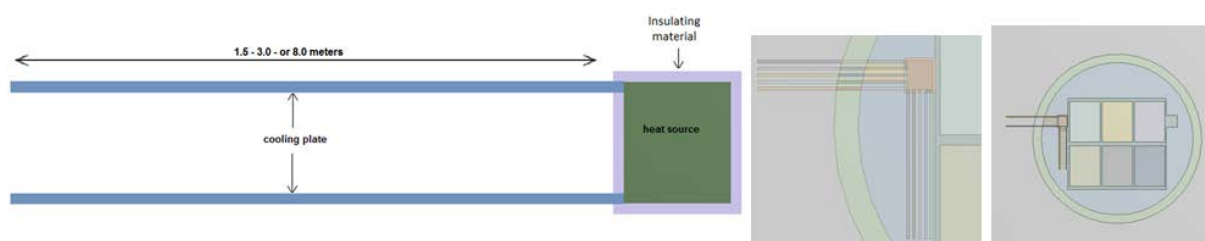
Figure 7-3. Schematic view of an RTG.

Modern2020 D3.3: Long-term power supply sources for repository monitoring
Dissemination level: PU
Date of issue of this report: 31/05/2019

Page 56
© Modern2020

Different designs of RTG have been tested:

- horizontal cooling plates going through the geological layer,

- vertical cooling plates going only through the concrete,

- different number (2, 3 or 5) of the cooling plates,

- different length and thickness of the cooling plates,

- different thicknesses of the insulation material (see report [23] for detail).

The following initial design parameters were considered:

- ILLL nuclear waste delivers a thermal power density of 5 Wth/m³.

- The RTG is supposed to deliver an electrical power of 5 We with an efficiency of 5%. (hence, its thermal power is equal to 100 Wth).

- The exterior limit of the geological layer is maintained at a temperature of 22 °C.

A two-dimensional steady state thermal numerical model has been developed with the commercial software ANSYS version 15 [32], [33]. The model is composed of the geological layer, the concrete of the disposal vault, 6 ILLL waste containers and different designs of the RTG (Figure 7-4).
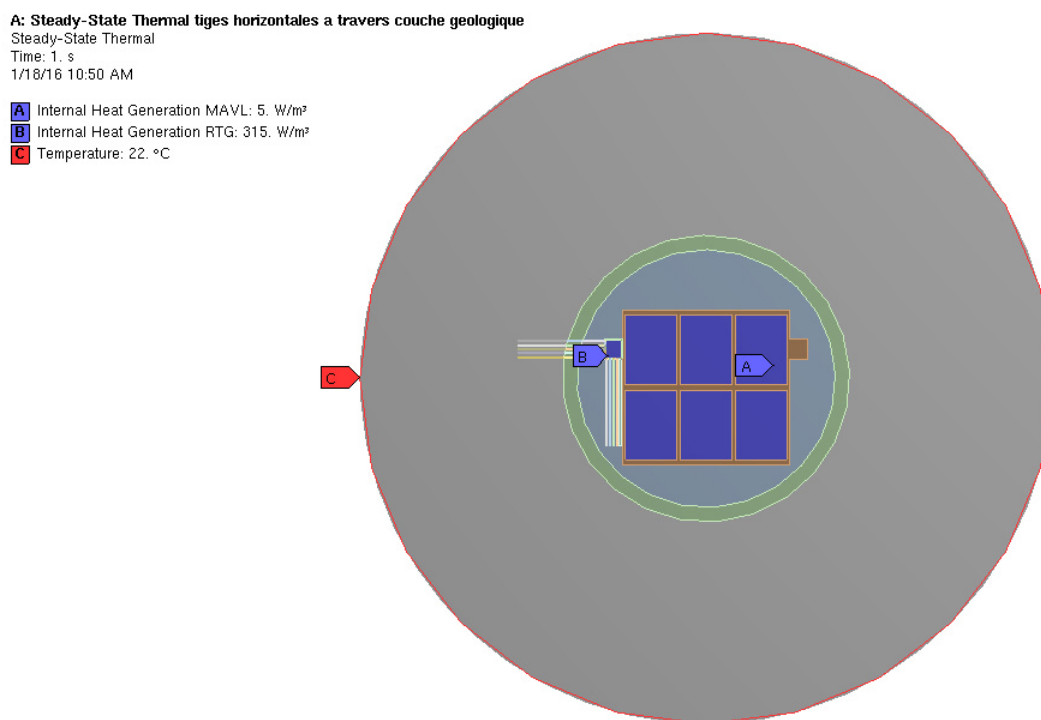
Figure 7-4. Schematic view of the numerical model.

Figure 7-5 presents the temperature field provided by the numerical model for the reference case (RTG with two 3 m long and 5 cm thick cooling plates). The model gave a temperature gradient of 6.9 °C between the hot and cold side of the cooling plates with a hot side of 57.2°C near the radioisotope source. With this design, the concrete thermal criteria is met.

Modern2020 D3.3: Long-term power supply sources for repository monitoring
Dissemination level: PU
Date of issue of this report: 31/05/2019

Page 57
© Modern2020
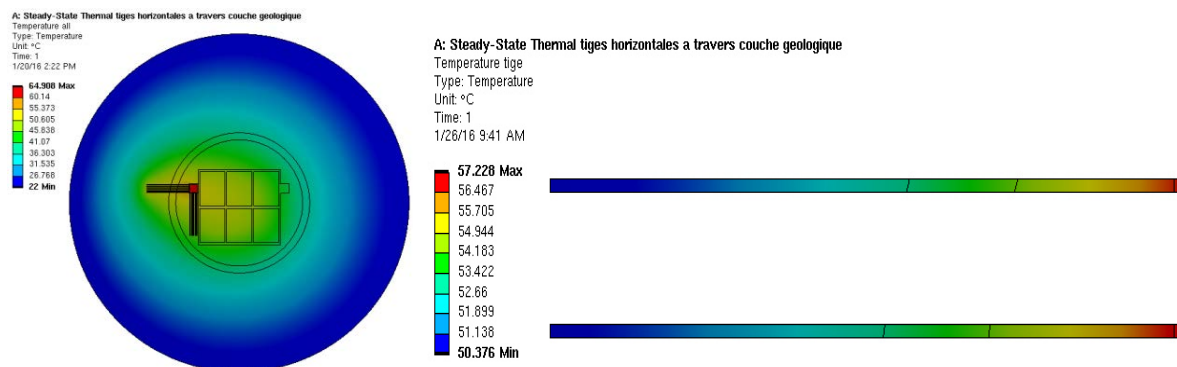
Figure 7-5. Temperature field on the entire model (left) and zoom on the cooling plates (right) for the reference case.

A parametric study has been performed as well. The impact of the concrete thermal conductivity, the length of cooling plates, the thickness of cooling plates and the thickness of the insulation material have been evaluated. The thermal criterion on the concrete is always met.

The difference of temperature between the hot and cold side of the cooling plates is almost constant in the range of the thermal conductivity tested and the highest with 2 cooling plates. Vertical cooling plates going only through concrete generates the same range of temperature difference with a higher temperature on both hot and cold side compared to horizontal cooling plates.

The numerical modelling showed that it is possible to evacuate the heat released by an RTG delivering 5 We electric power inside a geological underground disposal facility, while respecting the thermal criterion on the concrete.

It could be argued that driving the heat using cooling plates going inside the geological formation could be not admissible because they will constitute a preferential path for water and radionuclides. Nevertheless, using vertical cooling plates going only through concrete generates the same temperature differences compared to horizontal cooling plates, while the thermal criterion on the concrete is still met.

7.5 Economical aspects and potential commercialization

As already stated in the introduction, RTGs are as of today regarded as a potential solution to the autonomous power supply in a deep geological disposal, in which neither energy harvesting nor wireless energy transfer are manageable. The purpose of the ongoing project and the further developments (see Chapter 7.6) is to pave the way for the feasibility demonstration of such an application. Beside the technical feasibility, future commercialization is an additional issue. Industrial and commercial development of [241]Am based RTGs will be derived from the actual needs, as well as from the standard drivers and optimizations.

On one hand, the nuclear cycle industry already has the technological capacity to separate [241]Am and to transform it into an RTG source of the appropriate design. However, decision to develop an industrial capacity will have to be backed by reasonable and robust ROI expectations, which will depend on whether [241]Am is regarded as a by-product from existing installations or as a dedicated product from installations to be adapted or developed.

On the other hand, enhancing other application perspectives, not restricted to power supply for repositories, would be a crucial support to the commercialization. Such perspectives may be solidified when considering the requirements of the space industry. While [241]Am delivers only 20% of the power from [238]Pu (the most used isotope in the RTGs for space missions so far), it enhances power stability and longer term production (by about 5 times). [241]Am is also much cheaper to produce than [238]Pu (insofar as one has a reprocessing plant available), and is not liable to the proliferation regulations or safeguards, thus releasing part of the constraints. The space industry has historically voiced several times

Modern2020 D3.3: Long-term power supply sources for repository monitoring
Dissemination level: PU
Date of issue of this report: 31/05/2019

Page 58
© Modern2020

expectations from the nuclear cycle about Am powered RTGs. Discussions have been initiated; the development will take some time, and the constraints of the space missions environment (especially during the launch of vehicles) will have to be assimilated and taken care of.

In the end, the commercialization of the studied RTG concept will potentially depend on a global optimization and capabilities to use ^{241}Am as a power source in different domains, based on the present knowhow of nuclear (and space) industry.

7.6   Conclusion

The main conclusion of the work is that RTG's are a prospective powering alternative for monitoring operations within geological disposal and further steps for the design and prototyping studies are relevant. Proposed detailed steps for this are:

1) to define a reference design of the RTG,
   a) to define the heat source (on the basis of an expected global efficiency),
      i) to define the appropriate compound (Am_2O_3, AmO_2, other…),
      ii) to define the size of the elementary pellet,
      iii) to define the needed encapsulation of one or several pellets (size, material, …) to meet the nuclear safety requirements as a sealed source,
      iv) to estimate the quantity of the Am compound needed and consequently the number of pellets/sealed sources,
      v) to define the assembly the sealed sources to create the hot source,
   b) to choose the appropriate thermoelectric materials,
   c) to define the expected characteristics of the TEG built of the chosen materials,
   d) to model, from a thermal point of view, the RTG taking into account the expected size and thermal conductivity of the TEG, the size and thermal conductivity of the hot source,
   e) to check that the modelled RTG is mechanically feasible,
   f) to check that the modelled RTG meets the expected requirements (thermal flux in the TEG, hot side and cold side temperatures across the TEG), if not, the process has to be looped to c), b) or a) depending on the results,
   g) to study thermal fluxes system uncertainties on a specific RTG selected configuration,

2) to build a RTG prototype according to the reference design,

3) to perform tests on this prototype,
   a) in laboratory,
   b) in the site.

These steps have not been investigated within the Modern2020 project; they are provided as potential guidelines for future developments towards an RTG prototype. Despite the large number of these additional steps to be performed, building an RTG prototype for monitoring operations within geological disposal is a realistic objective. Figure 7-6 shows an example of a prototype that has been developed by AREVA TA for ESA (European Space Agency) according to given specifications. Practical prototyping has taken dedicated activities of a few years. This is possible to be repeated for developing another prototype for geological disposal applications.

The development work in Modern2020 was focused to a novel RTG concept, in which the RTG is placed in a disposal vault. The work in Modern2020 involved elaboration of this concept and proving the feasibility of it by numerical modelling. Practical experiments for this were not yet carried out in project Modern2020. Thus, the TRL achieved in project Modern2020 is 3.

Modern2020 D3.3: Long-term power supply sources for repository monitoring
Dissemination level: PU
Date of issue of this report: 31/05/2019

Page 59
© Modern2020
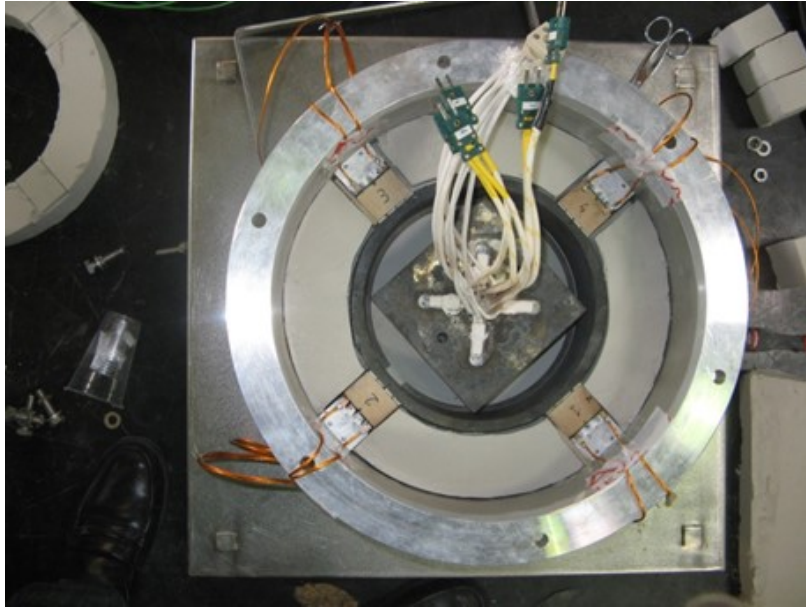
Figure 7-6. An European small-scale RTG with 5 – 50 We power range (an example of a prototype for ESA by Areva TA).

Modern2020 D3.3: Long-term power supply sources for repository monitoring
Dissemination level: PU
Date of issue of this report: 31/05/2019

Page 60
© Modern2020

8. Energy storage

8.1 Introduction

As discussed in Chapter 4 dealing with the wireless sensor units (WSUs) for repository monitoring in general, the intermittent power consumption of the WSU combined with the limited and sometimes intermittent supply capability of the power source calls for a rechargeable, intermediate energy storage between the power source and the power consuming parts of the WSU. This chapter summarizes the energy storage technology analysis performed by Arquimea to obtain a suitable solution for this.

The objective of this chapter is to provide a complete picture of the problem related to the intermediate energy storage in WSUs for repository monitoring from a system point of view. A WSU system view analysis is provided, since the energy storage solution is tightly connected to the WSU system architecture. This chapter is subdivided into the following sections:

- requirements analysis: compilation of the specific energy storage requirements of the repository monitoring WSUs, including numerical values of a case WSU with a specific operation scenario, the energy demand of which is also compared to the energy availability estimated in Chapter 5 and Chapter 6.
- state-of-the-art and analysis of existing energy storage technology solutions,
- summary and conclusions.

8.2 Requirements

The requirements of the WSUs for repository monitoring listed in this chapter are limited to the ones that are relevant for the energy storage subsystem. These requirements will vary depending on the monitoring concept and applied power source of the WSU. Nevertheless, with the objective of establishing a common set of requirements, a specific set of parameters has been selected with numerical values for a case WSU with a reference scenario ("reference WSU"). The selection of the ranges provided in this section intends to point out to the most representative values. After initial individual analysis of each main requirement, a summarizing table of the reference WSU is provided to point out the most representative values.

The reference WSU defined in this chapter is based on the Arquimea wireless system that will be installed at LTRBM demonstrator (Modern2020 Task 3.2 and Task 4.2). The system is composed by two buried WSUs with two new type of psychrometers (developed under Modern2020 Task 3.4), one pore pressure transductor and one capacitive relative humidity sensor. A third unit will be placed in the gallery and will collect data from the buried ones.

8.2.1 Environmental requirements

For the envisaged location of the WSUs in the repository installation, the following environmental conditions are considered:

- temperature range: 25 ºC - 45 ºC,
- humidity range: 50 % - 100 %,
- electromagnetic conditions: no other EMI than the generated from the application itself is expected,
- maximum estimated radiation exposure conditions: total dose of 12 Mrads (20 years).

8.2.2 Lifetime requirements

One of the most relevant requirements for the WSU is a long operating lifetime. Any maintenance operation is not feasible after initial installation. The expected lifetime of the WSU is between 20 to 50 years. End of life of the WSU is defined as the moment when the WSU is not able to provide any useful monitoring information.

8.2.3 Operation timing requirements

The operation of each buried WSU consists of successive operation cycles, each of which involves a long-lasting sleeping period and a short activity cycle. During the activity cycles, the WSU will perform the measurements and transmit the data. The operation scenario of the reference WSU implies two transmissions per day, i.e. once in every 12 hours, the WSU shall repeat the activity cycle that lasts 2 minutes. Between the activity cycles, the WSU is in the sleep mode with extremely low power consumption.

8.2.4 Supply voltage requirements

The sensor payload and the communication parts of the WSU are powered by a DC supply voltage within the following margins:

- DC voltage level: 3.00 to 3.63 V,
- ripple: 100 mV$_{pp}$.

8.2.5 Self-discharge

The self-discharge causes the energy storage to lose part of the accumulated energy before it is used. In general, if the supply power comes from an energy harvester with a constant output power level, the power dissipated by the self-discharge should be remarkably lower than the output power of the energy harvester.

8.2.6 Energy supply requirements

The energy demand of the WSU is completely dependent of the WSU configuration (number and type of the sensors in the payload) and time between the measurements or activity cycles in general. With the objective of scaling the capacity of the energy storage system, the following parameters have to be considered:

- operation scenarios:
  - o number and type of individual sensors in the payload,
  - o energy consumed by each activity cycle of the WSU,
  - o rate of the activity cycles with measurements and communication,
- supply voltages,
- peak current consumption.

Table 8-1 shows the energy budged analysis of the reference WSU, which is based on the Arquimea wireless system installed at the LTRBM demonstrator. The system is composed of two buried wireless units (WSN nodes) with two new type psychrometers (developed under Modern2020 Task 3.4), one pore pressure transductor and one capacitive relative humidity sensor. A third unit is placed in the gallery and will collect data from the buried ones. The operation of each buried wireless unit is based on 12 hours operation cycles. Each operation cycle consists of a long-lasting sleeping period with extremely low power consumption and a short activity cycle. During the activity cycles, the WSU performs the measurements and transmits the data obtained to the next node or to the gallery node. The reference operation scenario implies two transmissions per day. A 3.3 V primary power supply is considered for current consumption estimations in this table. The supply voltage requirements are analysed closer in Chapter 8.2.4.

Modern2020 D3.3: Long-term power supply sources for repository monitoring
Dissemination level: PU
Date of issue of this report: 31/05/2019

Page 62
© Modern2020

Table 8-1. Calculation of the energy consumption per operation cycle of the reference WSU.

Operation	Current consumption (mA)	Supply voltage (V)	Operation timing per cycle (s)	Energy consumption (mWh)
Stand-by current (12 h)	0.001	3.6	43080	0.043
Data Transmission	400	9	0.1	0.1
Ack reception	0.512	3.6	20	0.01
Active Node	5	3.6	120	0.6
Psychrometer (2 units)	170	5	35	8.26
Pore pressure (4...20 mA) + Capacitive Relative Humidity sensor	20	9	5	0.25
Total				9.26

Figure 8-1 shows the distribution of the energy consumption of the WSU activity cycles in the reference scenario without sensors and with sensors. The figure shows that 92 % of the energy is consumed by the sensor payload installed in the WSU, the major part of which (89 %) by the 2 psychrometer units. Any other payload configuration will change drastically this energy distribution, e.g. in the case of having four pore pressure sensors and no psychrometers, the measurements energy consumption will decrease to the 57 % of the total consumed energy.

The estimated energy consumption of the reference WSU during each 12 hours' operation cycle is 9.26 mWh (33.3 J) that can be divided into a base consumption of 0.15 J to cover the stand-by current and 33.15 J consumed by the 2 minutes activity cycle.

From the power supply point of view, Figure 8-2 shows the expected power and energy demand during the 2 minutes activity cycle. Independently of the sensors payload, the maximum instantaneous power demanded for the system is due to the data transmission (3600 mW).
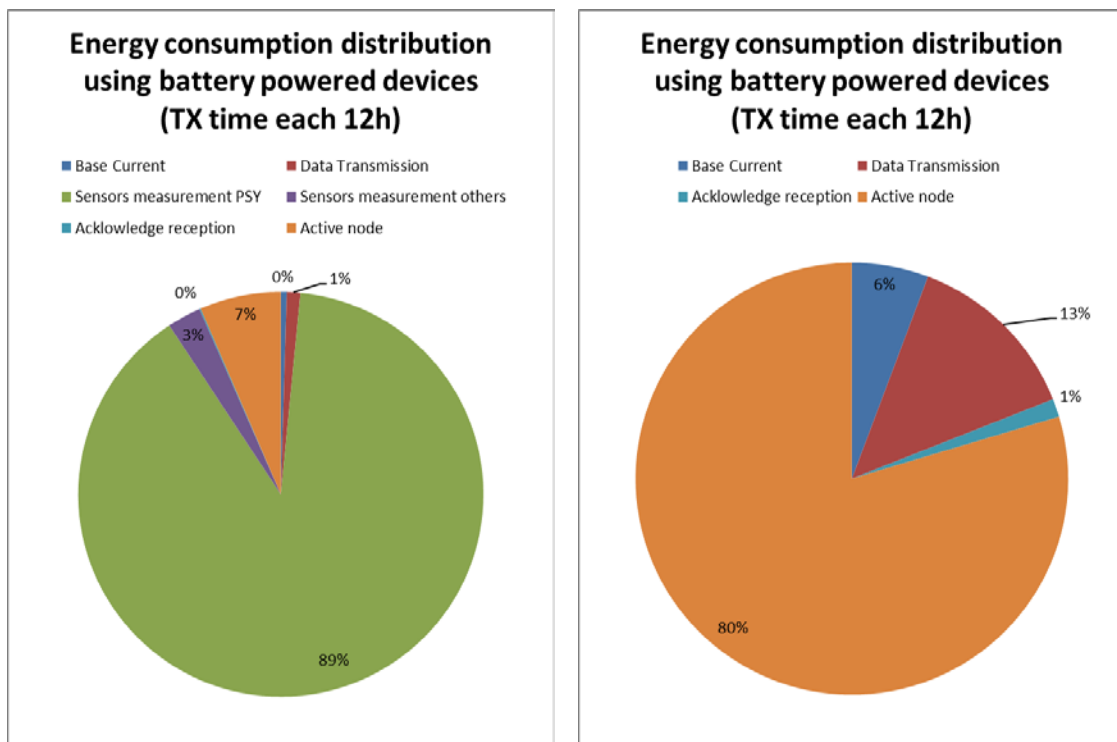
Figure 8-1. Energy consumption distribution for the reference WSU with sensors (left) and without sensors (right)

Modern2020 D3.3: Long-term power supply sources for repository monitoring
Dissemination level: PU
Date of issue of this report: 31/05/2019

Page 63
© Modern2020
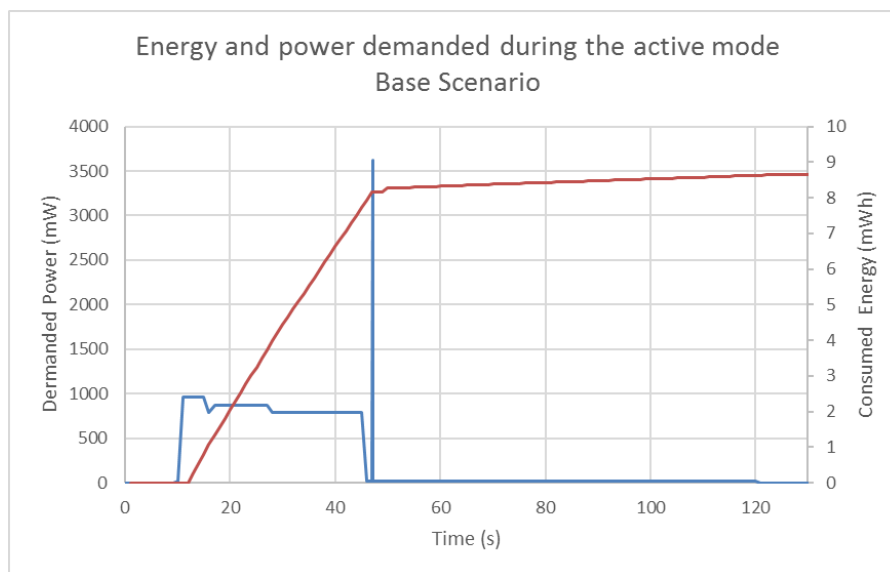
Figure 8-2. Profile of the consumed energy and power of the of the reference WSU during the activity cycles.

8.2.7 Energy demand vs. energy availability

The energy demand of the reference WSU (33.3 J during 12 h) can be compared to the power output capacity of the thermal energy harvesting and wireless energy transfer systems presented in Chapter 5 and 6. Referring to Figure 5-11 and Table 6-4, the 12 hours energy accumulation capacity of the presented power sourcing case implementations are:

- TEH-1L immediately after the disposal (1 mW): 43 J,
- TEH-2L 50 years after the disposal (0.07 mW): 3.0 J,
- wireless energy transfer 10 m through host rock with low conductivity (0.05 mW): 2.2 J with pilot antennas according to Chapter 6.3.1.

The previous numbers are rough estimations and depend much on the design parameters. The numbers exclude the power losses of the energy storage (e.g. self-discharge) and the supply voltage conversions between the energy storage and the sensor payload. A general conclusion is that some adjustment of the WSU operation scenario and/or the design parameters of the energy source is needed to match between the energy demand and energy availability. This concerns especially the wireless energy transfer system used as an example and can be solved e.g. by applying larger antenna diameters.

8.2.8 Requirements summary table

The requirements of the reference WSU are summarized in the table below.

Modern2020 D3.3: Long-term power supply sources for repository monitoring
Dissemination level: PU
Date of issue of this report: 31/05/2019

Page 64
© Modern2020

Table 8-2. Requirements summary table.

#	Name	Description	Min	Nom	Max	Unit
1.1	Temperature	Temperature range	25	-	45	°C
1.2	Humidity	Humidity range	50		100	%
1.3	TID	Total Ionizing Dose		12		Mrads
2.1	Life	Life duration	20		50	Years
3.1	Operational cycle	Time between active cycles of the WSN node		12		Hours
4.1	Voltage level	DC power supply voltage range	3.00		3.63	V
4.2	Voltage ripple level	Voltage	0		100	mV
5.1	Total energy demand	Total energy demand during 1 complete cycle every 12 hours			33	J
5.2	Peak current consumption	Maximum current consumption peak demand (0.1s)			400	mA

8.3 Energy storage technologies

The requirements presented in Chapter 8.2 represent a substantial challenge to the design of the energy storage subsystem for a repository monitoring WSU. From the different requirements, it is possible to remark the following ones, which together result in that any direct solution from the current commercial state-of-the-art cannot be directly used:

- Ultra-low power availability from harvesting source. This low power generation makes that all the systems involved in the energy storage shall be highly efficient avoiding any consumption in the storage process that could reduce the energy availability for final application. The energy storage self-discharge and the DC/DC voltage conversion for charging the storage energy device become significant challenges to be considered for the final solution.
- Long operating lifetime in years. For many energy storage technologies, this depends strongly on the operation temperature and the charging state. 20 years is a significant complex requirement especially in combination with the 25-45°C operational temperature range.
- Finally, peak current consumption of the payload will also significantly limit the applicability of the available technologies.

Different available technologies for energy storage applied to low power energy harvesting are analysed. For this document, three different group of technologies have been selected for analysis and comparison:

1. Rechargeable batteries,
2. electrostatic double-layer capacitors (EDLC),
3. electrochemical pseudocapacitors and hybrid capacitors devices.

A common used method for generic comparison of the previous energy storage technologies is the Ragone plot. Ragone plots provide the available energy of energy storage devices for constant active power request [34]. Traditional batteries and supercapacitors (EDLCs) are located in opposite corners when represented in this kind of graphs.

Modern2020 D3.3: Long-term power supply sources for repository monitoring
Dissemination level: PU
Date of issue of this report: 31/05/2019

Page 65
© Modern2020
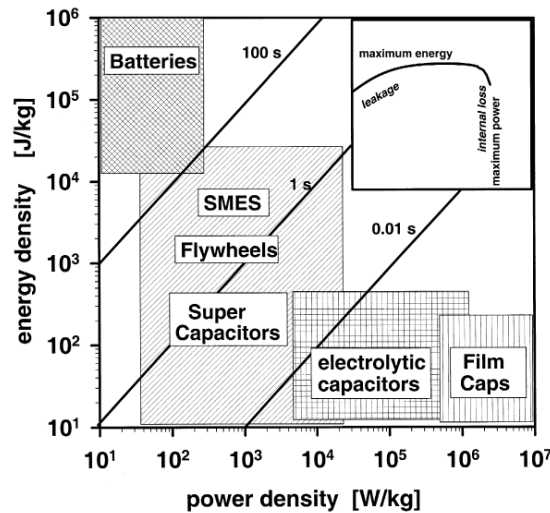
Figure 8-3. Ragone plot of various Energy Storage devices (extracted from [34]).
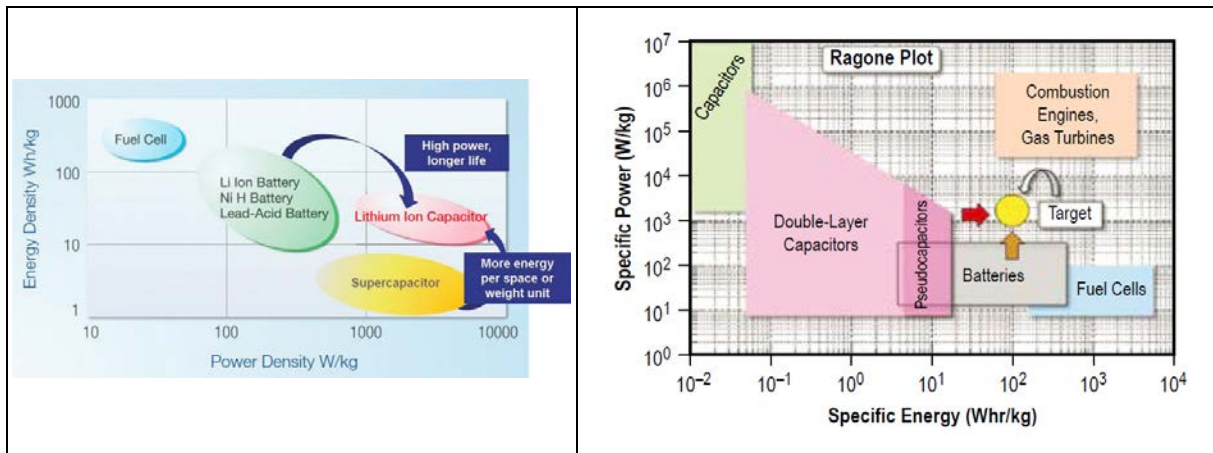
Figure 8-4. Ragone plots of various rechargeable batteries, EDLC, battery-supercapacitor hybrid and pseudocapacitors devices (extracted from [35] left and [36] right).

As described in [37], [36] and [38], new advances provide (and are in the way of providing) energy storage devices located in between and above the traditional batteries and EDLCs with the objective of obtaining the best of the two technologies. Chapter 8.3 present an analysis of the pros and cons of the three different groups of energy storage devices.

8.3.1 Rechargeable batteries

Rechargeable (secondary) batteries are well-known devices used in wireless applications. Rechargeable batteries are based on galvanic cells that store energy in chemical form and are able to convert this to electrical energy on demand, typically by means of an electrochemical oxidation/reduction. Rechargeable batteries can be charged by reversing the internal chemical reaction. Figure 8-5 illustrates the voltage of different cell chemistries. Li-ion based batteries have the highest cell voltage output. Moreover, Li-ion batteries have higher power density (see Figure 8-4), lower self-discharge rate and higher charge-discharge efficiency.

Modern2020 D3.3: Long-term power supply sources for repository monitoring
Dissemination level: PU
Date of issue of this report: 31/05/2019

Page 66
© Modern2020
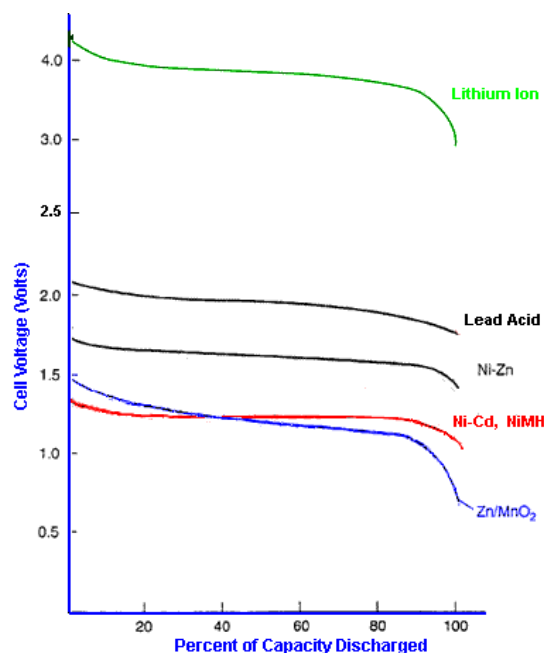
Figure 8-5. Cell voltage in function of percent of discharge for different batteries technologies (extracted from [39]).

For WSN powered by energy harvesting, the analysis of the rechargeable batteries in this chapter is focused in two technologies that presents better characteristics for this application: NiMH and Li-based. As described in [40], in addition to the previous mentioned characteristics, lithium based batteries do not suffer from memory effect (loss of energy capacity due to repeated shallow recharge). They have reasonably high energy, power density and number of recharge cycles. Though NiMH batteries do suffer from memory effect, the effect can be eluded by fully discharging the battery after charging it. Charge-discharge efficiency of the NiMH batteries is lower than that of the lithium based batteries.

An advantage of the batteries is that they provide a nearly constant voltage during a great part of the state of charge cycle (see Figure 8-5). On the other side are the following drawbacks that make them non-applicable for the repository monitoring WSUs: aging (short lifetime), high pulse current limitation (internal impedance), temperature efficiency (also directly related with the life of the battery) and depth of discharge (DoD).

Aging of batteries is a rather complex process affected by the environmental conditions and unwanted chemical reactions that change active chemicals of the batteries (e.g. passivation problems, corrosion of some of the active chemicals, chemical loss though evaporation). In the case of Li-ion batteries, the aging means a progressive degradation of their characteristics, mainly related with the reduction of its initial capacity. Usually there is not an abrupt moment when the battery stops to work, rather there is a moment when the battery, due to aging degradation, does not fulfil applications requirements any more, which can be considered to be the end-of-life of the battery. Clearly, if we define the end-of-life in this way, it will change from application to application. Manufacturers usually provide capacity degradation information for describing battery aging characteristics of their products. Nevertheless, capacity reduction is not the main aging problem for our application: the chemical processes related to aging generates a significant increase of the battery internal impedance what, as later described, is important for our application. Unfortunately, information about how this parameter evolves with aging is usually not provided by manufacturers. On the other hand, temperature significantly affects the aging process (refer to Figure 8-6). Aging process is increased with temperature, which has also to be considered in the case of the reference WSU described in Chapter 8.2 (maximum operational temperature of 45 ºC).

For determining the lifetime of a battery, two different parameters are usually used: calendar life and cycle life [41]:

- Calendar life is just the time that the battery is expected to work independently of the way the battery is charged and discharged during its life. Calendar life is defined by applying the state of charge (SoC), i.e. by the percentage of the total charge of the battery that is usable along the lifetime of the battery at a determined temperature.
- Cycle life represents the number of cycles that the battery will last for a determinate temperature and in function of the DoD.

Figure 8-6 presents two graphs that represents the typical behavior of Li-ion batteries for these two parameters. The figure illustrates clearly the drawbacks that prevent the direct use of Li-ion batteries (and conventional batteries in general) in the long-term repository monitoring scenarios. For the minimum requirement of 20 years' operating life (14600 charging discharging cycles with 12 hours' operation cycles) and a maximum operational temperature of 45°C, the degradation of the battery capacity by aging will be significant (loss of more than 50% of the initial charge capacity).
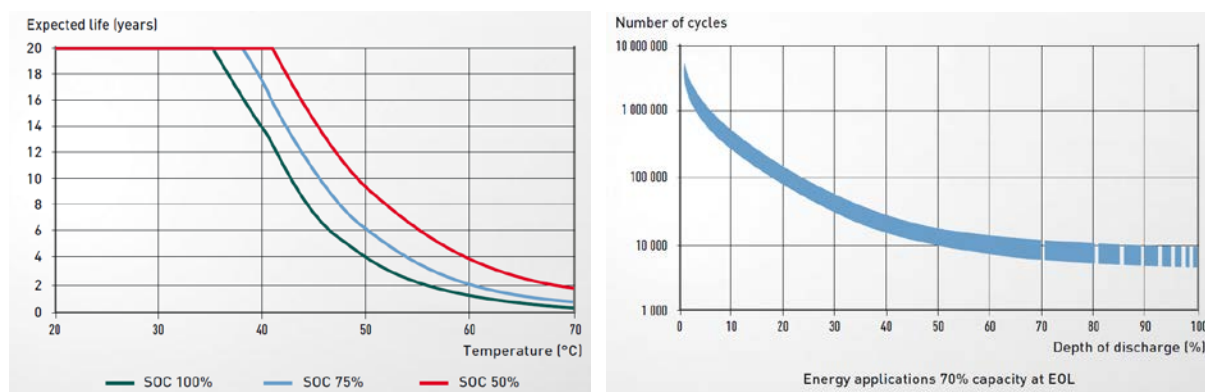
Figure 8-6. Calendar life (left) and cycle life at 25 ºC (right) for Saft Li-ion batteries (extracted from [41]).

Finally, another relevant characteristic is the internal impedance of the conventional batteries. As indicated in Chapter 8.2.6, the WSU will abruptly vary its current consumption during short periods (transmitting), demanding a high peak of current. This requirement is highly related with the internal impedance of the storage device. For batteries, the effect of the internal impedance will imply a voltage drop in the output, thus reducing the available power provided and potentially provoking malfunction of the transmission especially when the SoC of the battery is low. The use of conventional large capacitors (excluding the ultracapacitors that are discussed later) in parallel with the battery would increase the self-discharge and reduce the long-term reliability of the energy storage subsystem (e.g. leakage current increase with time).

The conclusion is that conventional batteries would be an appropriate solution during the initial years of the WSU, but the degradation of the batteries due to aging will reduce their applicability. Considering the state-of-the-art of the battery technologies and the requirements of the reference WSU, it will be very difficult to fulfil all requirements, particularly the lifetime requirement close to the 20 year that was set as the minimum in Chapter 8.2.2. Table 8-3 summarizes some available batteries in the market that are closest to the requirements.

Modern2020 D3.3: Long-term power supply sources for repository monitoring
Dissemination level: PU
Date of issue of this report: 31/05/2019

Page 68
© Modern2020

Table 8-3. Commercially available long-life rechargeable battery technologies.

Model/Manufacturer	Vout [V]	Maximun Peak current [mA]	Calendar life [years]	Comments
UMAL361421B024TA01 (MuRata)	2.3V	600mA	20	Low voltage output will imply the use of two batteries in series, thus duplicating impedance of the energy storage system, Nevertheless, UMAL batteries provide significant improvements to traditional batteries w.r.t the problems commented before.
THINERGY MEC202 (Infinite Power solutions)	3.9	200 mA (@ 45°C)	15	Maximum current parameter out of the requirement margins.

8.3.2 Supercapacitors

Supercapacitors, also called ultracapacitors or electrostatic double-layer capacitors (EDLCs), are basically large capacity electrolytic capacitors that can be used as energy storage devices. They consist of a positive electrode, a negative electrode a separator between them and some kind of electrolyte filling the curves and porosities of the electrodes and the separator. Supercapacitors take advantage of the small distance between the opposite charge charges (between electrolyte and electrodes) and the huge surface of the electrodes in comparison with traditional capacitors. The construction of the supercapacitors is usually done by rolling up the previous described structures in cylindrical or rectangular containers [42], [43], [44].
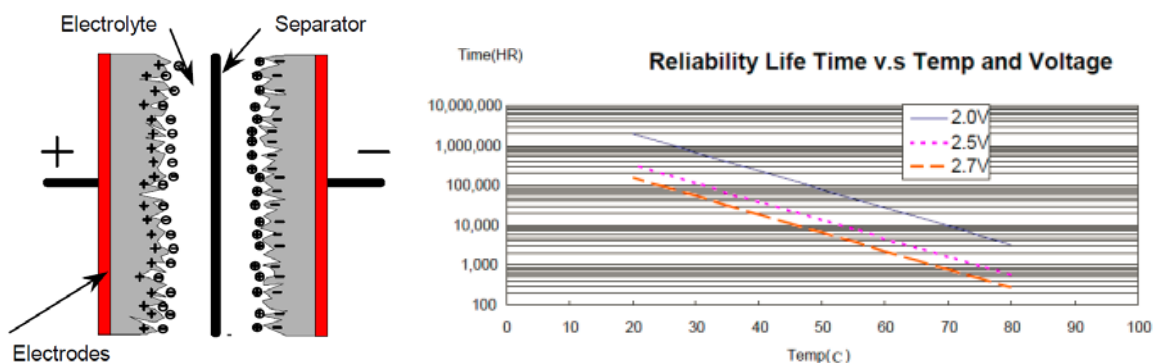
Figure 8-7. Supercapacitor scheme, extracted from [44] (left). Reliability lifetime vs. temperature and voltage, extracted from [45] (right).

In the following paragraphs, an analysis of supercapacitors for the repository monitoring WSUs is provided. The objective is to analyze the advantages and disadvantages of this storage technology with respect to the requirements in Chapter 8.2.

When compared to the batteries, the main advantage of the supercapacitors is their capability of supplying high current pulses. This capability is thanks due to the supercapacitors fast charge and discharge capabilities and low equivalent series resistance (ESR). Low ESR permits the supercapacitor to deliver high pulses of current by low voltage drop at the output, i.e. the supercapacitors are able to

provide a more constant voltage under variant current consumption conditions. In the WSUs powered by energy harvesting, this is of paramount importance as can also be concluded from Figure 8-2. Even though the relatively low ESR of the supercapacitors (in the order of a few hundreds of mΩ in most of the cases), some attention to this as well as to the voltage drop due to discharging has to be paid.

Another important advantage of supercapacitors with respect to batteries is their large cycle life ($1 \cdot 10^5$-$1 \cdot 10^6$ cycles typically). However, the supercapacitors suffer from aging that limits their calendar life. The aging of the supercapacitors depends on the combination of the operating temperature and the operating voltage ([46], [47]). A complete analysis of how aging affects supercapacitor systems can be found in [46]. The effects of the aging are increased ESR and a reduced total capacitance that have to be considered when doing the design and specifying the required energy storage capacity.

The temperature highly influences the aging of the supercapacitors. Several studies (e.g. [47]), determines that the aging effect on the capacitance and the ESR can be predicted using the Arrhenius law, therefore it is possible to consider the aging drift in capacitance and ESR during the design phase. Concerning the operation voltage, supercapacitors are able to work between their rated voltage and 0 volts, but voltages close to the rated voltage will reduce the lifetime considerably and should thus be avoided (see Figure 8-7).

Considering a calendar life of 20 to 40 years and a corresponding cycle life of 14600 to 29200 cycles, it would be possible to select the capacitor (and related electronics) for the reference WSU as described in Chapter 8.2 as follows:

- The rated maximum operating voltage of a supercapacitor cell is typically around 2.5V (commercial supercapacitors with around 5 V maximum operating voltage typically involve two separate cells in series). As our application requires 3.6 V, two or three capacitor cells in series will be required. This disposition will have a significant advantage of reducing the operational voltage per capacitor, thus increasing the lifetime of the capacitors. However, the total capacitance will be reduced with the serial connection. Another important drawback is that there will be need of including a charge-balancing circuit with the objective of ensuring the balanced charging of all the supercapacitors in series [46]. Considering the low power available from the harvesting system, a topology for this balancing circuit with much lower power consumption than the harvested power would be required.

- Considering the drift of the capacitance, the ESR of each capacitor, the final application current profile in each cycle and the Arrhenius law, it will be possible to size the supercapacitors and design the related electronics so that it will comply with the minimum requirements at the end of the system life in the following way:

   1. The required lifetime is defined.
   2. For a determinate operational voltage and ambient temperature, the capacitance and ESR aging drift values of the supercapacitors are calculated using the Arrhenius law for the lifetime defined in step1.
   3. Previous drift values are included in the discharge curves of the supercapacitors so that the circuit design ensures that the charge-discharge curves comply with the payload powering requirements.
   4. Initial capacitance and ESR obtained in previous steps are compared with commercially available supercapacitors.

If there are commercially available supercapacitors in the market with the parameters values worked-out by previous steps, the procedure is finished. If not, iteration of the lifetime, voltage per supercapacitor and number of supercapacitors in series has to be done. Temperature and current demand are considered invariant parameters.

In addition, another feature of the supercapacitors that has to be considered is the self-discharge [48], [45], [49]. Supercapacitors can lose their energy very rapidly compared to batteries. The self-discharge is caused by the parasitic leakage current that makes the capacitor to lose its charge without load. This parameter is dependent on the operational voltage and temperature and it increases as the total capacitance increases.

As a conclusion by following the design considerations described above, the needed capacitance of the reference WSU would be at least 100 farads. Leakage currents of the current state-of-the-art

Modern2020 D3.3: Long-term power supply sources for repository monitoring
Dissemination level: PU
Date of issue of this report: 31/05/2019

Page 70
© Modern2020

supercapacitors of this size are higher than e.g. the wireless energy transfer system according to Chapter 6.3.1 can supply, thus hindering the utilization of the supercapacitors for the application or requiring higher power from the power source.

8.3.3 Electrochemical pseudocapacitors and hybrid capacitors

Lithium-Ion capacitors

Classified as hybrid capacitor devices, Lithium Ion capacitors (LICs) have been recently commercialized with the objective to solve the drawbacks of supercapacitors and batteries discussed in the previous subsections, i.e. to solve the self-discharge (leakage current) problem and to be a safe and reliable high-energy density storage device with long lifetime.

Lithium Ion Capacitors are hybrid capacitors that use a carbon-based material as the negative electrode that can be doped with lithium. Just as in a conventional EDLC, they use activated carbon for the positive electrode [49].

Even though Li-ion capacitors seems to comply in a better way with proposed requirements, it is important to note that calendar life and cycle life characteristics are under analysis and information about long lifetime (20-40 years) is not available. Studies as [41] demonstrate that Li-ion supercapacitors calendar aging is highly dependent on temperature and the state of the charge (voltage) along the operational time. Some of the commercially available Li-ion capacitors are summarized in Table 8-4.

Table 8-4. Commercially available Li-Ion capacitors.

Model and manufacturer	Voltage range [V]	Maximun peak current [mA]	Cycle life [cycles]	Leakage current [µA]	Operation temperature [ºC]	Comments
SLC1016 family (FANSO)	3.6 – 2.0	500		0.25 (@25ºC)	-40 to 85	Voltage range, current capabilities and self-discharge very interesting for the repository monitoring WSUs. No information provided for cycle life in the datasheets.
ULTIMO laminate cell 1100F (JSR Micro)	3.8-2.2	>1000	>10000		-30 to 70	More orientated to high power demand applications.
(Taydo Yuden)	3.8-2.2		>10000	Specified in % per month	-25-85	

Pseudocapacitors

Pseudocapacitors are an evolution of supercapacitors with the objective of improving the drawbacks with respect to Li-ion batteries [36]. Commercial pseudo capacitors are available [50], nevertheless their performance with respect to lifetime and self-discharge is not as good as Li-ion capacitors discussed above.

Battery-supercapacitor storage devices

Other interesting approach is the combination of supercapacitors/pesudacapacitors and batteries. Different studies such as [51], [52], [53] analyse the potential of combining battery and supercapacitors.

8.4   Summary and conclusions

As discussed in Chapter 4, the energy sourcing of energy harvesting WSUs is typically comprised of three subsystems: power sourcing (energy harvesting), intermediate energy storage and energy management for connecting the previous and the power consuming subsystems (sensor and communication payloads) together. The intermediate energy storage subsystem is necessary for matching the limited and sometimes intermittent supply capability of the power sources with the variable power need of the sensor and communication payload. Chapter 8 presents a technology review and a critical evaluation of the applicability of the existing and emerging state-of-the-art energy storage technologies.

The performance and the reliability of the energy storage subsystem is a key issue for the repository monitoring WSUs. The requirements of the energy storage are in general related to the requirements of the entire WSU, which is discussed in Chapter 8.2. The most essential requirements concerning especially the requirements of the energy storage are:

- environmental requirements that are variable from case to case,
- lifetime requirement that can be targeted to be 20 years or more,
- low self-discharge (leakage power) that has to be remarkable lower than the sourced mean power,
- sufficient energy storage capacity, which can also be adjusted by connecting several energy storage components together,
- sufficient current output capacity to supply the power peaks of the sensor and communication payload (typically during data transmission), which can also be adjusted by connecting several energy storage components in parallel,
- proper voltage range, which can also be adjusted by DC/DC power converters or connecting several energy storage components in series.

The basis for the design and defining the previous parameters (except the environmental and lifetime requirements) and the performance requirements of the energy sourcing of the WSU is the power and energy demand of the WSU sensor and communication payload. The demand can be characterized by energy budged analysis, which is also strongly related to the operation scenario of the WSU. Balancing between the energy availability, the energy demand and the performance of the intermediate energy storage for finding a proper overall solution often requires iterative approach. Chapter 8.2.6 illustrates an example of the energy budged analysis by using a reference WSU developed in project Modern2020. Chapter 8.2.7 discusses briefly the possibilities to power the reference WSU by the thermal energy harvesting and wireless energy transfer solutions investigated in Chapter 5 and 6.

When considering the current state-of-the-art of the commercial energy storage technologies, the most fundamental features that have to be addressed in the selection of the energy storage technology for a specific repository monitoring WSUs are the aging that limits the lifetime and the self-discharge that dissipates part of the sourced energy. The aging can be characterized as cycle life (number of charge-discharge cycles) and calendar life. Since the aging typically decreases the energy storage and energy output capacity gradually, it is possible to extend the lifetime more or less by oversized energy storage capacity (component derating). In addition, the energy storage capacity, the current output capacity and the voltage range have to be addressed, which features however can be adjusted by connecting several energy storage components in parallel or in series if possible within the size and the self-discharge requirements. Among the available energy storage technologies for WSUs are rechargeable batteries (Chapter 8.3.1), supercapacitors (Chapter 8.3.2), electrochemical pseudocapacitors (Chapter 8.3.3), and hybrid capacitors combining several energy storage technologies (Chapter 8.3.3).

In general, conventional batteries would be an appropriate solution during the initial years of the WSU, but the degradation of the batteries due to aging will reduce their lifetime, which concerns especially the cycle life. There are some commercial batteries, for which the manufacturer declares calendar life close to 20 years, but the exact calendar life depends much on the environmental and operational conditions,

Modern2020 D3.3: Long-term power supply sources for repository monitoring
Dissemination level: PU
Date of issue of this report: 31/05/2019

Page 72
© Modern2020

which have to be considered case by case. Moreover, in typical repository monitoring WSU, the required capacity of the battery (or the number of the batteries to be connected in parallel) is driven rather by the required current output capacity than the energy storage capacity. Thus, the energy storage capacity of the battery system has to be unnecessary high, which increases the leakage power.

Even though the energy storage capacity (per unit volume) of the supercapacitors is much lower than that of the batteries, the supercapacitors provide remarkably higher current output capacity and longer cycle life than the batteries. Concerning the repository monitoring WSUs, the supercapacitors suffer from relatively short calendar life and high self-discharge.

Electrochemical pseudocapacitors and hybrid capacitors such as lithium-ion capacitors and battery-supercapacitor storage devices have recently been commercialized with the objective to solve the drawbacks and to combine the best features of the batteries and supercapacitors. As they represent novel technologies, these energy storage devices lack currently reliable data about the effects of the aging to the performance parameters in different environmental and operation conditions. In the long run, these technologies are potential to enable better energy storage solutions for repository monitoring WSUs than the batteries and supercapacitors.

For some repository monitoring WSUs with relatively low rate of activity cycles and low energy consumption, a potential power and energy sourcing technology can also be a long term primary (non-rechargeable) battery that is based on Lithium Thionyl Chloride chemistry. The long lifetime of these batteries is based on low self-discharge rate (below 1 % per year according to the manufacturers). Up to 40 years lifetimes are announced by the device manufacturers, but in practice the lifetime in typical WSU applications is probably remarkably shorter because of the pulsed nature of the supply power. Examples of commercial devices are Tadiran TL-4930 and TLP-93111/A/SM. The latter model also features an internal capacitor to enable higher pulse supply currents and to extend the lifetime.

Modern2020 D3.3: Long-term power supply sources for repository monitoring
Dissemination level: PU
Date of issue of this report: 31/05/2019

Page 73
© Modern2020

9. Overall conclusions

9.1 Main conclusions in brief

The work in Modern2020 Task 3.3 has mainly focused to the development and demonstration of the energy sourcing as a separate subsystem without other functionalities of the prospective complete WSUs such as sensor measurements and wireless communication. The achieved TRL levels are 3 – 5 depending on the investigated technology. The volume of the needed further research and development work in each alternative is not directly proportional to their TRL.

The analyses and pilot systems indicate that the proposed three power sourcing technologies (thermoelectric energy harvesting, wireless energy transfer, nuclear generators) are relevant and feasible for powering repository monitoring wireless sensor units (WSUs). By theoretical analyses and by the implementation of some concrete pilot set-ups of the above mentioned power sourcing technologies and their verification results in the environment that partly represents the final repository environment, the project has improved the understanding about scaling the capacity of the power sourcing by adjusting the design parameters. Moreover, the activities have improved the understanding of the effects of the repository environment on the behavior and performance of the power sourcing. Both of these will be of great importance in the follow-on actions towards complete wireless repository monitoring systems.

Even though the performance and other features of each power sourcing option depend much on the design parameters and operation environment, a rough comparison of the three technical options can be given in Table 9.1.

Table 9-1. A rough comparison of the investigated energy sourcing options.

Power sourcing option / Required/ desired feature	Thermoelectric energy harvesting from the HLW containers	Wireless energy transfer through the repository barriers	RTG nuclear battery
Typical output power capacity	tens of µW to a few mW per unit	tens of µW to several mW, depending strongly on the thickness of the barriers and the available space for the antennas.	several W
Operation mode	continuous power output	continuous or discontinuous power output	continuous power output
Temporal variations in power output	slowly decreasing power output, depending on decay heat of HLW	constant power output, can be adapted on demand by adjusting the power level of the power transmitter	slowly decreasing power output, depending on selected radionuclide(s)
Placement	one or more units can be placed in a disposal cell; application limited to heat-generating waste	placement preferably close to the sealing plug; application in all waste sections possible	flexible unit placement possible; consideration of heat transport necessary; application in all waste sections possible
Expected impact on the disposal concept	low impact, placement in single barrier is possible with minor alteration of the overall heat flow	low, due to placement close to the plug	safety assessment of introduced radionuclides necessary, interactions between heat pipes and the EBS need to be considered
Specific future research needs	energy storage options, long-term reliability	energy storage options, long-term reliability, interactions with electrically conductive and magnetic permeable materials in the EBS, (automatic) antenna tuning	safety and long-term reliability, heat transport in specific placements, energy storage options in applications with high peak power consumption

Limited power sources such as typical thermoelectric energy harvesters or wireless power transfer systems are not able to supply typical repository monitoring WSUs during their activity cycles directly. For this, the powering of the WSUs also requires an intermediate energy storage that accumulates the sourced energy for the further need of the sensor and communication payload. Typically, the monitoring application allows long (e.g. several hours or even several days) energy accumulation periods between short activity cycles with sensor measurements and wireless communication. In this low duty-cycle operation scenario of the WSU, the sensor and communication payloads are kept in an ultra-low power sleep mode or even totally unpowered, and are activated periodically by an ultra-low power wake-up circuit. With this kind of WSU arrangement, which is also commonly applied in energy harvesting wireless devices in general, power sourcing levels even down to around 10 µW can be exploitable if the leakage power of the energy storage can be kept below this.

The work in Modern2020 Task 3.3 has also improved the understanding for designing the intermediate energy storage subsystem. Depending on the power sourcing capacity, power needs of the sensor and communication payload, and the required lifetime and environmental conditions, the energy storage subsystem can be a critical part for the performance and the reliability of the entire repository monitoring WSU. This concerns especially the lifetime (aging), the self-discharge of the energy storage components, and the maximum output power than can be supplied. Even though several energy storage technologies such as rechargeable batteries, electrostatic double-layer supercapacitors and newer type pseudocapacitors are commercially available, the design of an energy storage subsystem that can fulfil all requirements of typical repository monitoring WSUs can be a challenging task. The design of the

energy storage subsystem may also set additional requirements to the capacity of the power sourcing and to the sensor and communication payload design concerning e.g. its operation scenario.

With the basic features of the proposed technologies well understood and its principal working demonstrated in this research, the follow-on steps after project Modern2020 should be targeted to the further development, demonstration and verification of the energy sourcing parts as more complete building blocks. This should be started with closer numerical energy demand requirement capture that is based on case-by-case analysis of the target WSUs. Beyond this, the follow-on steps should also be targeted to integration, demonstration and verification of more complete pilot repository monitoring systems. In addition to the power sourcing, these pilot systems should also include the intermediate energy storage with appropriate energy management, sensor and communication payloads, an encapsulation that can tolerate the target repository environment, and external parts behind the EBS. The verification of these comprehensive repository monitoring pilot systems should take place in a testing environment that emulates as much as possible the final repository environment, including e.g. the ambient bentonite with moisture saturation, pressure and temperature drift. For thermoelectric energy harvesting, this could be based e.g. on a real-scale heater experiment. For wireless energy transfer, the testing environment should also involve all metallic and magnetic permeable components with potential effects to the magnetic field. Since monitoring behind safety relevant barrier usually does not allow accessing the devices after the installation, the future actions should also involve measures for improving the reliability such as redundancy, design by drift margins and component derating, and qualification and screening procedures.

9.2   Power sourcing

Three alternative power sourcing technologies were investigated closer in project Modern2020:

1. thermoelectric energy harvesting by exploiting the heat generated by the HLW (high-level waste),
2. wireless energy transfer through the repository barriers by LF (low frequency) magnetic fields,
3. RTG (radioisotope thermoelectric generator) type nuclear battery inside ILLL (intermediate level long lived) waste vaults.

Chapter 5 reports a feasibility study and laboratory experiments of a thermoelectric energy harvester pilot based on a TEG of size 40 mm x 40 mm and exploiting the heat generated by the HLW in the Dutch OPERA disposal concept. It concludes that the proposed energy harvester concept is an appropriate power sourcing option for wireless repository monitoring sensors and provides a relatively simple technical implementation. Assuming a long interim storage of 100 years, thermoelectric harvesting still allows providing energy over a period of more than 100 years after disposal. The output power capacity is limited by the temperature gradient across the barrier in which the harvester is placed. However, a higher output power might be achieved for waste with a shorter interim storage history (i.e. < 100 years), or if the harvester device bridges more than a single barrier component, as is conservatively assumed here. To increase the output power, several TEGs can also be applied in a TEH, and several TEHs can also be distributed over a disposal cell. The low output voltage of the TEG (typically in tens of millivolts) results in a rather small efficiency of the voltage step-up converter that is necessary at the TEG output. The decay of the heat production of the HLW will drop the output power capacity in the course of the repository operation. This is not necessarily a problem, assuming that the intervals between the sensor activity cycles will become longer in the course of the repository operation, which is relevant due to the slower changes of the HLW and the EBS after few decades. Still, output power levels of several hundreds of microwatts at the beginning and some tens of microwatts after 100 years operation are possible with the pilot concept. This can power low duty cycle operation of various wireless sensor nodes by use of an intermediate energy storage to accumulate the energy for the activity cycles of the sensor payload and the communication parts. Further research is needed when it comes to qualifying the used materials and components with respect to long-term reliability and moderate radiation field as present in the proposed concept.

Modern2020 D3.3: Long-term power supply sources for repository monitoring
Dissemination level: PU
Date of issue of this report: 31/05/2019

Page 76
© Modern2020

Chapter 6 reports the feasibility studies and pilot experiments of inductive wireless energy transfer between two loop antennas at the opposite sides of the repository barriers. It concludes that this is also a relevant power sourcing option for wireless repository monitoring sensors. For example (referring to Table 6-4), supplying some tens of microwatts by a 100 W power transmitter to a WSU behind a 10 m repository barrier comprised of low-conductivity host rock is possible with a 2 m x 2 m power transmitter antenna and a 180 mm diameter power receiver antenna in the WSU. Energy transfer through an electric conductive media is shown to be feasible as well, if interactions are understood and covered in the design of the energy transmitter. With an optimized antenna design, link efficiencies of several hundred ppm were achieved, despite of interactions with the conducting medium. For the wireless distance of interest (10 m), interactions with the medium need to be considered in the case of argillaceous host rocks, (saturated) bentonite or cementitious materials. In case of higher conductivities (> 50 mS/m), lower frequencies than 125 kHz should be preferred. For reasonable power levels, resonance tuning of the antennas is necessary. The operation distance and powering capacity can be improved by increasing the antenna diameters that can be adapted to meet the powering needs of the sensor and the size constraints of the repository environment. In general, LF (e.g. 125 kHz) magnetic fields can penetrate through the host rock and the EBS, but larger metallic parts in the repository structures may degrade the powering capacity due to field attenuation, and may also require additional effort for keeping the antennas tuned. On the other hand, materials with high magnetic permeability can also enhance the powering capacity, and careful analysis and testing of each application case is necessary to optimize the power transfer efficiency. As with the thermoelectric energy harvesting, accumulation of the energy into an intermediate energy storage with associated sleep mode arrangements of the sensor payload and communication parts is typically necessary. A useful option in the wireless energy transfer is the implementation of wireless communication by shared antennas and RF front end, which makes the overall system more compact and eliminates possible co-existence problems and double efforts of the adaptation of two independent inductive systems. An advantage of the wireless energy transfer is also the absence of wearing parts, even though the temperature variations and long-term aging of electronic components may cause performance degradation, especially because of antenna detuning. Another advantage of the wireless energy transfer is its lower impact to the disposal concept in general, since its components can be placed e.g. close to sealing plug. A general conclusion from all the previous is that the wireless energy transfer systems have to be adapted carefully to the specific repository environment, which also calls for additional research efforts.

Chapter 7 reports a generic state-of-the-art of nuclear batteries, which is followed by a feasibility analysis, conceptual design and thermal modelling of an RTG type nuclear battery in an ILLL disposable vault. It concludes that further steps for developing an RTG prototype are relevant, for which the results also give guidelines. The RTG is composed of a specific radioisotope heat source with alpha particle emission and a TEG. Thus, the physical operation principle of the RTG is much the same as that of the thermoelectric energy harvester that exploits heat generated by the HLW. However, the power output capacity of RTG's is much higher due to the higher temperature gradient across the TEG. In many cases, the high output power can cancel the need of the intermediate energy storage that is prone to limit the lifetime of the WSU. According to the estimations in Chapter 7.3, an RTG with 1 kg Am_2O_3 heat source can produce several watts of electric power, which can be enough for continuous powering of many types of repository monitoring sensor nodes even without any intermediate energy storage. Due to the relatively long half-life of [241]Am (433 yr) compared to the main isotopes that dominate heat production in HLW, the decay of the output power capacity is slower than with the proposed thermoelectric energy harvesting concept.

9.3 Energy storages

In WSUs, the peak power consumption during measurements or data transmission can be larger than what is continuously supplied by a power source. Here, a rechargeable intermediate energy storage subsystem is necessary for buffering the sourced energy. To define the requirements of the energy storage subsystem, an energy budged analysis of the WSU is a useful tool. Chapter 8.2.6 gives an example for this.

Modern2020 D3.3: Long-term power supply sources for repository monitoring
Dissemination level: PU
Date of issue of this report: 31/05/2019

Page 77
© Modern2020

The energy storage subsystem is a critical component, affecting the performance and reliability of the repository monitoring WSUs. This concerns especially the lifetime (aging) and the self-discharge of the energy storage subsystem. In addition to the energy storage technology, these features depend much on the environmental conditions such as the temperature, and on the operational conditions such as the terminal voltage, charging state or the rate of charge-discharge cycles. In addition, the energy storage capacity, output current capacity and the voltage range of the energy storage components have to be addressed in the design. The design of the energy storage subsystem should also address the optimal configuration of the energy storage components in series and in parallel, the voltage conversions between the power source and the WSU payload, and energy storage component derating (selecting oversized capacity). The combination of all these requirements makes the design of the intermediate energy storage subsystem a challenging task.

Currently, the intermediate energy storage subsystem of energy harvesting wireless sensors is typically based on small rechargeable batteries or supercapacitors, which are not optimal for repository monitoring WSUs, especially because of their limited lifetime, which can be characterized as both calendar life and cycle life (maximum number of the charge-discharge cycles). In many repository monitoring application cases, the self-discharge (concerning especially supercapacitors) and the output current capacity (concerning especially batteries) of the energy storage components may also cause problems. Since the aging of the batteries and supercapacitors depends much on the operation temperature, WSUs operating at relatively high temperatures should be avoided.

To overcome the above mentioned problems of the rechargeable batteries and supercapacitors, the component manufacturers have developed novel energy storage technologies such as electrochemical pseudocapacitors and hybrid capacitors, which are potential energy storage technologies for future repository monitoring WSUs but currently lack reliable data about the effects of aging. There are also novel long-life non-rechargeable (primary) batteries based on Lithium Thionyl Chloride chemistry that, combined with a capacitor for supplying peak currents, can be a possible energy sourcing solution for repository monitoring WSUs with relatively low energy consumption.

9.4   System integration

The work behind this document has been focused to the development and evaluation of the energy sourcing technologies as separate building blocks according to the concepts illustrated in Chapter 4 without any actual integration into entire repository monitoring WSUs or systems. Thus, the follow-on activities after Modern2020 should also involve the integration and verification of the energy sourcing parts as a building block of more complete systems that also involve the sensor payload, wireless communication, encapsulation and the necessary parts behind the repository barriers. Moreover, this work should also be connected to the overall design of the monitoring systems with possibly several wireless sensor nodes.

For the repository monitoring WSU integration, a key issue is the matching of the power/energy sourcing capacity and the power/energy consumption demand, which may require scaling either or both of these parts. With limited energy sources such as thermal energy harvesting from the HLW or wireless energy transfer, an intermediate energy storage and WSU energy budged analysis are necessary. The energy budged analysis should address e.g. the energy consumed by each activity cycle of the sensor (joules), the rate of the activity cycles (measurements per hour/day/week), and the peak power consumption during activity cycles (watts). The power/energy consumption may be scaled e.g. via the rate of the activity cycles and the sensor configuration in each activity cycle. The power/energy sourcing may be scaled e.g. via the number of the TEGs or the size of the power transmitter and power receiver antennas, in which the design constraints due to the repository environment have to be taken account of.

9.5   Reliability improvements

Since monitoring devices that are installed behind safety relevant barriers do not allow access after the installation, among the most important future design drivers of the energy sourcing parts (as well as the

Modern2020 D3.3: Long-term power supply sources for repository monitoring
Dissemination level: PU
Date of issue of this report: 31/05/2019

Page 78
© Modern2020

repository monitoring WSUs in general) will be maximizing their reliability. For this, following measures are applicable:

- redundancy,
- anticipating drift margins and component derating,
- qualification and screening.

Redundancy, i.e. the duplication of critical components or functions of a system, is conventionally being applied e.g. in spacecrafts. In the case of the energy sourcing parts of repository monitoring WSUs, the redundancy can mean e.g. including several thermoelectric energy harvesters, a combination of thermoelectric energy harvester with a wireless energy transfer system, or including several energy storage subsystems by cold redundancy, i.e. keeping the redundant subsystems unpowered.

Allowing drift margins for changing environmental conditions (e.g. temperature) and component aging, as well as component derating (operating a device below its maximum rating in order to extend its lifetime) are also widely used design methods in critical systems. For example, ensuring the long-term performance of wireless energy transfer systems requires drift margins for the antenna tuning, which may also call for some autotuning arrangements. Component derating concerns especially the energy storage devices, the aging of which depends typically much on their operating conditions such as the voltage and the temperature. Nevertheless, the aging of the energy storage devices reduces their capacity, and thus some capacity drift margin is necessary, too. It is also important to minimize the environmental stress of the WSUs in the repository monitoring system design, for example by placing the devices in low and constant temperatures as much as possible.

Qualification means a procedure of actions for providing that a system or its component perform correctly under the requirements. The qualification procedure can be applied to the whole system or to its critical subsystems or components. As examples, the qualification of the energy storage subsystem can involve performance tests by accelerated aging at high temperatures or accelerated charge-discharge cycles, and qualification of the electrical components and subsystems may involve radiation tests if the effects of the radiation are assessed as a risk. The same procedures can also be applied e.g. to screening the energy storage component lot for the final implementation.

Modern2020 D3.3: Long-term power supply sources for repository monitoring
Dissemination level: PU
Date of issue of this report: 31/05/2019

Page 79
© Modern2020

10. Appendices

1. Thermal analysis of the OPERA disposal design (NRG)

2. General outlines of disposal cell geometries (NRG)

Modern2020 D3.3: Long-term power supply sources for repository monitoring
Dissemination level: PU
Date of issue of this report: 31/05/2019

Page 80
© Modern2020

11. References

[1] "MoDeRn. Monitoring Reference Framework Report. MoDeRn project Deliverable D-1.2.1," 2013.

[2] A. Bitschi, Modelling of thermoelectric devices for electric power generation, PhD. thesis ETH, 2009.

[3] J. L. Bierschenk, Optimized Thermoelectrics For Energy Harvesting Applications, In: Priya, S., Inman, D.J. (ed): Energy Harvesting Technology, SpringerScience+Business Media, 2009, p.337-351.

[4] E. Verhoef, E. Neeft, J. Grupa and A. Poley, Outline of a disposal concept in clay, OPERA-PG-COV008, COVRA N.V., 2014.

[5] E. Strömmer, M. Jurvansuu, T. Tuikka, A. Ylisaukko-oja, H. Rapakko and J. Vesterinen, "NFC-Enabled Wireless Charging," in *4th International Research Workshop on Near Field Communication, NFC 2012*, Helsinki, Finland, 2012.

[6] K. Finkenzeller, RFID Handbook, Chichester, England: John Wiley & Sons Ltd, 2003.

[7] Y. Lee, "Antenna Circuit Design," Microchip AN710, 2003.

[8] P. C. Clemmow, An Introduction to Electromagnetic Theory, Cambridge, U.K: Cambridge University Press, 1973.

[9] G. Lehner, Elektromagnetische Feldtheorie für Ingenieure und Physiker. 6th ed., Heidelberg: Springer Verlag, 2008.

[10] N. J. Cassidy, Electrical and magnetic properties of rock, soils and fluids. In: Jol, H.M. (ed.). Ground Penetrating Radar Theory and Applications, Amsterdam: Elsevier Science, 2009, pp. 41-72.

[11] J. H. Scott, Electrical and magnetic properties of rock and soil. Technical Letter Special Projects-16, Colorado: United States Department of the Interior, Geological Survey, Denver, 1966.

[12] T. J. Schröder and E. Rosca-Bocancea, Wireless Data Transmission Demonstrator: from the HADES to the surface, MoDeRn Deliverable D.3.4.2, 2013.

[13] J. R. Wait, "Complex Resistivity of the Earth," *Progress In Electromagnetics Research,* vol. 1, pp. 1-173, 1989.

[14] J. R. Wait, Criteria for Locating an Oscillating Magnetic Dipole Buried in the Earth, Proc. IEEE, 59 (6), 1971, pp. 1033-1035.

[15] J. R. Wait and K. P. Spies, Electromagnetic Fields of a Small Loop in a Stratified Earth, IEEE Trans. Antennas and Propagation, AP-19 (5), 1971, pp. 717-718.

[16] S. F. Pichorim and P. J. Abatti, Design of Coils for Millimeter- and Submillimeter-Sized Biotelemetry, IEEE Transcations on biomedical Engineering, 51 (8), 2004, pp. 1487-1489.

[17] M. B. Kraichman, Impedance of a Circular Loop in an Infinite Conducting Medium, Journal of Research of the National Bureau of Standards - D. Radio Propagation, 66D (4), 1962, pp. 499-503.

[18] R. R. Harrison, Designing Efficient Inductive Power Links for Implantable Devices, IEEE International Symposium on Circuits and Systems, 2007, pp. 2080-2083.

[19] K. Schuylenbergh and R. Puers, Inductive Powering: Basic Theory and Application to Biomedical Systems, Springer Science + Business Media B.V., 2009.

Modern2020 D3.3: Long-term power supply sources for repository monitoring
Dissemination level: PU
Date of issue of this report: 31/05/2019

Page 81
© Modern2020

[20] [Online]. Available: www.oceanologyinternational.com/files/AUV_Marketplace_John_Westwood.pdf.

[21] [Online]. Available: http://www.futura-sciences.com/fr/news/t/terre-3/d/lobservateur-sous-marin-qui-ne-remontera-jamais_10643/.

[22] ANDRA, "CGNTAMTD150056, Spécification technique de besoin. Alimentation autonome pour la transmission sans fil en condition de stockage géologique. Modern2020 WP3.3, (2015), 15 pages.".

[23] "Modern2020 project Milestone number MS11 – final report on "Using Nuclear Batteries for Geological Disposal Monitoring: State of the Art", 47 pages.," 2016.

[24] A. Harmon, "NASA's Radioisotope Power System Program. Science Mission Directorate. OPAG.," 2007.

[25] R. L. Cataldo and G. L. Bennett, "U.S. Space Radioisotope Power Systems and Applications: Past, Present and Future," NASA Glenn Research Center and Metaspace Enterprises, USA, 2011.

[26] M. A. Prelas, C. J. Weaver, M. Watterman, E. Lukosi, R. Schott and D. A. Wisniewski, "A review of nuclear batteries," *Progress in Nuclear Energy,* vol. 75, pp. 117-148, 2014.

[27] S. T. Revankar and T. E. Adams, "Advances in Betavoltaic Power Sources," *Journal of Energy and Power Sources,* vol. 1, no. 6, pp. 321-329, 2014.

[28] W. R. Corliss and R. L. Mead, "Power from Radioisotopes, Understanding the atom series," United States Atomic Energy Commission, Division of Technical Information, 1971.

[29] D. Leone, "Plutonium Still Scarce, Production Restart Still Slow for Needy NASA," 2015. [Online]. Available: http://spacenews.com/doe-to-crank-out-new-plutonium-238-in-2019/.

[30] McNutt, "RL Physics and Chemistry of Space-certified RPS : what do you need to know," The John Hopkins University applied physics laboratory. Committee on Astrobiology and Planetary Science Space Study Board, 2014.

[31] R. D. Abelson, "Big Things Come in Small Packages: Mission Concepts Potentially Enabled by Small Radioisotopes Power Systems. Systems & Mission Architecture Section," in *CalTech*, 2005.

[32] "DLC 037 0017 Rév. 2, Document logiciel Calcul - ANSYS - Dossier de validation théorique," AREVA, 2015.

[33] "DLC 037 0019 Rév. 2, Document logiciel Calcul - ANSYS – Manuel utilisateur," AREVA, 2015.

[34] T. Christen and M. W. Carlen, "Theory of Ragone plots," *Journal of Power Sources,* vol. 91, no. 2, pp. 210-216, 2000.

[35] Murata, *Small Energy Device Laminate type (UMAL). C2M1CXS-313(E),* 2016.

[36] D. S. Tucker and S. Paley, "Flexible Hybrid Battery/Pseudocapacitor," NASA, 2015.

[37] W. Zuo, R. Li, C. Zhou, Y. Li, J. Xia and J. Liu, "Battery-Supercapacitor Hybrid Devices: Recent Progress and Future Prospects," *Advanced Science,* vol. 7, no. 4, 2017.

[38] A. Sato, "TAIYO YUDEN Lithium Ion Capacitors: An Effective EDLC Replacement," TAIYO YUDEN.

[39] "Battery and Energy Technologies," Electropaedia, [Online]. Available: https://www.mpoweruk.com/index.htm.

Modern2020 D3.3: Long-term power supply sources for repository monitoring
Dissemination level: PU
Date of issue of this report: 31/05/2019

Page 82
© Modern2020

[40] S. Sudevalayam and P. Kulkarni, "Energy Harvesting Sensor Nodes: Survey and Implications," *IEEE Communications Surveys & Tutorials,* vol. 13, no. 3, pp. 443-461, 2011.

[41] *Lithium-ion battery life,* Saft, 2014.

[42] Tecate Group, "Ultracapacitor & Supercapacitor Frequently Asked Questions," [Online]. Available: https://www.tecategroup.com/ultracapacitors-supercapacitors/ultracapacitor-FAQ.php.

[43] P. Mars, "Coupling a supercapacitor with a small energy-harvesting source," *EDN-Electronic Design News,* pp. 39-42, 7 June 2012.

[44] A. Schneuwly and R. Gallay, "Properties and Applications of Supercapacitors From the State-of-the-art to Future Trends," in *Proceeding PCIM2000*, Rossens, Switzerland, 2000.

[45] Tecate Group, *Tecate PowerBurst Ultracapacitors Technical Guide Document,* Tecate Group document no. 9100760000 Rev M .

[46] D. Linzen, S. Buller, E. Karden and R. W. De Doncker, "Analysis and evaluation of charge-balancing circuits on performance, reliability, and lifetime of supercapacitor systems," *IEEE transactions on industry applications,* vol. 41, no. 5, pp. 1135-1141, 2005.

[47] G. Alcicek, H. Gualous, P. Venet, R. Gallay and A. Miraoui, "Experimental study of temperature effect on ultracapacitor ageing," in *European Conference on Power Electronics and Applications*, Aalborg, Denmark, 2007.

[48] *Product Guide – Maxwell Technologies BOOSTCAP Ultracapacitors,* Maxwell Technologies Doc. No. 1014627.1, 2009.

[49] Y. Diab, P. Venet, H. Gualous and G. Rojat, "Self-Discharge Characterization and Modeling of Electrochemical Capacitor Used for Power Electronics Applications," *IEEE Transactions on Power Electronics,* vol. 24, no. 2, pp. 510-517, 2009.

[50] *2.3V 50F Pseudocapacitor Cell,* Maxwell Technologies doc. no. 3001969-EN.2, 2018.

[51] X. Jiang, J. Polastre and D. Culler, "Perpetual environmentally powered sensor networks," in *Fourth International Symposium on Information Processing in Sensor Networks (IPSN 2005)*, Boise, ID, USA, 2005.

[52] F. S. Garcia, A. A. Ferreira and J. A. Pomilio, "Control Strategy for Battery-Ultracapacitor Hybrid Energy Storage System," in *Applied Power Electronics Conference and Exposition (APEC 2009)*, Washington, DC, USA, 2009.

[53] F. Ongaro, S. Saggini and P. Mattavelli, "Li-Ion Battery-Supercapacitor Hybrid Storage System for a Long Lifetime, Photovoltaic-Based Wireless Sensor Network," *IEEE Transactions on Power Electronics,* vol. 27, no. 9, pp. 3944-3952, 2012.

[54] C. Auvigne, Electrical and Magnetical Modeling of Inductive Coupled Power Transfer Systems, Thesis, Ecole Polytechnique Federale de Lausanne, 2015.

[55] MoDeRn, "Monitoring Reference Framework Report," MoDeRn Deliverable D-1.2.1, 2013.

Modern2020 D3.3: Long-term power supply sources for repository monitoring
Dissemination level: PU
Date of issue of this report: 31/05/2019

Page 83
© Modern2020